UNIVERSITÀ
DEGLI STUDI
DI PADOVA

Sede Amministrativa: Università degli Studi di Padova
Dipartimento di Medicina Molecolare

CORSO DI DOTTORATO DI RICERCA IN: Biomedicina

CURRICOLO: Medicina Molecolare

CICLO: XXIX

TITOLO TESI

Towards the identification of small molecules inhibiting he dimerization of HCMV DNA polymerase processivity factor UL44

Tesi redatta con il contributo finanziario del Fondazione Cariparo

Coordinatore: Ch.mo Prof. Stefano Piccolo

Supervisore: Ch.mo Prof. Ignazio Castagliuolo

Co-Supervisore: Ch.mo Prof. Gualtiero Alvisi

Dottorando: Veronica Di Antonio

Index

Abstract

Human cytomegalovirus (HCMV) is a leading cause of congenital defects in humans. Currently available antivirals utilized for the therapy against HCMV infections have a series of contraindications due to their high cost, low bioavailability, high toxicity and the uprising of resistant viral strains. Furthermore no vaccine is available and no drugs are approved to prevent vertical transmission during pregnancy, therefore new, effective antiviral are highly needed.

HCMV DNA polymerase accessory protein UL44 plays an essential role in viral replication, conferring processivity to the DNA polymerase catalytic subunit UL54 by tethering it to the DNA. Binding of UL44 to dsDNA occurs in the absence of ATP and clamp loaders, and depends on UL44 homodimerization. Indeed, our research group recently demonstrated that the protein can dimerize in cells and point mutations disrupting protein self-interaction also prevent DNA binding and abolish viral oriLyt-dependent DNA replication in transient transcomplementation assays. Therefore, disruption of UL44 homodimerization represents an attractive target for the development of new anti-virals. Based on these observations, using the recently published crystal structure of UL44 homodimers our research group previously performed a virtual screening with the Glide software in combination with a library of 1.3 x 10^6 small molecules (SMs) to identify SMs potentially interfering with UL44 homodimerization. After three rounds of screening (HTVS: high-throughput virtual screening, SP: standard precision, XP: extra precision), followed by an in depth analysis of compounds chemical properties, 18 SMs were selected for further analysis. Selected compounds were obtained from a commercial supplier, to be tested in a variety of assays for their ability to inhibit UL44 homodimerization both in cells and in vitro, as well as on HCMV replication.

To this end, we applied a number of in cells and in vitro assays to monitor the effect of the SMs on UL44 dimerization. In cells methods included Fluorescent Resonant Energy Transfer (FRET) and Bioluminescence Resonant Energy Transfer (BRET), while as GST pull-down assays was chosen as the in vitro method.

FRET acceptor photobleaching was capable of detecting both UL44 homodimerization and UL44 binding to the catalytic subunit C-terminal domain (residues 1125-1242). Such interactions were sensitive to point mutations specifically impairing the two processes, highlighting the specificity of this technique. Therefore, we were able to confirm that UL44 forms dimers in cells. However, data acquisition and analysis proved quite time consuming and dependent on high fusion proteins expression levels.

BRET assays allowed to quickly and precisely quantitatively monitor UL44 self-interaction and binding to UL54 in living cells, and through saturation experiments allowed to precisely calculate B_{max} and B_{50} values, relative to homodimerization or binding to UL54 for a number of single amino acids substitution derivatives of UL44 impaired for dimerization, binding to UL54 or to dsDNA, as well as for nuclear targeting. These data allowed gaining insights relative to the formation of HMCV DNA polymerase holoenzyme, suggesting conformational changes within UL44 upon DNA binding in complex to UL54. Furthermore, calculation of B_{max} and B_{50} values was used to establish three different cellular systems expressing ideal amount of UL44 for screening purposes, in that they generated a BRET ratio similar to half of the B_{max}. These included a fully stable expression system, whereby both RLuc-UL44 and YFP-UL44 are stably expressed in HEKA derived cells, a stable/transient system whereby YFP-UL44 is stably expressed and RLuc-UL44 is transiently expressed, or a fully transient system whereby both fusion proteins are transiently expressed. Competition assays performed overexpressing increasing amounts of FLAG-tagged UL44 as a competitor revealed that no inhibition could be obtained for the fully stably expressing system. This result highlighted the difficulty in disrupting a pre-existing protein complex and suggested to focus our attention on transient systems.

Keeping this in mind, a first small-scale screening was performed to study the impact of 18 SMs on UL44 dimerization by BRET using the stable/transient system. The 18 selected SMs were resuspended in DMSO and their toxicity was evaluated in cell culture, before being added at sub-toxic concentration to the YFP-UL44 cell line, six hours post-transfection with RLuc-UL44. Our analysis identified only compounds slightly inhibiting the BRET ratio relative to UL44 homodimerization.

Based on these disappointing results, we revaluated the BRET assays setup, by decreasing the time of SM incubation before assaying their effect from 42 to 18h, by switching to a completely transient system, and by decreasing the amount of expressed proteins. The last modification required a

change in the substrate used for generation of bioluminescent signal from RLuc-fusion proteins from CTZ to hCTZ.

A new screening was performed, which resulted in very similar results to those obtained using the original setup. Furthermore when hit candidates were re-evaluated for their effect using a negative control, their effect on BRET ratio of UL44 proved unspecific. Additionally, BRET - similarly to FRET - failed to detect a specific effect on the UL54/UL44 interaction by a SM known to disrupt such interaction. Therefore we conclude that, with our current settings, BRET and FRET are not the ideal techniques to search for SM inhibitors of protein-protein interactions

We then focused on in vitro methods, starting with a GST pull-down assay, which was performed using UL44 C-terminal domain (residues 1-290), either fused to GST of a 6His-tag. Our results indicated that GST pull-down was capable of detecting differences in binding between wild-type UL44 and a dimerization-impaired mutant, suggesting a possible application for the screening of SMs. GST pull-down is currently being implemented for this purpose, and preliminary data suggest that a number of tested SMs could impair UL44 dimerization.

In summary, we have developed a number of assays to monitor UL44 dimerization. Whereas in cells RET based assays confirmed that UL44 form dimers in living cells, they proved suboptimal for screening proposes. On the other hand, in vitro methods such as GST pull-down might prove more sensitive and are currently being implemented for the identification of SMs inhibitors of UL44 dimerization

Riassunto

Cytomegalovirus (CMV) è un importante patogeno di interesse umano. Al momento gli antivirali disponibili ed utilizzati per la terapia contro l'infezione da CMV presentano una serie di controindicazioni dovute all'alto costo, bassa biodisponibilità, alta tossicità ed il presentarsi di ceppi virali resistenti. Inoltre non è disponibile un vaccine ed ancora non è ancora stato approvato l'uso di alcun farmaco per prevenire la trasmissione verticale durante la gravidanza. Per questi motivi, sono necessari nuovi ed efficaci farmaci antivirali.

La proteina accessoria UL44 della DNA polimerasi di CMV, svolge un ruolo essenziale nella replicazione virale, conferendo processività alla subunità catalitica UL54 ancorando il complesso oloenzimatico al DNA.

Il legame di UL44 al dsDNA avviene in assenza di ATP e dei clamp loaders, e dipende dalla omodimerizzazione di UL44. Infatti, il nostro gruppo di ricerca ha recentemente dimostrato che la proteina può dimerizzare in cellule e che mutazioni puntiformi in grado di inficiare tale dimerizzazione prevengono il legame con il DNA ed aboliscono la replicazione del DNA virale oriLyt-dipendente in saggi di transcomplementazione transiente.

Perciò, la distruzione dell'omodimerizzazione UL44 rappresenta un potenziale allettante bersaglio per lo sviluppo di nuovi anti-virali. Partendo da queste osservazioni ed usando la struttura cristallografica recentemente pubblicata degli omodimeri UL44, il nostro gruppo di ricerca ha eseguito un virtual screening con il software Glide in combinazione con una libreria di 1.3 x 10^6 piccole molecole (SMs) per identificare SMs che potenzialmente potessero interferire con l'omodimerizzazione di UL44. Dopo tre rounds di screening (HTVS: high-throughput virtual screening, SP: standard precision, XP: extra precision), seguiti da un'analisi delle proprietà chimiche dei composti, sono state selezione 18 SM per ulteriori analisi. I composti selezionati sono stati acquistati presso un fornitore commerciale, per essere testati in diversi saggi per valutare le loro abilità di inibire l'omodimerizzazione di UL44, sia in cellule che in vitro.

A questo scopo, abbiamo utilizzato diversi saggi in cellule e in vitro per monitorare l'effetto delle SMs sulla dimerizzazione di UL44. Nei saggi cellulari, le tecniche utilizzate includono Fluorescent Resonant Energy Transfer (FRET) e Bioluminescence Resonant Energy Transfer (BRET), mentre per saggi in vitro è stato utilizzato il saggio GST-pull down.

I nostri dati indicano che la metodica FRET acceptor photobleaching è in grado di rilevare sia l'omodimerizzazione di UL44, sia il legame con il dominio C-terminale della subunità catalitica (residui 1125-1242). Queste interazioni sono sensibili all'introduzione di mutazioni puntiformi che alterano i due processi, evidenziando la specificità di questa tecnica. Siamo stati quindi in grado di confermare che UL44 forma dimeri in un contesto cellulare. Purtroppo, l'acquisizione dei dati e la loro analisi richiedono un lungo tempo e dipendono da alti livelli di espressione delle proteine di fusione.

Per contro, il saggio BRET permette un rapido e preciso monitoraggio quantitativo dell'omodimerizzazione di UL44 e il legame con UL54 in cellule viventi. Inoltre, attraverso esperimenti di saturazione, che permettono di calcolare in modo preciso i valori di B_{max} e B_{50} relative all'omodimerizzazione o al legame con UL54 per varianti di UL44 che contengono singole sostituzioni amminoacidiche che affliggono la dimerizzazione di UL44, il suo legame a UL54 o il DNA, nonché il trasporto al nucleo della proteina.

I dati ottenuti possono aiutare a comprendere il processo di formazione dell'oloenzima della DNA polimerasi di CMV, suggerendo cambiamenti conformazionali nel complesso olenzimatico in seguito a legame con il DNA. Inoltre, il calcolo di B_{max} e B_{50} è stato usato per sviluppare tre differenti sistemi cellulari esprimenti un'ideale quantità di UL44 da utilizzare come piattaforma per lo screening di SM, poiché sono in grado di generare valori di BRET ratio simili al 50% della B_{max} .Questi includono un sistema di espressione completamente stabile, in cui sia RLuc-UL44 che YFP-UL44 sono stabilmente espresse in cellule derivate da HEK293 A, un sistema ibrido stabile/transiente, in cui YFP-UL44 è stabilmente espressa e RLuc-UL44 è espressa in transiente, o un sistema completamente transiente in cui entrambe le proteine sono espresse transientemente.

Saggi di competizione eseguiti sovra-esprimendo quantità crescenti di UL44 fusa a un FLAG tag hanno evidenziato che nessun inibizione può essere ottenuta per il sistema completamente stabile, probabilmente per la difficoltà di distruggere un complesso proteico preformato piuttosto che prevenirne la formazione. Per questo motive ci siamo focalizzati su sistemi transienti di espressione piuttosto che sul sistema interamente stabile.

Sulla base di questi dati, un primo screening su piccolo scala è stato eseguito per studiare l'effetto di 18 SMs sulla dimerizzazione di UL44 usando il sistema BRET stabile/transiente. Le 18 piccole molecole sono state risospese in DMSO e la loro tossicità è stata valutata in coltura cellulare, prima di essere aggiunte a concentrazioni subtossiche alla linea YFP-UL44, sei ore dopo la trasfezione per

esprimere RLuc-UL44. La nostra analisi ha identificato solo composti che inibivano blandamente il BRET ratio relativo alla dimerizzazione di UL44.

Per questo motivo abbiamo ri-valutato il set up del saggio BRET, diminuendo il tempo d'incubazione delle SM prima di testare i valori BRET da 42 a 18 ore, utilizzando un saggio completamente transiente e diminuendo la quantità di proteine espresse. Per quest'ultima è stato necessario cambiare il substrato utilizzato per generare il segnale bioluminescente da CTZ a hCTZ.

È stato eseguito un nuovo screening, con risultati molto simili a quelli ottenuti utilizzando il setup originale. Inoltre, quando i candidati migliori sono stati rivalutati usando un controllo negativo, il loro effetto sul BRET ratio è risultato aspecifico. Ulteriormente, la BRET, come la FRET, non è riuscita a rilevare uno specifico effetto nell'interazione UL44/UL54 di una SM in grado di distruggere questa interazione. Possiamo quindi concludere che BRET e FRET non sono tecniche ideali per la ricerca di SM inibitrici dell'interazione tra le proteine.

Ci siamo poi focalizzati su metodi in vitro, partendo dal saggio GST-pull down, il quale è stato effettato utilizzando il dominio C-terminale (residui 1-290) di UL44, fuso o con GST o con 6His-tag. I risultati ottenuti mostrano che la tecnica GST-pull down è in grado di rilevare differenze nel legame tra UL44 wild-type e i mutanti con mutazioni nel sito di dimerizzazione, suggerendo una possibile applicazione di GST-pull down per lo screening delle SMs. Questa tecnica è stata implementata per questo studio, e i dati preliminari suggeriscono che il numero di SMs testate potrebbe portare all'inibizione della dimerizzazione di UL44.

In conclusione, abbiamo sviluppato diversi saggi per monitorare la dimerizzazione di UL44. I saggi cellulari basati su RET confermano che UL44 forma dimeri in cellule viventi, e dimostrano di essere subottimali per lo screening. D'altro canto, i metodi in vitro come GST-pull down dimostrerebbero un maggiore sensibilità e sono stati implementati per l'identificazione degli inibitori della dimerizzazione di UL44.

4. INTRODUCTION

1.1 Human Cytomegalovirus (HCMV)

Human Cytomegalovirus (HCMV), also known as Human Herpesvirus-5 (HHV-5), is a member of the *Herpesviridae* family, subfamily *Betaherpesvirinae*. CMVs from other mammals also belong to this subfamily. HCMV is a species-specific ubiquitous virus which only rarely causes diseases in immunocompetent individuals, but it is responsible for a variety of pathologies in immunocompromised patients. It is also one of the major causes of congenital defects in newborns.

The name Cytomegalovirus derives from the fact that the virus causes enlargement of the infected cells (cytomegaly), inducing the formation of inclusion bodies in the nucleus and in the cytoplasm containing neo-formed viruses and lysosomes. HCMV shares several characteristics with the others Herpesviridae members, such as viral particle and genome structure, the ability to induce acute infections associated with a highly productive lytic cycle, persistent infections with low replicative levels, or latent infections without production of viral particles [1]. In addition to infectious virions, HCMV infected cell cultures also produce the Non-Infective Enveloped Particles (NIEPS) and the Dense Bodies (DB). The NIEPS differ from the infective virions because they lack the viral genome; the DB, instead, are completely devoid of both capsid and genome [2]. The relative presence of the three forms depends on the cell culture passages and on the viral strain [3].

1.2 Epidemiology and Pathogenesis

HCMV is a ubiquitous pathogen that causes a variety of diseases both in adults and children. It is widespread in the population, 50-90% of adults being seropositive worldwide. The seroprevalence depends on socio-economic factors and on the geographic area [4].

HCMV comes in contact with the body through mucous membranes or parenterally (blood, or stem cell, organ transplants) and can lead to general infection with involvement of the whole organism, causing a wide range of symptoms such as encephalitis, retinitis, hepatitis and splenomegaly. The transmission can be vertical or horizontal. The frequency of vertical transmission the is of about 0.5-1%, and can occur either transplacentally from the mother to the foetus/child, or via cervical/vaginal secretions as wells as via breast milk. Vertically transmitted CMV infections represent the major cause of congenital defects in newborns. The horizontal ways, instead, are sexual or oral transmission, trough urine or after organs or hematopoietic stem cells transplant [5]. In immunocompetent individuals, most HCMV infections are asymptomatic, even though the levels of viremia are very high. After the primary infection, which is usually followed by a 4-8 weeks viremic incubation period, the virus remains latent in the host lifelong in blood cells or bone marrow (involving monocytes, macrophages and dendritic cells), and it reactivates periodically when the immunity system control fails [6]. Only rarely HCMV infections display minor symptoms similar to that of mononucleosis [7]. However, there are four cases in which HCMV can cause dangerous consequences: in congenital primary infection and in immunocompromised individuals; in primary infection; in reinfection; in reactivation. Congenital infections can be asymptomatic or symptomatic, and in both cases they can lead to serious consequences. In fact, in 10-17% cases of asymptomatic infections there can be neuronal or hearing impairment; in 5-10% of cases instead, the infection is symptomatic and causes the classic HCMV symptoms such as encephalitis, hearing loss, motor deficits, and rarely myopathies and retinitis. In immunocompromised patients, such as transplanted individuals, or HIV infected people, consequences are more serious with the risk of transplant reject, pneumonia, retinitis and finally death [8].

1.3 HCMV structure

HCMV viral particle is composed by a host cell membranes-derived viral envelope, in which several glycoproteins are embedded, an icosahedral nucleocapsid and, between them, the so called tegument which is a phosphoprotein layer [9] (Figure 1.1).

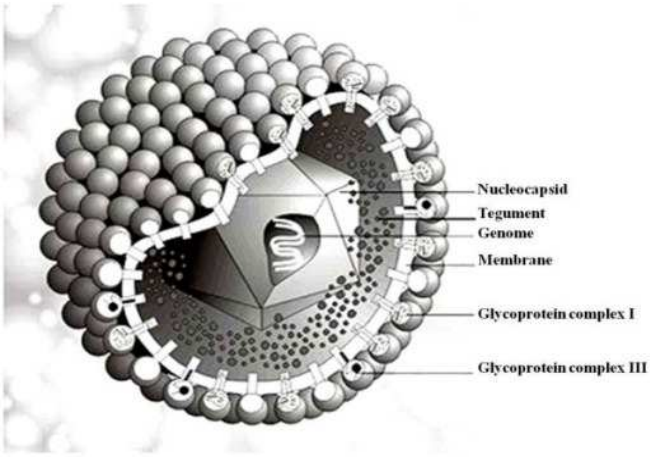

Figure 1.1: HCMV viral particle structure. From: http://www.virology.net/big_virology/bvdnaherpes.html website.

The viral capsid is made up of 162 capsomers subdivided into 12 pentons and 150 exons which are composed by four main proteins: UL86 (major capsid protein), UL48-49, UL85 (minor capsid protein), and UL46 (minor capsid binding protein). The envelope contains six viral encoded glycoproteins, which are essential for the virus entry into the host cell, cell-to-cell diffusion as well as for virus maturation: gpUL55 (gB), gpUL73 (gN), gpUL74 (gO), gpUL75 (gH), gpUL100 (gM), and gpUL115 (gL). The tegument contains the majority of viral proteins, most of which are phosphorylated and able to interact with the cytoplasmatic portions of envelope and capsid proteins, thus bridging the two viral elements [10]. When the virus is released into the cytoplasm, the tegument proteins become functionally active and play an important role in all the phases of the viral cycle, including virus entry, gene expression, evasion from the host immune response, assembly, maturation and release [11]. Many tegument proteins are of particular interest for the role

they play in the HCMV replication cycle. The most abundant of them are pp150 (ppUL32, or basic phosphoprotein), and pp65, which is used as target for rapid diagnosis test of infection.

1.4 Genome structure

HCMV is a double stranded non segmented DNA virus with a very large linear genome of about 235kbp. HCMV genome is the largest among the Herpesviruses and with the highest amount of G-C content. Its genome can be divided into two main regions: a unique long (UL), and a unique short (US), which are flanked by terminal (TRL and TRS) and internal (IRL and IRS) inverted repeats (Figure 1.2). UL and US can be orientated in both directions, so the viral progeny can present any of the four possible isomers of the genome. In the terminal part of the genome and in the junction between the UL and US, there is a direct repeated sequence, responsible for the inversion of the two regions, and, through cis elements called pac-1 and pac-2, for the cleavage and packaging of theDNA [12].

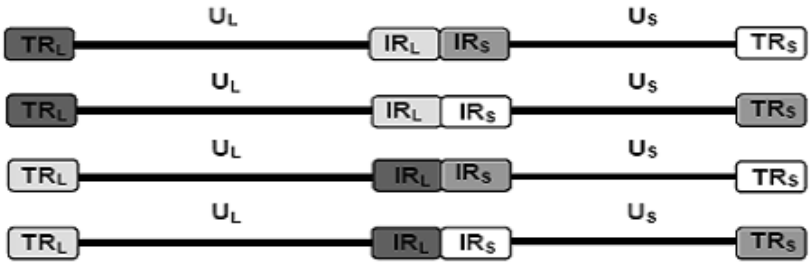

Figure 1.2 The 4 isomers of the HCMV genome with the UL region and US region flanked by terminal and internal repeats. From: [11].

HCMV genome contains a large number of protein coding genes, whose transcription is driven by a series of ORFs (Open Reading Frames) named by the region and numerical order in which they occur [13]. The gene products of more than 40 ORFs are very similar to proteins encoded by α- and γ-herpesviruses [14], and of these ORFs, c. 25% encode for functions relative to metabolism and replication of the viral DNA, while c. 75% are involved in maturation and structural organization of

virions. The products of more than 50 ORFs, instead, are not essential for a productive viral replication, and the function of many ORFs has not been characterized yet. In addition to the coding genes there are also polyadenylated non-coding RNAs (some in antisense with respect to protein coding regions, and some which do not overlap with them) and non-polyadenylated RNAs such as micro-RNAS [13].

1.5 Genome expression

Expression of HCMV genome starts within one hour post infection (pi), without protein synthesis, from the viral origin oriLyt. There is an initial circularization of the genome within four hours pi, followed by the synthesis of the DNA with a bidirectional θ mechanism from the oriLyt [15]. The viral genome is synthetized by a virally-encoded DNA polymerase via a rolling circle mechanism, producing concatamers which are then cleaved in monomers ready to be packed in the viral capsids. The dsDNA is transcribed by the host RNA polymerase II, but numerous viral proteins are also involved in every step of the infection. Transcription and synthesis of gene products is strictly regulated both transcriptionally and post-transcriptionally. During productive infection, the replication of the virus occurs in the nucleus in a temporally ordered manner: in fact, as soon as the virus enters the host nucleus through the nuclear pores, there is first the expression of the immediate early (IE) genes, which are transcriptional regulators necessary for the transcription of the early genes (E). The early genes, the second class of genes, are instead involved in DNA replication. Once replication begins, the third class of genes, the late genes [15] are transcribed to produce mainly structural and assembly proteins. Some genes can be assigned to more than one temporal class.

HCMV genome replication is a complex process requiring the activity of several proteins endowed with different enzymatic activities. Pioneeristic studies demonstrated that 11 viral genomic loci are

required to transcomplement oriLyt dependent DNA replication in transient transfection based assays [16]. Six of them encode for replication fork proteins, as identified by similarity to homologous proteins in Herpes Simplex Virus type 1 (HSV-1). Such proteins are the DNA polymerase catalytic subunit UL54 and its processivity factor UL44, ssDNA binding protein UL57 as well as heterotrimeric a trimeric helicase-primase complex, whose function is to unwind dsDNA and synthesize a RNA primer. composed by the helicase UL105, the primase and a cofactor UL102. During viral DNA replication, the trimeric helicase-primase complex unwinds dsDNA and synthesize RNA primers [17]. Subsequently, UL57 binds and stabilizes the ssDNA strand released by the helicase primase complex, while the DNA polymerase holoenzyme mediated DNA synthesis. The remaining five loci do not have obvious homologous proteins in other herpesviruses. Such loci comprise three immediate early (IE) regulatory regions such as UL122-123, UL36-38 and Internal Repeated Sequence 1/Terminal Repeated Sequence 1 (IRS1/TRS1), as well as two early (E) proteins such as UL112-113 and UL84.

The UL122-123 regions are localized under the control of the extremely strong Major Immediate Early (MIE) promoter/enhancer, containing several binding sites for cellular transcription factors (TFs). It primarily encodes the IE-72 and IE86 proteins, which are the main viral trans-activators, driving the expression of several cellular and viral genes. The UL36-38 region generates several different transcripts, based on the activation of different promoters and the use of a number of splicing sites [18]. Such genes encode for a number of proteins endowed with anti-apoptotic function such as viral Inhibitor of Caspase-8-Induced Apoptosis (vICA), encoded by UL36, a protein able to bind to pro-caspase 8 preventing its auto-proteolytic activation, and subsequently Fas-binding and apoptosis [19]. UL37 encodes proteins gpUL37 e pUL37x1 (pUL37exon1). gpUL37 is a glycoprotein also known as viral Mitochondria-localized Inhibitor of Apoptosis, (vMIA), which inhibits Fas-mediated apoptosis by localizing to mitochondria and preventing cytochrome c release. pUL37x1, prevents cytochrome c release by interacting with mitochondrial

Adenosine Nucleoside Transporter (ANT) [20]. Also the UL38 gene product encodes an anti-apoptotic factor blocking caspase-mediated apoptosis [21].

The two highly homologous proteins IRS1/TRS1 cooperate with other IE proteins in viral mediated transactivation of viral and cellular promoters [22].: for example, they can activate expression of ß genes together with IE1-72 and IE2-86 and increase the activity of the MIE promoter cooperating with UL69 [22].

Genes UL112-113 can generate four different phosphoproteins as a consequence of alterative splicing events. Such proteins have different molecular weights (34, 43, 50 e 84 kDa), and are differently expressed and localized at different stages of the viral life cycle. Such proteins bind to dsDNA and recruit UL44 to replication sites [23, 24]. Furthermore, the 84 kDa protein appears to regulate nuclear transport of the other UL112-113 proteins [25].

Finally, the UL84 protein is a nucleocytoplasmic shuttling protein, with structural and functional homology to DExD/H box helicases, a family of nucleocytoplasmic shuttling RNA helicases with transcriptional regulation activities [26]. Indeed, UL84 a multitasking factor which shuttles between the nucleus and the cytoplasm, it is endowed with transcriptional regulation abilities and it is the proposed origin binding protein. Its transcriptional properties are exemplified by its ability to bind IE2, inhibiting its activity, while such complex activates a bidirectional promoter present at the oriLyt, most likely starting the replication process. UL84 is also capable of binding RNA and possess UTPase activity [27-30]. Its role as origin binding protein is supported by the interaction in vivo with HCMV oriLyt, in a region containing RNA/DNA hybrid structures and stem-loops, with in vitro studies suggesting it can change the structure of such stem loop structures possibly priming the assembly of the replication complex [31]. Furthermore, UL84 is able to bind both UL44 and UL57 [27M, 32].

1.6 Herpetic DNA polymerase holoenzyme general characteristics

All known *Herpesviridae* members encode their own DNA polymerase holoenzymes, essential for viral DNA replication. Sequence alignments shown that all herpetic DNA polymerases have conserved structures and functional domains. Furthermore, such polymerases are composed by two distinct subunits, a catalytic and an accessory protein, whose physical interaction is essential for replication of viral DNA (Table 1.1).

Virus	Catalytic Subunit	Accessory Subunit	Reference
HSV-1	UL30	UL42	[33]
HSV-2	POL	ICSP34, 35	[34]
VZV	POL	ORF16	[35]
HCMV	UL54	UL44	[36]
HHV-6	Pol6	p41	[37]
HHV-7	U38	U27	[38]
HHV-8	Pol-8	PF-8	[39]

Table 1.1: Human *Herpesvridae* members DNA holoenzyme subunits.

For all known *Herpesviridae* members, the catalytic subunit is of the DNA Polymerase holoenzyme is a large protein (110-140 kDa), constituted by six conserved functional domains: a pre Nh2 domain, with 6 highly conserved residues, most likely involved in the interaction with the helicase/primase complex; a NH2 domain, probably endowed with RNA binding ability and hypothesized to be involved in RNAse activity; a domain possessing 3'-5' esonuclease activity; a palm domain involved in catalytic activity; a fingers domain responsible for nucleotide binding; a thumb domain, binding dsDNA. Such catalytic subunit thus possesses a 5'-3' DNA polymerase activity, being able to extend DNA templates as well as RNA primers. It also possesses an intrinsic 3'-5' proofreading a activity as well as 3'-5' and 5'-3' esonuclease activities. However, the catalytic DNA polymerase has a much lower activity as compared to the holoenzyme (therefore defined basal activity). Binding to the smaller accessory subunit, results in increased holoenzyme DNA polymerase and DNA binding activities, as well as in higher nucleotides incorporation rates and processivity, thus making the holoenzyme capable of replicating the entire viral genome. The essential role of the association between the two subunits has been proved by the fact that mutations impairing such intermolecular association also prevent viral replication [40, 41].

The current biochemical model, universally accepted for all known *Herpesviridae* DNA polymerase holoenzymes, is mainly based on studies on the HSV-1 holoenzyme, formed by the catalytic subunit UL30 and the processivity factor UL42. UL42 is known to be able to simultaneously bind to dsDNA and UL30 using different protein domains, thus tethering it to dsDNA [40, 41].

1.7 HCMV DNA Polymerase Catalytic subunit

DNA polymerases are classified in seven different families. Herpetic DNA polymerases belong to the B family. Such family comprises several viral and cellular DNA polymerases, all containing 7 conserved regions, designed I, II, III, IV, V, VI and VII. Such regions play an important role in enzyme catalytic activity. Regions I to V, along with an additional region called region C, shared by all *Herpesviridae* DNA polymerase catalytic subunits, are involved in binding to substrates and antiviral nucleoside analogs. The N-terminal domain possesses RNAse H activity and interacts with several viral proteins, while the intrinsic exonuclease 3'-5' activity has been mapped to region IV and the C region [42]. In the catalytic site, three highly conserved regions (Exo I, II and III) possess 5'-3' exonuclease activity.

The most conserve region is the one N-terminally located, with regions I, II and III being extremely conserved in all known DNA polymerases (from bacteriophages to mammals), thus suggesting they could fulfil all catalytic functions. Region I in involved in substrate recognition, including dNTPs and PPi, since several mutants mapping in this region exhibit resistance to nucleoside and pirophospahte analogues, or affect its catalytic activity. Furthermore, several mutations affecting sensibility to nucleoside or pirophoasphate analogues map to regions II and II suggesting a direct role in dNTPs binding and pirophospahte hydrolysis [43]. Finally, regions V and VII are less conserved and characterized, and their role has still to be defined. In The HCMV DNA polymerase is called UL54 and it is a 140 kDa protein of 1242 amino acids. Regions I to VII are located within residues 379-1100 [44], so that the catalytic core is located in the central part of the protein. On the other hand, the N-terminal part of the protein contains the three regions (Exo I, II, III) responsible for the 5' -3' exonuclease activity [45], while the C-terminal domain is responsible for binding to UL44 and nuclear transport of the protein. Indeed, UL54 C-terminal 22 residues are necessary and sufficient to mediate binding to its accessory subunit UL44 [46]. In addition, UL54 C-terminal domain contains two NLSs. The first to be discovered was an atypical, poorly characterized

hydrophobic NLS (hNLS), which lies within the protein UL44 binding domain (PRRLHL-1127), and thus appears to be active only when UL54 is not associated with UL44 [46, 47]. UL54 also contains a classical NLS (cNLS), located upstream of the UL44 binding domain (PAKKRAR-1159). Such NLS is active also when UL54 is in complex with UL44 and confers energy- and Ran-dependent nuclear targeting to reporter proteins, as well as recognition by the IMPα/β heterodimer through direct interaction with IMPα [48, 49].

1.8 HCMV DNA polymerase accessory subunit UL44

HCMV DNA polymerase accessory subunit, UL44 is a 52 kDa phosphoprotein essential for HCMV genome replication [50]. UL44 has been shown dimerize, thus being able to bind to dsDNA in the absence of clamp loaders and ATP, and to directly interact with UL54, thus stimulating its holoenzyme activity [17, 51]. UL44 can be functionally and structurally divided in a N-terminal domain (residues 1-290), and a C-terminal domain (residues 291-433). The N-terminal domain retains all known UL44 biochemical properties, including the ability to bind to dsDNA and UL54 and to stimulate to latter activity [51]. The C-terminal domain is largely unstructured, containing five stretches of glycine which confer extreme flexibility. Its main function described so far appears that of regulating the nuclear import process of UL44 thanks to a C-terminally located NLS A functional cNLS (PNTKKQK-431) is located at the very C terminus of the protein, driving the protein into the nucleus upon binding to IMPα/β binding [52]. In addition, UL44 C-terminus (residues 409-433) is the target of extensive post-translational modifications. These include multiple phosphorylation sites (S413, S415, S418 and T42T) and a sumoylation site (K410), which regulate UL44 subcellular localization by controlling its ability to interact with host cell proteins [48, 52-55], although the exact role of UL44 sumoylation is still unknown [54]. UL44 N-terminal portion (residues 1-290) has been recently crystallized [56]. UL44 forms heat to head dimers, and

each monomer shares a very similar structure to that of other processivity factors such as proliferating nuclear antigen (PCNA) monomers, and the monomeric HSV-1 UL42 (Figure 1.3), despite lacking high sequence homology [57, 58].

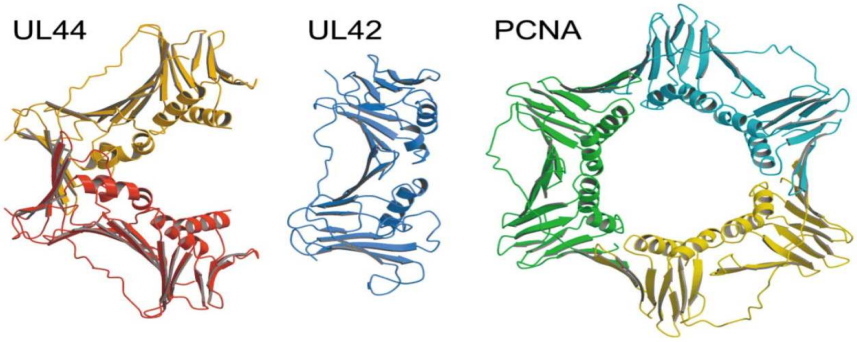

Figure 1.3 Comparison of the UL44 dimer, the UL42 monomer, and the PCNA trimer. Adapted from [59].

Each monomer forms two topologically similar domains. They share a central β-sheet and are connected by a long connector loop running along the front face of the molecule which is important for binding to other protein partners, including UL54 [59] (Figure 1.4).

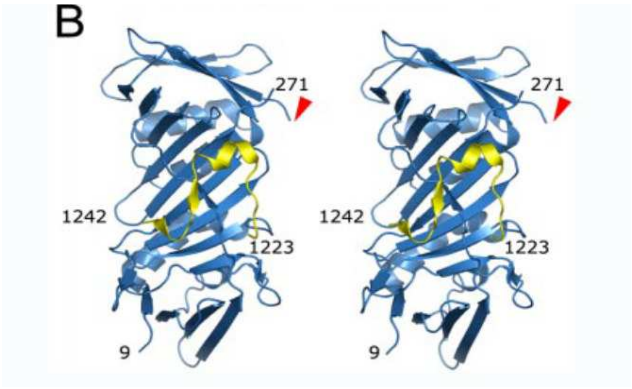

Figure 1.4: Representation of the UL44-UL54 complex (blue and yellow, respectively). From: [59].

The back face of UL44 is flanked by four helices and is rich in basic residues involved in DNA binding [60]. Dimerization relies on the interaction between the two most N-terminal B-sheets of each monomer, with six main chain hydrogen bonds formed. The interaction involves also extensive packing of hydrophobic side chains at the interface, with F121, M123 and L93 of each

monomer is being packed against L86 and L87 of the opposite monomer (Figure 1.5).

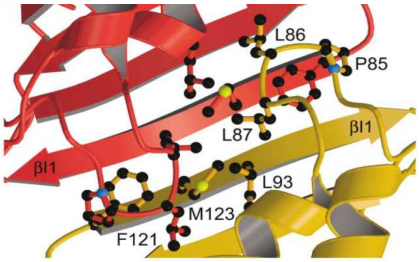

Figure 1.5. Structural representation of UL44 dimerization interface with crucial residues depicted in ball and stick. Adapted from [59].

Intriguingly, dimerization appears a prerequisite for DNA binding by UL44. Upon dimerization, the basic face of each monomer contributes to the formation of a positively charged central cavity which is involved in DNA binding via electrostatic interaction [60]. Accordingly, point mutations impairing dimerization – such as the L86A/L87A double mutant, strongly impair binding to dsDNA. Also the F121A mutant is impaired for DNA binding although to a lesser extent as compared to the L86A/L87A double mutant, and it has been speculated that it could possess weak DNA binding upon dimerization. Importantly, the L86A/L87A double substitution prevented viral DNA replication as shown by the failure of such mutants to sustain *ori*Lyt dependent DNA replication in transient trans-complementation assays, suggesting that UL44 homodimerization is essential for viral genome replication [61]. Therefore, UL44 dimerization can be considered a potential target of therapeutic intervention to interfere with HCMV replication.

Furthermore, each UL44 monomer possesses a basic face containing several basic lysine residues which, upon dimerization, forma a basic cavity binding to dsDNA via electrostatic interactions. In

addition, each UL44 monomer has a 13 aa long flexible loop (FL), not visible in the electron density map [PHTRVKRNVKKAP-172], which has been modelled as protruding towards the back face and potentially contacting dsDNA. In vitro modelling and mutagenic studies have shown that basic residues within the back face and the FL of UL44 are important for DNA binding: their substitution to alanine strongly impaired DNA binding [60]. The importance of UL44-FL in cells has been recently demonstrated by our research group in cells: substitution of UL44-FL basic residues with hydrophobic ones impaired DNA binding, and its ability to form nuclear speckles, simultaneously increasing its intranuclear mobility upon transfection in Mammalian cells. Such mutation also abolished HCMV *ori*Lyt-dependent DNA replication in transient transcomplementation assays, implying that the UL44-FL is important for DNA binding during viral replication [62]. Furthermore, overexpression of such UL44 mutant (called UL44Dloop) in the presence of wild-type UL44, abolished HCMV oriLyt-dependent DNA replication in transient transcomplementation assays, suggesting a transdominant negative phenotype [62]. Indeed, transient relocalization assays suggested that UL44Dloop could still interact both with UL54 and to interact with UL44, implying that the formation of DNA defective UL54/UL44 and UL44/UL44 complexes could be detrimental for viral replication [62].

1.9 UL54 and UL44 mutants used in this study

Point mutations (substitutions) in UL44 are known to affect several UL44 biochemical properties such as the interaction between UL44-UL44 homodimers, the formation of UL54-UL44 complex, as well as its ability to bind dsDNA and were used in different combination in this study, as expressed from a variety of Mammalian expression plasmids (see Appendix §6.4).

In particular, UL44-F121A and UL44-L86/L87A mutants possess amino acid substitutions that interfere with the dimerization of UL44, without affecting binding to UL54 neither in vitro nor in

living cells [49, 61]. Importantly such mutants exhibit reduced DNA binding ability in filter binding assays [56], and are not compatible with viral DNA replication in *ori*Lyt replication assays, suggesting that UL44 homodimerization is essential for viral life cycle [61]. The UL44-I135A mutant, instead, has an amino acid substitution in the connector loop of UL44. Such mutation does not affect UL44 DNA binding ability or dimerization ability [56, 61] but completely disrupts the UL54-UL44 interaction preventing DNA replication [62]. On the other hand, UL44Δloop, containing hydrophobic substitutions in place of basic residues within UL44-FL (see above), retains the ability to dimerize and bind to UL54 in cells but is defective for DNA binding, as shown by cellular subfractionating experiments and by subcellular localization assays [62]. Such mutant, intriguingly, does not support HCMV oriLyt-dependent HCMV DNA replication, where it behaves as a trans-dominant-negative mutant [62]. Finally, the UL44DNLS mutant bears point mutations within UL44-NLS (PNTKKQK-431), impairing its nuclear localization, without affecting its ability to bind to UL54 and self-interact [48, 52].

1.10 Currently available HCMV antivirals

The treatment against HCMV infections could be prophylactic or preventive.

The prophylactic treatment starts immediately after an organ or stem cells transplant and continues for the next 90-100 days to prevent the appearance of the virus [63]. Even though the prophylactic therapy doesn't exclude the possibility of infections, without it 20-30% of transplanted patients are infected in the subsequent 90 days post transplantation.

The preventive treatment, instead, starts when in asymptomatic patients is diagnosed the presence of the virus, also at very low levels (sign of primary infection or viral reactivation). Antivirals are administered to prevent the progression of the asymptomatic viremia.

Currently available antivirals utilized for the therapy against HCMV infection, have a series of contraindications due to their high cost, low bioavailability, high toxicity and the uprising of resistant viral strains. Indeed, several viral strains have developed resistance or cross-resistance to them causing serious issues, especially to immunodeficient patients [64].

The majority of the antiviral drugs are analogues of the DNA polymerase substrates, nucleoside or pyrophosphate analogues, because, being the herpetic DNA polymerases essential for the replication of the genome, it is a good target for antivirals. HCMV encodes for a protein kinase (UL97) able to monophosphorylate nucleosidic analogues, which are then di- and tri-phosphorylated by cellular kinases. The polyphosphorylated form acts as inhibitor of the HCMV DNA polymerase hindering the synthesis of the viral genome.

Ganciclovir (GCV) was the first antiviral approved for the treatment of HCMV infections and nowadays is the most commonly administered drug against HCMV [65]. It is a guanosine analogue, it requires the UL97-mediated phosphorylation to become active and causes the termination of the nascent viral DNA. GCV is available for intravenous or intraocular use.

Valganciclovir (VGCV) is the L-valyl ester of GCV, it is a prodrug which has a higher bioavailability (60%) and it is rapidly metabolized to the active form (GCV).

Cidofivir (CDV) is a nucleosidic analogue of dCMP, which becomes active after the tri-phosphorylation by cellular kinases. Similarly to GCV, it causes the termination of the DNA chain synthesis, acting as a competitive inhibitor of the viral DNA polymerase, not only of herpesviruses but also of other viruses. Despite its wide range of action, CDV has a very low bioavailability and it is highly toxic for kidneys. Foscarnet (FOS) is a non-nucleosidic inhibitor of herpetic DNA polymerases which acts blocking the release of pyrophosphate by the polymerase. It is mainly administered to patients resistant to GCV. Fomivirsen is a synthetic 21-mer phosphorothioate oligonucleotide which binds to the viral mRNA encoding the IE2 protein preventing its translation.

It is used in the treatment of cytomegalovirus retinitis (CMV) in immunocompromised patients, including those with AIDS. Currently, no drugs are approved for the treatment of infected pregnant women. Such issues stimulated the research of more active, specific and less toxic new compounds against HCMV. To this end, one possible strategy is hinder viral replication by dissociating viral protein-protein complexes can either be achieved via small molecules or peptidomimetic compounds mimicking one of the partners involved in the interaction between the subunits of the complex [66, 67]. A potential target for this inhibition of HCMV replication with this strategy is represented UL44 homodimerization. In fact, as mentioned previously, it was demonstrated that mutations of residues involved in UL44 homodimerization, reduce also its ability to bind dsDNA and so to support HCMV DNA replication [61].

1.11 Protein-protein interaction (PPI) as druggable targets in human disease

The importance of the complex network of direct interactions between proteins in both cellular physiology and development of disease is widely recognized. Despite this, small-molecule drugs that act by directly disrupting the interaction between two proteins are relatively rare and PPIs are viewed as challenging targets [68].

Inhibitors of protein–protein interactions have several potential advantages with respect to other kind of drugs. First of all, the extreme specificity of partner interactions offers the possibility of interfering with them in a highly selective fashion, making them attractive targets. Additionally, inhibitors of PPI could be less prone to drug resistance than are inhibitors that bind enzymes active site. This is especially important when considering viral enzymes, which are particularly prone to mutation. In fact, a single mutation in one subunit of protein-protein interfaces requires a complementary mutation in the other subunit to maintain the complex intact, making this event less

likely when compared to the probability of a single mutation on the catalytic site, which is often sufficient to confer drug resistance [67].

The first example in literature of successful disruption of protein–protein interactions regards an enzyme, the ribonucleotide reductase (RR) of herpes simplex virus type 1 (HSV-1) [69]. The results obtained with HSV-1 RR inhibitors encouraged further efforts in this direction. Screening of small molecules libraries bring to the identification of an inhibitor of the interaction between HSV-1 catalytic subunit (UL30) and accessory protein (UL42) leading to the inhibition of viral replication [70]. Other examples of successfully disrupted viral PPI include peptides and small molecules targeting dimerization of HIV protease, reverse transcriptase, or integrase, as well as small molecules targeting the Influenza A virus RNA polymerase PB1 and PA subunits. Notably, a high throughput screening approach recently identified AL18, a small molecule capable of interfering with the UL54-UL44 interaction, thus inhibiting HCMV replication in cells in the low micromolar range. This small molecule is able to inhibit in a dose dependent manner the of UL54-UL44 interaction, with an IC50 of 9-30 μM (as assessed by ELISA or fluorescence polarization assays, respectively), and with a selectivity index above 100 (as defined by the ratio between the CC50 - compound concentration causing death in 50% of cells, and the ED50, compound concentration causing a reduction of 50% in viral replication) [71].

1.12 Virtual screening of SMs potentially disrupting the UL44 homodimerization

Based on these observations, our research group recently performed a structure-based virtual screening of commercially available databases, with the aim of identifying small molecule inhibitors of the HCMV UL44 homodimerization (Federico Falchi, Unpublished). The Glide software (Schrödinger, NY, USA) was employed to dock molecules to the interface of the two

monomers. Three rounds of screening by docking were performed using the High throughput virtual screening (HTVS), Standard Precision (SP) and Extra Precision (XP) docking settings. After each docking round only the top-ranked molecules in term of docking score were selected for the following round. The resulting 500 molecules were further reduced by visual inspection, cluster analysis and on the basis of their commercial availability, 18 compounds were purchased and tested for their ability to disrupt UL44 dimerization (see Figure 1.6).

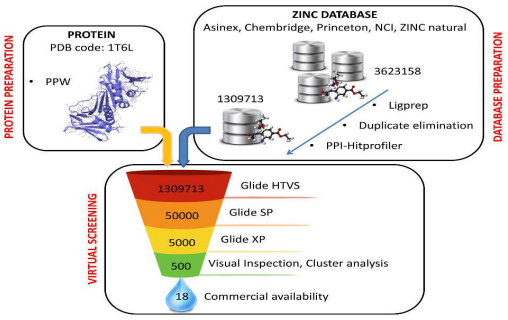

Figure 1.6. Use of Virtual screening to identify SMs potentially interfering with UL44 homodimerization. Falchi et al., unpublished.

1.13 Methods to detect protein-protein interaction (PPI)

Biological systems are made up of very large numbers of different components interacting at various scales. Most genes, proteins and other cell components carry out their functions within a complex network of interactions, and protein–protein interactions (PPIs) are crucial events of virtually all cellular processes. The investigation of these PPIs is essential for the comprehension of how gene functions and regulations are integrated within an organism [72]. PPIs are conceived as physical contacts with molecular docking between proteins that occur in a cell or in a living organism *in vivo*. Therefore, the interaction interface should be intentional and not accidental, and should be non-generic but evolved for a specific purpose. PPIs can be characterized as stable or transient and both can be either strong or weak. The investigation of these PPIs requires different

experimental techniques designed to characterize protein complexes and PPI network. There are two main approaches for the investigation: *in vitro* methods and *in* cells methods. *In vitro* methods comprise a broad range of techniques adopted for both interaction discovery and confirmation. These methods rely on the natural affinity of binding partners for each other (see Table 1.2).

In vitro *method*	***Description***
Co-immunoprecipitation	An immunoprecipitation (IP) experiment designed to affinity-purify a bait protein antigen together with its binding partner using a specific antibody against the bait.
Pull-down Assays	An affinity chromatography method that involves using a tagged or labelled bait to create a specific affinity matrix that will enable binding and purification of a prey protein from a lysate sample or other protein-containing mixture.
Crosslinking Reagents	Strategies involve chemical crosslinking which may or may not be reversed. Nearest neighbours (suspected to interact) *in vivo* or *in vitro* can be trapped in their complexes for further study.
Protein Interaction Mapping	Uses an "artificial protease" on a bait protein to initiate contact-dependent cleavages in the prey protein in the presence of specific reactants. contact sites or interface of a known protein-protein interaction.
Surface Plasmon Resonance	Relates binding information to small changes in refractive indices of laser light reflected from gold surfaces to which a bait protein has been attached.
Mass Spectroscopy	Used in concert with affinity-based methods (such as co-IPs) to isolate binding partners and complexes and to identify the component proteins using standard mass spectral methods.

Table 1.2. *In cells* methods for PPIs analysis [Thermo Scientific Pierce Protein Interaction Technical Handbook. Version 2, Thermo Scientific, 2010].

In cells methods, instead, are a more restricted number and can be found listed in the Table 1.3 below.

In cells method	Description
Yeast Two-Hybrid System	Monitor complex formation through transcriptional activation of reporter genes.
Crosslinking Reagents	Incorporating functional groups into proteins which can react, trapping a protein complex.
Immunofluorescence/FRET/BRET	Detect co-localized signal from two different proteins or monitor complex formation thought fluorescent/bioluminescent resonance energy transfer.
Proximity Ligation Assay	Two primary antibodies recognize the target antigens of interest. Secondary antibodies (PLA), each with a unique short DNA strand attached, bind to the primary antibodies. When the PLA probes are in close proximity, the DNA strands can interact forming DNA oligonucleotides. After their joining, oligonucleotides are amplified using a polymerase, and labelled complementary oligonucleotide probes highlight the product.
Biomolecular Fluorescence Complementation (BiFC)	Based on the association of fluorescent protein fragments that are attached to components of the same macromolecular complex.

Table 1.3: In cells methods for PPIs analysis [Thermo Scientific Pierce Protein Interaction Technical Handbook. Version 2, Thermo Scientific, 2010].

Each method has its own advantages and disadvantages. In vitro methods allow great sensitivity, but often rely on the use of non-physiological systems, such as bacterial cells, to produce proteins to a large extent, so that their conformation might result different from what expected. Furthermore, in vitro methods, detect interactions occurring outside their physiological context, i.e. the cell. On the other hand, in cells methods, overcome these issues. The proteins of interest are directly expressed

in their preferred cell type, and localization is readily detectable. However, such methods, are more limited, offer reduced flexibility, and are less sensitive as compared to *in vitro* ones.

1.14 Fluorescent Resonant Energy Transfer (FRET)

Fluorescent Resonant Energy Transfer (FRET) is a nanotechnology able to give information on PPIs. FRET technique is based on the energy transfer between two fluorophores called donor and acceptor. The energy transfer is possible only when the donor fluorophore, once excited at an appropriate wavelength, transfers part of its energy to the acceptor fluorophore by means of a dipole-dipole interaction. To this end, it is necessary that donor and acceptor fluorophores are located within 10 nm. Another necessary condition to have a FRET signal is that the emission spectrum of the donor has a sufficient overlap with the excitation spectrum of the acceptor. In this study the two fluorophores used were two proteins derived from the GFP (Green Fluorescent Protein): CFP (Cyan Fluorescent Protein) as donor, and YFP (Yellow Fluorescent Protein) as acceptor. To evaluate the interaction between two proteins, donor (CFP), and acceptor (YFP), are fused to the proteins of interest, and the fusion proteins are expressed in cells. If the two proteins of interest interact, donor and acceptor will be in close proximity to generate an energy transfer and so a FRET signal. One of the most common methods to measure FRET efficiency, is the Acceptor Photobleaching. The basic principle of this technique, is that the energy transferred from the donor to the acceptor will be reduced, or eliminated, if the acceptor is bleached by laser excitation at maximum power for an opportune time. FRET efficiency is calculated on the bases of donor fluorescence intensity variations pre- and post-bleaching of the acceptor, using the following equation:

$$FRET\ efficiency\ \% = \frac{Dpost - Dpre}{Dpost} \times 100$$

Where Dpost is the donor fluorescence intensity post-bleaching, and Dpre the donor fluorescence intensity pre-bleaching. FRET is an in cell method to detect PPIs, usually *ex vivo* but can be also performed *in vivo* with the use of more sophisticated confocal scanning microscopes. It also allows to detected the cellular compartment were the interaction take place. However, it requires complex setup for data acquisition and processing, which cannot easily be automated for high throughput screening without sophisticated apparatuses.

1.15 Bioluminescent Resonant Energy Transfer (BRET)

Bioluminescence Resonance Energy Transfer (BRET), is a nonradioactive resonance energy transfer occurring between a light-emitting bioluminescent donor and an acceptor fluorescent protein, whose emission and excitation spectra significantly overlap. As for FRET, when donor and acceptor are brought into close proximity (1-10 nm), and are properly oriented each other, the donor can transfer energy to the acceptor, which then emits light at a specific wavelength. Since light emission from the donor takes place at a different wavelength than that from the acceptor, the energy transfer can be easily detected by measuring the ratio of the acceptor to the donor emission intensities. Such output allows to compensate for well-to-well aspecific signal variations (e.g., due to different cell numbers in each well or signal decay across the plate). Because BRET strictly depends on the molecular proximity between donor and acceptor, it is suitable for monitoring the activation state of any protein (e.g., receptor or transcription factor) that undergoes association or conformational changes. A strong advantage of BRET assays over other *in vivo* methods such as FRET and BiFC (Figure 1.7) is the fact that is easily scalable to multiwell plate formats. This phenomenon can either be observed *in vitro*, using purified proteins, or directly within the cells where the fusion proteins were produced. Differently from FRET, BRET does not require a light source, therefore it is not affected by photobleaching, light scattering or autofluorescence and direct

excitation of the acceptor cannot take place. The intrinsic low background of BRET allows either detection of weak interactions and performing experiments with low concentrated proteins. BRET is also able to analyze millions of cells in a very short time, making possible the analysis of multiple samples simultaneously.

Usually, detection of protein-protein interactions by BRET, requires fusion of one of the protein of interest to a donor protein and of its binding partner to an acceptor protein. The most commonly used donor and acceptor proteins are Renilla Luciferase (RLuc) and Yellow Fluorescent Protein (YFP),

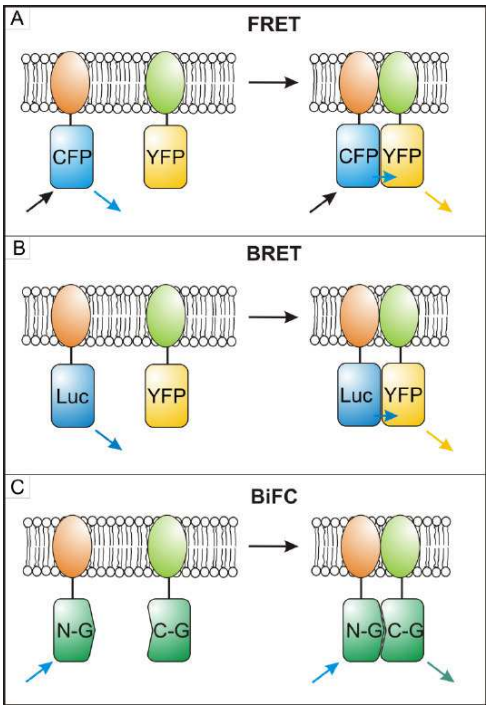

Figure 1.7. Comparison between FRET, BRET and BiFC

respectively. Addition of the natural substrate of Rluc, Coelenteraine (CTZ), leads to the emission of blue light (with a maximum at a 480 nm) with an emission spectrum that overlaps with the excitation spectrum of the YFP. If the two fusion proteins do not interact, only blue light is emitted

upon substrate addition. Instead, if the two fusion proteins interact, thereby placing the donor and acceptor molecules within a distance less than 10 nm, resonance energy transfer occurs and an additional light signal corresponding to the acceptor reemission can be detected (with a maximum at 535 nm in the case of YFP). The typical readout of a BRET experiment is the calculation of the BRET value and the BRET ratio (see § 3.27).

The BRET value is defined as the ratio between the YFP and RLuc signals calculated for a specific BRET pair, according to the formula:

$$BRET = \frac{YFP\ signal}{RLuc\ signal}$$

Similarly, the BRET ratio is defined as the difference between the BRET value relative to a BRET pair and the BRET value relative to the BRET donor (RLuc) alone, is calculated according to the formula:

$$BRET\ ratio = \frac{YFP\ signal}{RLuc\ signal} BRET\ pair - \frac{YFP\ emission}{RLuc\ emission} BRET\ donor$$

Usually a BRET ratio above 0.1 is considered indicative of PPI. A strong advantage of BRET assays is the possibility to discriminate between specific and non-specific interactions performing donor saturation experiments. In such experiments a fixed amount of donor molecule is expressed in the presence of increasing amounts of acceptor. In the case of a specific interaction, the BRET ratio augments in a hyperbolic manner and reaches a plateau (BRET max) representing complete saturation of all donors with acceptor molecules. On the other hand, in the case of non-specific interactions, the BRET ratio increases linearly with the increase of acceptor expression levels (see Figure. 1.8)

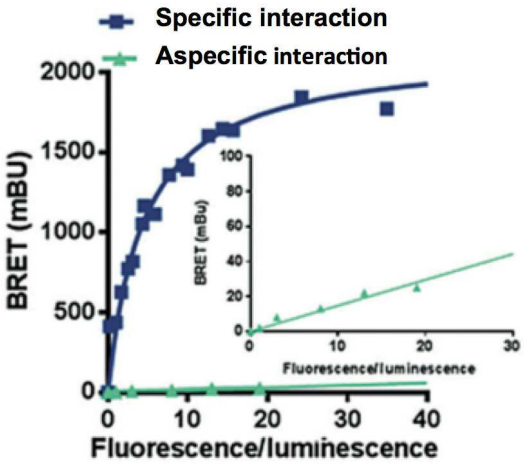

Figure 1.8: Example of the outcome of a BRET saturation experiment in the case of specific and aspecific protein-protein interactions. Adapted from [73].

1.16 Biomolecular Fluorescence Complementation (BiFC)

Biomolecular Fluorescence Complementation (BiFC) is a technique used to validate PPIs. BiFC relies on the association of fluorescent protein fragments fused to the proteins whose interaction has to be evaluated. In particular, the fluorescent protein is split into its N- and C-terminal domains, each one attached to one of the protein under investigation and expressed in live cells. If these two proteins interact, the two domains of the fluorophore will be close enough to reform their native 3D conformation and the so reconstituted fluorophore, under proper light excitation, can emit its fluorescent signal. The BiFC technique permits not only the detection and validation of PPIs *in vivo*, but can also localize the proteins in the cells and give information about the strength of the PPI, since the intensity of the fluorescent light emitted is proportional to the strength of the interaction.

2. Aim

Antiviral agents currently used for the treatment of HCMV infection have several disadvantages: toxic side effects, similar mechanisms of action and induction of resistant viral strains, leading to countless problems, especially in immunodeficient individuals (4).

Furthermore, HCMV is the leading cause of congenital viral infection and there are no drugs available during pregnancy. These problems have stimulated the search for new compounds that are less toxic, more active and more specific against HCMV. That is why we propose to inhibit viral replication through the dissociation of UL44 homodimeric complex using compounds that bind to homodimerization interface.

This strategy has two possible advantages. The first one is given by the fact that a protein-protein interaction - in this case, the dimerization of UL44 - is highly specific and therefore this paves the way for a virus-specific inhibition. Secondly, whereas a single point mutation in the catalytic site of an enzyme is sufficient to give rise to drug resistance, the homodimerization of UL44 would be restored by two different mutations, thus reducing the possibility of drug resistance onset.

3. MATERIALS AND METHODS

3.1 Lentiviral vectors productions

To produce Lentiviral pseudoparticles, 2 wells of a 6 well plate containing HEK293 T cells were transfected by Lipofectamine 2000 (Invitrogen)
using the following plasmids:.

- pCMVR8.74, Gag Pol expressing plasmid (6.4 μg).
- pMD.G, Encoding Vesicular stomatitis virus G protein (2.1 μg).
- Lentiviral plasmid coding the transgene of interest (6.4 μg), either pWPI–YFP-UL44puro or pWPIpuro empty vector.

After 24 hours, 8 x 10^4 cells HEK293A cells were seeded in a 12 well plate. The next day, Lentiviral pseudoparticles were harvested from HEK293 T cells and replaced by 3 ml of DMEM cpt w to the HEK293 T cells. Viral supernatants were collected at 48,52 and 72 hours post transfection, filtered through a 0.45 μ filter and stored in cryovials at 4°C or -80°C for short and long term use, respectively.

3.2 Generation of stable cell lines by Lentiviral transduction

HEK293 A cells were seeded in 12 well plates (8 x 10^4/ well). 24 hours later, media was replaced with 500 μl to 1000 μl of the filtered viral supernatants. When required, cells were transduced every 12 hours up to three times, in order to maximize transgene expression. 96 hours post transduction cells were grown in DMEM cpt containing with the appropriate amount of selection agent (see §

3.22). Media was changed every 3 days, and cells subcultured to a 6 well plate when reached confluence.

3.3 Generation of stable cell lines by Calcium Phosphate Transfection

HEK293 A cells, seeded on 2 wells of o 6 well plate, were transfected with a variable amount (5-15μg) of pre-linearized mammalian expression plasmid by Lipofectamine 2000. Plasmids were linearized using enzyme in order to promote integration in the host genome without interruption of any important sequence. 8h hours post transfection, media was changed and replace with DMEM cpt. Subsequently, 24h hours post transfection, the appropriate amount of selection agent was added to the cells (see § 3.22).

3.4 Determination of the optimal selection agent concentration for generation of stable cell lines

In order to select cells expressing the transgene of interest after either Lentiviral transduction (§3.20) or transfection (§3.21) we determined the optimal concentration of the appropriate antibiotics puromycin 0-6 μg/ml, (Clontech), blasticidin 0-20 μg/ml (Life Sciences) and neomycin 0-2000 μg/ml (Life Sciences). To this end, HEK293 A seeded $1x10^5$ in 24 well plates. 24 hour later, media was replaced with DMEM cpt containing a variable amount of antibiotic (see Table 6.3**)**. Media was replaced every 3 days, and cell viability was monitored daily for up to 10 days. For each antibiotic, the minimum concentration sufficient for killing all cells present in the well was selected for further experiments.

3.5 Generation of polyclonal and monoclonal cell lines

Polyclonal HEK293 A cell lines stably expressing the transgene of interest, were obtained by either transducing the parental cell line with a Lentiviral pseudoparticle (§3.20) or transfecting them with a linearized plasmid DNA (§ 3.21), followed by incubation in the presence of an appropriate amount of selection agent (§ 3.22). Cells were subsequently expanded from a 12 well plate to a 6 well plate, then to a T25 flask. When confluent cells were passaged to a T150 flasks, before being frozen. Such polyclonal cell lines were then either used for specific assays, or used to derive monoclonal cell lines. To this end, 0.5 cells/well in 200µl were seeded in each wel of a 96 well plate using a multichannel pipet (Eppendorf), in the presence of media containing the appropriate selective agent. Plates were monitored daily for appearance of colonies and media was changed every 3 days. When the colonies reached confluency, they were passaged to 24 well plates and subsequently to 6 well plates, before being further expanded and frozen for long term storage.

3.6 Preparation of glass coverslips for microscopic imaging

Poly lysine solution (SIGMA 6282) was used to treat glass coverslips to ensure a better adherence of the cells to the coverslips. One day before seeding, sterile glass coverslips (Assistent®, REF 1001/12, 12mm ø) were placed, under sterile hood, into 24 well plates and 300 µl of poly lysine solution were added to each well, ensuring that all the surface of the glass coverslip was covered, and then incubated for 2 h at 37°C by gently shaking. At the end of the incubation period, poly lysine was removed and the coverslips were washed, first with 1 ml of sterile H_2O MQ, and then with 1 ml of sterile PBS. After the removal of PBS, coverslips were positioned at 45° and dried ON at RT. HEK293 T cells were subsequently seeded on such Poly-Lysinated coverslips, and then transfected with the appropriate DNA mixtures using Lipofectamine. 48h p.t., culture media was removed from the wells and cells were washed with 1 ml of PBS to eliminate debris. Cells were then fixed for 10 minutes at RT with 350 µl of Paraformaldehyde (4% v/v in PBS, pH 7.4) and washed twice with 1 ml of PBS to remove residues of paraformaldehyde. Finally, glass coverslips

were mounted on microscope slides using 5µl of Fluoromount-G (Southernbiotech) as mounting media. Slides were equilibrated for 30 min at RT before being stored in the dark at 4°C.

3.7 Coelenterazine stocks preparation

Coelenterazine (native-CTZ; cat. 102171) and Benzyl Coelenterazine (h-CTZ; cat. 102181) were purchased from PJK GmbH. Native-CTZ (MW: 423.463 g/mol) stock solutions were prepared in the dark dissolving 1 mg of compound in 2.36 ml of MetOH, to obtain 1 mM stocks. h-CTZ (MW: 407.464 g/mol) stock solutions were prepared in the dark dissolving 1 mg of compound in 2.45 ml of MetOH, to obtain 1 mM stocks. Stocks were aliquoted in foil covered eppendorfs (50 µl/vials) and stored at -80°C until required.

3.8 Z^I factor analysis

The Z-factor is a parameter quantifying the suitability of a particular assay for use in high-throughput screen. An assay with 0.5 < Z-factor < 1 is considered to be excellent [74]. Z-factors were calculated according to the formula:

$$\text{Z-factor} = 1 - \frac{3(\sigma_p + \sigma_n)}{|\mu_p - \mu_n|}.$$

3.9 Bioluminescence Resonant Energy Transfer (BRET) measurements

HEK293 T were detached from culture flasks and 1 or 2 x 10^5 cells/well were seeded on 24 well plates and analysed 24h or 48h post transfection, respectively. Plates were incubated ON at 37°C in a 5% CO_2, 95% humidified incubator. The following day cells were transfected with the appropriate DNA mixtures containing BRET pairs expression plasmids, using Lipofectamine 2000. Cells were also mock transfected, to establish background levels of luminescence and fluorescence. Additionally, each Rluc-expressing plasmid was also transfected in the absence of a YFP construct to be used as a background for calculation of the BRET ratio. 16h post transfection cells were

observed using an inverted fluorescent microscope (Leica, DFC420 C) to verify cells conditions and to verify that the YFP-fusions were expressed as expected. At the established time post transfections, cells were processed for BRET assays. Culture media was removed from wells and cells were very gently washed with 1 ml of PBS, before being resuspended with 290 µl of fresh PBS. Using a p200 filter tip cells were further resuspended and 90 µl of mixture were transferred to a black bottomed 96-well plate (Costar®, REF 3916, 2018-04-12) well, in triplicate. When acquisition of fluorescent signal was required (YFPnet), the 96-well plate was first read with a spectrometer compatible with BRET measurements (VICTOR X2 Multilabel Plate Reader, Perkin) for the YFP fluorescent emission, using a fluorimetric excitation filter (band pass 485 ± 14 nm) and a fluorimetric emission filter (band pass 535 ± 25 nm). The **YFPnet** value corresponds to the acquired value relative to each well, subtracted the background value acquired relative to mock transfected cells. Subsequently, h-CTZ 1 mM stocks were appropriately diluted (1:20, 1:10 or 1:5, v/v in PBS) before being added to each well (10 µl/well) to reach the desired final concentration (5-20 µM). The plate was then read in luminometry, to allow acquisition of the YFP and RLuc signals. Initially it was acquired the **YFP signal**, using a luminometric 535 ± 25 nm emission filter. Subsequently, it was acquired the **Rluc signal**, using a luminometric 460 ± 25 nm emission filter. **YFP** and **RLuc emission** values relative to each condition were calculated by subtracting the **YFP** and **RLuc signal** relative to mock transfected cells to their **YFP** and **RLuc signals**. Luminometric readings were performed at 5', 15', 30', 45' and 60' after addition of the substrate. Before each reading, the plate was shacked for 1 sec. at normal speed and with double orbit. Details relative to the fluorimetric and luminometric readings are detailed in the Appendix section (§6.10).

Finally, the data obtained were analysed calculating to calculate the **BRET value**, defined as the ratio between the **YFP** and **RLuc signals** calculated for a specific BRET pair, according to the formula:

$$BRET = \frac{YFP\ signal}{RLuc\ signal}$$

Similarly, the **BRET ratio**, defined as the difference between the **BRET value** relative to a BRET pair and the **BRET value** relative to the BRET donor alone, was calculated according to the formula:

$$BRET\ ratio = \frac{YFP\ signal}{RLuc\ signal} BRET\ pair - \frac{YFP\ emission}{RLuc\ emission} BRET\ donor$$

3.9.1 BRET saturation curves

HEK293 T cells were transfected with appropriate amounts of BRET donor plasmids (RLuc; generally 2.5-10ng), sufficient to yield a RLuc signal clearly distinguishable from the background, in the presence of increasing amounts of BRET acceptor plasmids (YFP; generally 0-180ng), and of a variable amount of empty vector pCDNA3 (to 500ng final plasmid DNA). At the appropriate time post transfection (24-48h) samples were processed as above (see §3.27) to calculate the **BRET ratio**, The **YFPnet** and the **RLuc signal** values, relative to each condition. BRET saturation curves were then calculated using the GraphPad Prism software by plotting each individual **BRET ratio** value to the **YFPnet/RLuc signals (YFP/RLuc)** and interpolating such values using the one-site binding hyperbola function of PRISM. A specific BRET pair would then generate a logarithmic shaped curve and reach a plateau. This would thus allow calculation of BRETmax (Bmax) and BRET50 (B50) values, indicative of maximum energy transfer and relative affinity of the BRET pair tested. On the opposite, a non-specific interacting BRET pair would not reach plateau, resulting in a linear BRET ratio over Y/R curve.

3.9.2 Normalization of Y/R ratios using control molecule RLuc-YFP

When required Y/R ratios relative to each condition, were normalized to the Y/R ratio of control molecule RLuc-YFP, in order to reflect more accurately the relative number of RLuc and YFP

fusions expressed. To this end, different amounts of the RLuc-YFP control plasmid (h-CTZ: 3-9ng; CTZ: 45ng) were used to transfect HEK293 T cells along with the BRET pair expression plasmids, and similarly processed at the required time points (see §3.27). Both in the case of h-CTZ and CTZ, curves were normalized using the Y/R values 15 min post substrate addition normalized to the Y/R ratio of RLuc-YFP control molecule of the correspondent time point (15min).

3.9.3 BRET competition curves

Bret competition curves were performed to verify the possibility to detect inhibition of the interaction between the BRET pairs.

To this end appropriate amounts of BRET donor and acceptor plasmids (RLuc-UL44 2.5ng + YFP-UL44 40/22ng or RLuc-UL54 10ng + YFP-UL44 40/22ng) were transfected into HEK293 T cells together with increasing amounts of a competitor, YFP-UL44-FLAG. As negative control, a BRET competition curve was performed transfecting increasing amounts of YFP-UL42-FLAG competitor, which is known to not interact with UL44 nor with UL54. Variable amount of empty vector pCDNA3 were also added to reach a final plasmid DNA quantity of 500ng. At the appropriate time post transfection (24-48h) samples were processed as above (see §3.27) to calculate the **BRET ratio**, the **YFPnet** and the **RLuc signal** values, relative to each condition. BRET competition curves were then calculated plotting each individual **BRET ratio** value to the quantity of competitor transfected.

3.9.4 Evaluation of the effect of SMs on UL44 homodimerization by BRET assays

HEK293 T cells were seeded $1x10^5$ or $2x10^5$ in to 24-well plate and incubated ON at 37°C, 5% CO2 and 95% humidity. The following day cells were transfected with the appropriate DNA mixtures containing the BRET pairs expression plasmids, using Lipofectamine 2000. 6h post transfection mixtures were removed and added the SMs, two concentrations each compound

according to viability experiment (see §3.30.2). 24h or 48h later the cells were processed as above (see §3.27) to calculate the BRET ratio, the YFPnet and the RLuc signal values, relative to each condition. The BRET inhibition was calculated plotting each individual BRET ratio value to the quantity of BRET pair transfected.

3.9.5 Evaluation of the effect of AL18 on the UL54-UL44 interaction by BRET assays

According to viability experiments from **[71]** we decided to use two concentrations for the BRET experiments, 3µM and 30µM respectively.

HEK293 T cells were seeded into a 24-well plate, $2x10^5$, $1x10^5$ respectively for the 24h and 48h test, and incubated ON at 37°C, 5% CO2 and 95% humidity. The following day cells were transfected with the appropriate DNA mixtures containing the BRET pairs expression plasmids, using Lipofectamine 2000. 6h post transfection mixtures were removed and add AL18.

24h or 48h post transfection cells were observed using an inverted fluorescent microscope (Leica, DFC420 C) to verify cells conditions, localization and expression of the YFP-fusions.

24h or 48h time post transfection samples were processed as above (see §3.27) to calculate the BRET ratio, the YFPnet and the RLuc signal values, relative to each condition. The BRET inhibition was calculated plotting each individual BRET ratio value to the quantity of BRET pair transfected.

3.10 Fluorescence Resonant Energy Transfer (FRET)

HEK293 T were detached from culture flasks and 0.5 x 10^5 cells/well were seeded on 24 well plates containing poly-lysinated glass coverslips 12 mm ø (see §3.24). Plates were incubated ON at 37°C in a 5% CO_2, 95% humidified incubator. The following day cells were transfected with the appropriate DNA mixtures containing the FRET pairs expression plasmids, using Lipofectamine 2000. Subsequently, transfection mixtures were removed, 8h or 16h post transfection. 16h post

transfection cells were observed using an inverted fluorescent microscope (Leica, DFC420 C) to verify cells conditions and expression of the YFP- or CFP-fusions. At 24 or 48 hours post transfection, media was removed from 24 well plates containing cells grown on 12 mm glass coverslips and cells were then processed for Immunofluorescence as described in §3.32.

3.10.1 Localization analysis

Subcellular localization of CFP and YFP fusion proteins, was microscopically evaluated using a Leica SP2 Confocal Scanning Laser Microscope (CSLM) equipped with a 63X oil immersion objective and an argon laser. Samples were scanned at 200 Hz, using a line average of 3, image resolution of 512 x 512 pixels and zoom 2.5. CFP was exited at 458 nm, whereas YFP at 514 nm. Laser power, gain and offset were set in order to obtain an optimal signal to noise ratio. Digital images were subsequently analysed with ImageJ software to create panels of localization containing CFP and YFP fusions alone and a merge of the two.

3.10.2 FRET Acceptor Photobleaching analysis

Samples previously analyzed for the subcellular localization, were then subjected to FRET Acceptor Photobleaching using a Leica SP2 CSLM equipped with a 63X oil immersion objective and an argon laser. After an initial scanning (see §3.28.1), FRET Acceptor Photobleaching was performed following three basic steps, using the FRET acceptor bleaching function of the Leica Confocal software (version 2.61). 1) images of donor and acceptor fusion proteins were first acquired pre bleaching using the same parameters described in § 3.28.1; 2) acceptor was bleached with argon laser at maximum power (6 to 10 scans); 3) post bleaching images of donor and acceptor

were acquired, using the same settings as in step 1). FRET efficiency % was calculated on the basis of donor fluorescence intensity variations pre- and post-bleaching, using the following equation:

$$FRET\ efficiency\ \% = \frac{Dpost - Dpre}{Dpost} \times 100$$

Where **Dpost** is the donor fluorescence intensity post-bleaching, and **Dpre** the donor fluorescence intensity pre-bleaching. For each sample 10 to 30 cells in different areas of the slide were selected and subjected to FRET. We preferentially selected that cells which displayed comparable levels of expression between the donor and the acceptor and which were not saturated. Due to the different levels of expression of the different samples, we were not able to use a single setting for all the samples, but the same setting (laser potency, pinhole, gain and offset) was used for FRET pairs which were then compared the one to the other (i.e. CFP-UL54 + YFP-UL44 vs CFP-UL54 + YFP-UL44-I135A). Data obtained (FRET efficiency %, CFP and YFP expression levels pre bleaching) were then analysed using GraphPad Prism software.

3.10.3 FRET efficiency statistical analysis

FRET efficiency % between different samples was statistically compared with GraphPad Prism, to perform the parametric t test with Welch's correction relative to each FRET pair considered.

FRET correlation Analysis. To calculate correlation between FRET efficiency % with CFP and YFP expression levels, FRET efficiency % and fluorophore expression levels were analyzed with the correlation function of GraphPad Prism, computing the r between the two datasets, and using two tailed Pearson correlation coefficients with 95 % confidence interval. Pearson r values > than 0.5 or smaller than - 0.5 were considered indicative of positive or negative correlation, respectively.

3.10.4 Processing of digital images

8 bit CLSM images acquired using the Leica software were processed with ImageJ to generate tiff images. First, brightness was adjusted and images were smoothened, then the most significant area

of the image was selected and cropped (256 x 256). Subsequently a colour was assigned to each channel, green for CFP and red for YFP, before merging the two to obtain a composite image. The composite image was transformed in a RGB colour image and the merged channels were split again in 8 bit images. A scale bar of 10 μm was added to the merge RGB colour image before creating a stack of the three images (CFP on the left, YFP in the middle, merge on the right). To highlight protein-protein co-localization in HEK293 T cells confocal images acquired as in §3.19.1 and processed as described above, were analyzed with ImageJ. On a selected cell present in the merge image of the stack, a line was drawn on the entire surface of the cell. Subsequently a RGB profile plot of the selected area was obtained the plugins graphic option of ImageJ.

3.11 SMs stocks preparation in DMSO

SMs and AL18 were purchased from Vitas-M and Maybridge, respectively. According to each SM MW, molecules were diluted in appropriate amounts of DMSO 100% to obtain the following stocks concentrations: 20 mM, 10 mM, 5 mM, 2.5 mM, 1.25 mM, 625 μM, and 312.5 μM. Stocks were aliquoted in foil covered eppendorfs (20 μl/vials) and stored at -20°C until required.

3.12 WST-1 cell viability assay

Viability assays on HEK293 A cells were performed through a colorimetric assay using the nonradioactive cell proliferation reagent WST-1 (Roche, version 16). WST-1 is a stable tetrazolium salt which is cleaved to a soluble formazan by a bioreduction reaction dependent on the production of NAD(P)H in viable cells. The amount of formazan dye produced is directly proportional to the number of metabolically active cells in which the respiratory chain of mitochondria is functional. The quantification is measured with a scanning multi-well spectrophotometer and the recorded absorbance is proportional to the number of viable cells. HEK293 A cells were seeded into a 96-well plate, $1x10^4$/well for the 24h and $0.5x10^4$/well for 48h, and incubated ON at 37°C, 5% CO_2

and 95% humidity. The following day, cell culture medium was replaced with either different concentrations of DMSO or with freshly prepared dilutions of the SMs in 1% DMSO. To this end, SMs stocks in 100% DMSO were diluted 1:100, under sterility and in the dark, into DMEM (DMSO 1% final concentration v/v) in order to obtain different concentrations: 200 µM, 100 µM, 50 µM, 25 µM, 12.5 µM, 6.125 µM, 3.125 µM. After addition of SMs and the plates were incubated again at 37°C, 5% CO_2, 95% humidity. The test was done in duplicate and as controls some seeded wells were left with DMEM-DMSO 1%, and some wells without cells with DMEM-DMSO 1%. After 24h or 48h, the plates were observed under optical microscope to evaluate cells confluence and morphology as well as the presence of precipitates. Subsequently, 10 µl of WST-1 (1:10 v/v) were added to each well, and absorbance was determined with a spectrophotometer plate reader at 450 nm at different time points post addition of the substrate: 10', 20', 30', 40', 50', 60', 90', 120', 180'. Data acquired were analyzed with the software PRISM and fitted to a linear regression or 4 Parameter Logisitic Equation (Sigmoidal) to calculate the cell culture viability of 50% of cells (CC_{50}) values.

3.13 GST-pulldown assay

The recombinant 6His-UL44, 6His-UL44-L86/L87A, GST-UL44, GST proteins were purified as described [75]. 0.03 nmol of either GST- fusion proteins were incubated for 2 hours at 4°C with 0.12nmol of 6His-UL44 wild type in a final volume of 100 µl in Binding Buffer (see Appendix 6.1). After that 100 µl of samples were loaded onto columns previously activated with 100 µl of glutathione-sepharose columns (Biorad). Columns were washed with 2.5 ml of NETN buffer (see Appendix 6.1). 100µl of the last wash fraction were collected and used for subsequent analysis. The bound complexes were eluted with 300 µl of elution buffer (NETN buffer plus 15 mM glutathione). Samples derivate from Input, Wash fractions and Eluted fractions were analyzed by Western-Blot as described in § 3.34.

3.14 Immunofluorescence analysis

Cells were plated ($5x10^4$ per well) in 24 well with glass coverslips, previously treated with poly-lysine (see§ 3.24), and incubated, in order to allow adhesion. The following day, cells were fixed in 4% formaldehyde (see § 3.24) and permeabilized in PBS-0.5% Triton X-100 (Applichem) for 5 minutes at RT. Subsequently cells were washed with PBS and saturated with 3% PBS-BSA for 30 minutes. Samples were then incubated for 1 hour at RT with Anti-Rluc Mouse monoclonal antibody (Sigma-Aldrich, MAB4400) diluted 1:50 in 1% BSA in PBS- (weight/volume). Following three washes in PBS, cells were incubated with Alexa Fluor® conjugated secondary antibody (Molecular Probes) diluted in 1% PBS-BSA for 1 hour in the dark. Immunofluorescence signals were either visualized on inverted fluorescent microscope (Leica, DFC420 C), or with a Leica SP2 CLSM system.

3.15 Western-blot assays

The following primary and secondary antibodies and were diluted in PBS containing 5% milk at the concentrations reported below:

- Anti-Rluc Luciferasi mouse monoclonal, 1:4000 (Sigma, MAB4400)
- Anti-GFP rabbit polyclonal, 1:1000 (Santa Cruz Biotech sc-8335)
- Anti-Tubulin mouse monoclonal, 1:10000 (Sigma, T6074)
- Anti-6His tag, 1:2500 (Sigma, H-1029).
- Goat Anti-mouse IgG Peroxidase Conjugate 1:10000(Sigma, A4416)

  Goat Anti-rabbit Peroxidase Conjugate 1:10000 (Sigma, A6154).
- Goat Anti-mouse immunoglobulin Ab conjugated to horseradish peroxidase 1:2000 (sc-2055, Santa Cruz Biotech).

4. RESULTS

I. Study of UL44 dimerization in cells and *in vitro*

Since UL44 has been crystallized as a dimer, and point mutations affecting UL44 dimerization *in vitro* affected its DNA binding properties as well as *ori*Lyt dependent DNA replication, we speculated that UL44 dimerization could represent a therapeutic target. UL44 dimerization has not been detected only *in vitro*, but also in cells, by using subcellular localization assays by simultaneously co-expressing differently tagged nuclear and cytosolic versions of UL44 [49]. Such assays suggested that UL44 could also function as a dimer in cells, however they are not amenable to the screening of compounds interfering with dimerization given their non-quantitative nature. We therefore decided to develop new in cells quantitative assays to verify UL44 dimerization in cells, which would be potentially amenable to screening of UL44 dimerization in cells.

4.1 Study of UL44 dimerization in cells by Resonant Energy Transfer techniques

We initially focused on Resonant Energy Transfer (RET) techniques, which are based on the ability of a specific molecule, called "donor", to transfer energy to an "acceptor" molecule when the two are located in close proximity (< 10 nm) (see Introduction 1.15). To this end we used Fluorescence Energy Transfer (FRET) and Bioluminescence Energy Transfer (BRET).

4.2 Generation of Mammalian expression plasmids to study UL44 interactions by FRET

The first RET method we tested is FRET, based on the ability of a fluorescent donor such as CFP to transfer energy to a acceptor molecule such as YFP (see section 1.15). To this end, we generated

plasmids mediating the expression of N-terminally tagged versions of UL44 as fused to either CFP or YFP, using the Gateway™ technology. As a control, we also generated expression plasmids between such fluorescent protein and the C-terminal 95 amino acids of UL54 (residues 1125-1242) containing the NLS and the UL44 binding domain of the protein (see introduction) [46]. Additional control plasmids mediating the individual expression of YFP and CFP as well as a CFP-YFP fusion protein were also obtained [76].

4.3 Analysis of subcellular localization and molecular weight of expressed proteins.

Plasmids were transfected in HEK293 T cells $5x10^4$ containing poly-lysinated glass coverslips (see §3.24) and their subcellular localization investigated by CLSM 48h p.t. (see §3.28.1). As expected both CFP, YFP and CFP-YFP homogenously distributed throughout the cells with a diffuse pattern (Figure 4.1 A). On the other hand, fusion of UL44 to either CFP or YFP resulted in strong nuclear localization, often accompanied by a pointy intranuclear pattern, indicative of DNA binding and consistent with the presence of a NLS within the DNA binding protein UL44. Fusion to UL54 (1125-1242) resulted in proteins mainly localized to the cell nuclei with a diffuse pattern due to the presence of a NLS, but the lack of any DNA binding domain in UL54 C-terminus (figure 4.1A). We also evaluated that all fusion proteins were correctly expressed by Western blotting. To this end, HEK293 T cells were transfected with each expressing plasmid, and 48h p.t. samples were lysed, electrophoretically separated on 8.5 % bis-tris acrylamide gels and subjected to Western blotting (§ 3.34). The presence of specific bands relative to each fusion protein was detected using an anti GFP antibody (§ 3.34). Our results indicate that all fusion proteins could be readily detected at the expected molecular weight (Figure 4.1 B). In particular both YFP and CFP-UL44 fusions could be detected as 70 kDa discrete bands, whereas UL54 (1125-1242) fusions (apparent MW of 37 kDa) migrated slower than CFP and YFP as individually expressed (MW ca. 27 kDa), but slightly faster than the CFP-YFP fusion protein (MW ca. 54 kDa).

Overall, our results indicate that all the CFP and YFP expression plasmids employed mediate the expression of proteins exhibiting the expected subcellular localization (Figure 4.1 A) and molecular weight and could be therefore used for subsequent analysis (Figure 4.1 B).

4.4 Analysis of UL44 dimerization and its interaction with UL54 by FRET acceptor photobleaching

Based on these results, we decided to perform FRET acceptor photobleaching experiments. We used CFP-UL44 and CFP-UL54 (1125-1242) (from now CFP-UL54) as donor molecules, and YFP-UL44 along with a set of point mutant derivatives (L86/L87A, defective for dimerization; I135A, defective for UL54 binding) as acceptors. We additionally transfected cells with a positive control plasmid mediating expression of a CFP-YFP fusion, and with negative control plasmids mediating the expression of CFP and YFP as individual proteins. In this set of experiments, $5x10^4$ HEK293 T cells were seeded in 24 well plates, containing glass coverslips, before being transfected. In order to maximize the chance to obtain comparable expression levels between FRET pairs of interest (CFP-UL44/YFP-UL44 vs CFP-UL44-L86-L87A/YFP-UL44-L86-L87A and CFP-UL54/YFP-UL44 vs CFP-UL54/YFP-UL44-I135A), we transfected cells with two different amounts (Condition A, Condition B) of the relevant CFP-UL44/YFP-UL44 and CFP-UL54/YFP-UL44 FRET pairs expressing plasmids (Table 4.1). Subsequently, coverslips were processed (§3.24) before being observed by CLSM to determine the localization pattern of the proteins of interest (§3.28.1). In some cases, transfection mixtures were removed 8h p.t. in order to maximize cell viability. In other experiments, transfection complexes were removed after 16h in order to maximize transfection efficiency.

While performing FRET assays, we also evaluated the subcellular localization of each fusion protein, when expressed in the presence of its interacting partner. We first observed samples whose media was changed 16h p.t. As reported above, CFP localized with a diffuse pattern homogeneously distributed throughout the whole cell, and its localization was not affected by

simultaneous expression of YFP. Such subcellular distribution was undistinguishable from that of the CFP-YFP fusion (Figure 4.2). As expected, CFP-UL44 showed a nuclear localization with a spotty pattern dependent on its DNA binding ability, and such distribution was not affected by expression of YFP-UL44 (Figure 4.2). On the opposite, point mutant CFP-UL44-L86/L87A showed a more diffuse nuclear localization with decreased formation of speckles when expressed alone, most likely due to its inability to dimerize and therefore bind dsDNA, both in the presence and in the absence of its YFP-UL44-L86/L87A partner (Figure 4.2). On the other hand, CFP-UL54 showed a diffuse nuclear localization when expressed alone, whereas it strongly colocalized with YFP-UL44 in nuclear spots upon co-expression. Importantly, such co-localization was not observed when CFP-UL54 was expressed in the presence of YFP-UL44-I135A, a mutant derivative impaired in UL54 binding (Figure 4.2). In all cases, no difference was observed between conditions A and B and similar results were obtained when media was changed 8h p.t. (not shown).

FRET efficiency is expected to correlate with protein expression levels, therefore it is very important to compare values calculated for samples were similar levels of proteins are expressed. For this reasons we applied FRET acceptor photobleaching (see §3.28.2) to samples transfected with relevant FRET pairs at the different conditions (A and B; see Table 4.1), with identical settings (listed in Table 4.2). We first analyzed samples whose media was changed 8h p.t. As expected, we calculated a FRET efficiency of 33% for the positive control CFP-YFP, significantly higher than the 8% calculated for the negative control, represented by the simultaneous expression of CFP and YFP (Figure 4.3 A B). In order to avoid artifacts due to different protein expression levels between wt and mutant proteins, the same acquisition settings were used to analyze samples transfected according to the conditions represented in Table 4.3. Intriguingly, for both conditions the wt UL44 FRET pair revealed a FRET efficiency significantly higher than its dimerization impaired counterpart (Condition A: 23 ± 4 *vs*. 11 ± 5; Condition B: 27 ± 5 vs 7 ± 3) (Figure 4.3 A B). Similar results were obtained when comparing the FRET efficiency relative to expression of CFP-UL54 in the presence of YFP-UL44 and of the UL54-binding defective point mutant YFP-UL44-I135A

(Condition A: 19 ± 3 *vs*. 8 ± 4; Condition B: 18 ± 3 *vs*. 4 ± 2). Taken together, these results further confirm that UL44 forms dimers and binds to UL54 in cells, and that the L86A/L87A substitution within the dimerization site, as well as the I135A substitution within the connector loop, negatively affect these processes. Furthermore, these results indicated that acceptor bleaching could be used to monitor both the UL44 homodimerization and the UL54-UL44 interaction. Similar results were obtained for the relevant FRET pairs relative to cells whose media was changed 16h p.t. (Figure 4.3 C), as well as after pooling data from condition A and B (Figure 4.3D).

4.5 Analysis of YFP and CFP correlation with FRET efficiency

In order to determine the effect of relative acceptor and donor expression levels on FRET efficiency, we investigated if there was a correlation between the fluorophores expression levels and the FRET efficiency as described in §3.28.3, analyzing the two previous experiments in which media was changed 8h or 16h p.t.

Correlation was found more often between FRET efficiency and YFP as compared to CFP expression (40% vs 25% of cases, respectively) (Figure 4.4 and Figure 4.5). As expected, correlation between YFP and FRET efficiency was always positive (reaching maximum Pearson r value of 0.88), while that between CFP and FRET efficiency was preferentially negative (reaching a minimum Pearson r value of -0.68). These results suggest that, as expected, increasing the relative acceptor expression levels (YFP) also increases FRET efficiency, while increasing the relative donor levels (CFP) causes a decrease in FRET efficiency.

We therefore decided to investigate whether the observed differences in FRET efficiency between wt and point mutant-interaction impaired version of UL44 were due to altered expression protein expression levels. To this end, we compared CFP (Figure 4.6A, B) and YFP (Figure 4.6C, D) expression levels of the different FRET pairs relative to UL44 homodimerization (Figure 4.16 A, C) or to the UL54-UL44 interaction (Figure 4.6, D) of samples whose media was changed 8h p.t.. Our

analysis revealed no marked differences between conditions examined, thus showing that decreased FRET efficiency observed for UL44 mutants is a specific effect due to reduced PPI and does not depend upon altered fluorophores expression levels. Similar results were obtained also for samples whose media was changed 16h p.t. (not shown).

5 BRET-based analysis of UL44 dimerization

Our FRET-based results clearly indicated that UL44 dimerizes and binds to UL54 in cells, and that such interactions are affected by specific amino acids substitutions (see Figure 4.3.). However, FRET is sensitive to protein expression levels, and thus does not easily allow precise quantitation of inhibition of such PPIs. Furthermore FRET is extremely time consuming and not easily scalable to SMs screening. To overcome these limits, we decided to test if UL44 dimerization and binding to UL54 could also be monitored by an alternative RET method, such as Biolominescent (B)RET. BRET is based on non-radioactive energy transfer between a bioluminescent donor molecule, such as Renilla luciferase (Rluc) to a fluorescent acceptor molecule, such as YFP (see section 1.15).

5.1 Subcellular localization and expression analysis of RLuc-fusion proteins

To this end, we generated plasmids mediating the expression of N-terminally tagged versions of UL44 and UL54 as fused to RLuc, using the Gateway™ technology. As a negative control for UL44 dimerization, we generated the RLuc.UL44 (405-433) expression plasmid. UL44 (405-433) contains a NLS, responsible for nuclear targeting the protein, but lacks UL44 N-terminal domain responsible for all known biochemical activities, including the ability to self-associate, and therefore represents an ideal negative control for BRET assays. As a positive control, we also generated expression plasmids driving the expression of the YFP-RLuc and RLuc-YFP fusion proteins (Table §8.5).

HEK293 T cells were seeded in 24 well plate containing poly lysinated coverslip glasses and after 24h p.t. the cells were transfected with RLuc expressing plasmids and the subcellular localization of expressed proteins was investigated by inverted fluorescent microscope (Leica, DFC420 C), 48 h p.t. (see § 3.28.1). As expected, both RLuc-UL44 and RLuc-UL54, as well as the RLuc-UL44 (405-433), localized to the cell nuclei (see Figure 4.7). On the other hand, YFP-RLuc localized mainly in the cytosol, whereas Rluc-YFP appeared more nuclear.

We also evaluated that all fusion proteins were correctly expressed by Western blotting. To this end, HEK293 T cells were transfected with each expressing plasmids, and 48h p.t. samples were lysed, electrophoretically separated on 8.5 % bis-tris acrylamide gels and subjected to Western blotting (§ 3.34). The presence of specific bands relative to each fusion protein was detected using an anti RLuc antibody (§3.34). Our results indicate that all fusion proteins could be readily detected at the expected molecular weight (see Figure 4.7). In particular RLuc-UL44 fusions could be detected as ca. 100 kDa discrete band, whereas RLuc-UL54 (1125-1242) fusion (apparent MW of 46) migrated quicker than RLuc-YFP and YFP-RLuc fusion proteins (apparent MW ca.63 kDa). Very little degradation was detected relative to each fusion protein.

Overall our results indicate that all RLuc- expression plasmids employed mediate the expression of proteins exhibiting the expected subcellular localization and molecular weight and could be therefore used for subsequent analysis.

5.2 Analysis of protein expression levels mediated by BRET plasmids

Similarly to FRET, BRET is also sensitive to protein expression levels. Strong BRET signals, resulting in highest BRET ratio values (see § 3.28) are obtained under low RLuc and high YFP expression conditions. In order to evaluate the possible BRET ratio relative to UL44 dimerization, as compared to the BRET ratio relative to a negative control BRET pair, such as those represented

by the interaction of RLuc-UL44 (405-433) with YFP-UL44, we initially decided to compare the expression levels of fusion protein mediated by the aforementioned expression plasmids. To this end, we therefore seeded $1x10^5$ HEK293 T cells per well of a 24 well plate, and 24h later, transfected cells using Lipofectamine 2000 with increasing amounts of plasmids (from 0 to 500 ng) mediating the expression of either the YFP-UL44, the RLuc-UL44 or the RLuc-UL44(405-433) fusion proteins. 48h p.t. cells were processed for detection of fluorimetric (YFP-fusions) and luminescent (RLuc-fusion) expression by using a plate reader, 5' after addition of RLuc substrate CTZ (5μM, see §3.25). Our results indicate that the signals could be readily detected (Figure 4.8). Interestingly, while the signal relative to YFP-UL44 continued to increase with the increase of transfected plasmid (Figure 4.8 A, up to 500 ng), expression from both RLuc expression plasmids did not seem to increase linearly with the increase of transfected plasmid (Figure 4.8 B, C). Importantly, the RLuc-UL44 (405-433) protein appeared to be much more stable than the RLuc-UL44, with 50ng of expressing plasmid already resulting in a RLuc signal higher than that generated after transfection with 500 ng of RLuc-UL44 (Figure 4.8 B, C).

5.3 Detection of UL44 dimerization in living cells by BRET

We then decided to evaluate the ability of UL44 to form dimers in living cells. To this end $1x10^5$ HEK293 T cells were seeded and transfected as above with either RLuc-UL44 or RLuc-UL44 (405-433) alone, or in combination with YFP-UL44. Appropriate amounts of each plasmids were chosen in order to mediate the expression of comparable amounts of the RLuc-fusions. To this end, cells were transfected with either 100 ng of RLuc-UL44 or 12.5 ng of RLuc-UL44 (405-433). Where required, transfections were performed in the presence of an excess of YFP-UL44 expressing plasmid (500 ng), to allow calculation of the BRET signal. 48h p.t. later cells were processed for BRET analysis. Per each condition, the YFP fluorescent signal generated after excitation at 485 nm (YFP-Net, see §3.27) was recorded, and subsequently the YFP and RLuc emission values relative to

each condition was performed in luminometry, at different times after the addition of RLuc substrate CTZ (see § 3.27).

Luminometric measurements were recorded at different times points post CTZ substrate, in order to follow variations in the signals. As expected, RLuc (Figure 4.9 A) and YFP (Fig. 4.9 B) rapidly decreased over the 45' considered period. On the opposite, the BRET signal increased, reaching a maximum at 45' post CTZ addition, and was used as the selected time point to calculate BRET measurements post CTZ addition. These results, suggest that UL44 homodimerization can be successfully monitored by BRET assays (Figure 4.9 C). Importantly, RLuc-UL44 and RLuc-UL44 (405-433) were expressed to comparable levels (Figure 4.10 A), similarly to the YFP-UL44 (Figure 4.10 B). When individually expressed, RLuc-UL44 generated a BRET value of 0.31±0.03, similarly to the 0.32±0.02 BRET value calculated for Rluc-UL44 (405-433), and corresponding to the background signal. Importantly, co-expression of YFP-UL44 increased the RLuc-UL44 BRET value to 0.67±0.05, resulting in a BRET ratio of 0.36±0.10. On the other hand, BRET value of RLuc-UL44 (405-433) was not increased by co-expression with YFP-UL44 (0.35±0.01), resulting in a BRET ratio of 0.03±0.00 (Figure 4.10 C, D).

5.4 Probing the specificity of UL44 dimerization by BRET

Our results suggest that BRET might be suitable to detection UL44 interaction in living cells. However, the BRET signal generated by the presence of RLuc and YFP tagged version of UL44 could also result from aspecific interaction between the two proteins. The most common way to prove such specificity is by performing saturation experiments, whereby increasing amount of acceptor (YFP)- expression plasmid are transfected in the presence of fixed amounts of RLuc expressing plasmids (see § 3.27.1). To this end, HEK293 T cells were seeded $1x10^5$ in 24 well plates and transfected with either 25 ng of RLuc-UL44 or 6.25 ng of RLuc-UL44 (405-433), in the presence of increasing amounts of the YFP-UL44 (range: 0 to 900 ng). 48h later cells were

processed for BRET analysis. Per each condition, the YFP fluorescent signal generated after excitation at 485 nm (YFP-Net, see §3.27) was recorded, and subsequently the YFP and RLuc emission values relative to each condition was performed in luminometry, 45' after the addition of RLuc substrate CTZ (0.5 μM see § 3.25). Our analysis indicates that the BRET ratio relative to the RLuc-UL44/YFP-UL44 BRET pair rapidly increases with the increase of the ratio between YFP and RLuc expressed proteins (Y/R), reaching a plateau at the higher Y/R. Importantly, the data could be fitted to a one site-specific binding curve (R^2 = 0.982) to generate a logarithmic shaped curve, which reached a plateau, indicative of a specific interaction (Figure 4.11). On the opposite, the BRET ratio relative to the RLuc-UL44 (405-433)/YFP-UL44 BRET pair slowly increased in a linear fashion, without reaching a plateau, indicative of random interaction due to protein overexpression (Figure 4.11).

Such result is of a great importance because, like FRET, BRET is indeed also very sensitive to protein expression levels. Indeed the ability to correlate Y/R to the BRET ratio relative to different BRET pairs has implications to the study of the affinity of a PPI and to the potential identification of SMs disrupting such interaction. Indeed saturation experiments allow to calculate the Bmax (defined as the maximum energy transferred between donor and acceptor) and the B50 (define as the ratio of YFP/RLuc sufficient to generate a BRET ratio equal to 50% of Bmax), respectively depending on the distance and orientation of the two interacting molecules and on the affinity of such interaction (for more details, see §). For RLuc-UL44/YFP-UL44 BRET pair this first set of experiments allowed to calculate a Bmax of 0.65 and a B50 of 3.76.

Our previous results suggested that FRET could detect differences between wild type and mutant versions of UL44 in terms of binding to either UL44 itself or its catalytic subunit. However, differences in FRET values were extremely sensitive to expression levels, and data acquisition was rather complex and time consuming. On the other hand, BRET measurements can be easily performed on thousands of cells in a few seconds. In addition, they offer the possibility to estimate differences in binding affinity by comparing B50 values relative to different BRET pairs. To this

end we decided to compare the effect of a set of amino acids substitutions affecting several UL44 functions on protein dimerization and binding to UL54.

To this end, plasmids mediating the expression of several UL44 mutants N-terminally fused to both YFP and RLuc were generated (see APPENDIX 8.5). These included the dimerization defective UL44-F121A and UL44-L86A/L87A, the UL54 binding impaired UL44-I135A, UL44-Δloop, which bears point mutations within UL44 basic loop and it is therefore impaired in DNA binding, and UL44ΔNLS lacking the NLS. We also included plasmids driving the expression of a fragment of the catalytic subunit UL54 (1125-1242), containing both UL54 NLS and the binding site for UL44 as well as plamsids encoding for UL54 (1145-1213), devoid of the UL44 binding site (see § 1.7). To this end, we transfected $1x10^5$ HEK 293T cells, 24h later seeding in a 24 well plate, using different amount of plasmids mediating the expression of RLuc and YFP plasmids fused to the protein of interest. 48h p.t. cells were processed for detection of fluorimetric (YFP-fusions) and luminescent (RLuc-fusion) expression by using a plate reader, 5' after addition of RLuc substrate CTZ (5μM, see § 3.27). Data showed that most of the point mutations introduced in UL44 mutants fused with RLuc caused reduced protein expression levels (see §4.12). A similar trend was also observed when analysing YFP-UL44 fusion (data not show).

We also analyzed the expression levels of UL54-RLuc fusion proteins. Our data shows that UL54 (1125-1242) expressed less than UL44, impaling reduced stability. However the mutants UL54 (1145-1213) expressed to higher level (Figure 4.12). For subsequent experiments we chose the amount of each plasmid based on the signal generated by RLuc. We have chosen the following amounts of plasmids: 25 ng for RLuc-U44, RLuc-UL44F121A, RLuc-UL44L86/L87, RLuc-UL44Δloop, RLuc-UL44ΔNLS, 50 ng RLuc-UL44I135A, 100 ng for RLuc-UL54 (1125-1242), RLuc-UL54 (1145-1213).

5.5 BRET can accurately quantitate differences in binding affinity between UL44 dimerization defective and UL54 binding impaired mutants in living cells

We decided to use such plasmids to test the ability of BRET to quantitatively detect differences in binding affinity between expressed proteins. To this end, we transfected $1x10^5$ HEK 293T cells, 24h later seeding in a 24 well plate, using different amount of plasmids mediating the expression of RLuc and increasing amount of YFP fusions (0 to 900 ng), processed samples for fluorimeteric/luminometric detection, and calculated saturation curves using data obtained 45 min after CTZ addition. We could detect marked differences in terms of Bmax and B50 (see in §3.27.1) relative to mutant and wild-type proteins, indicating that our assay is able to discriminate even point mutations (see figure §4.7.2). We calculated similar Bmax and B50 values for UL44 self interaction and for its interaction with UL54 (Bmax = 0.64 $\pm$ 0.09 (8) *vs*. 52$\pm$0.15(5), and B50 = 19,04 $\pm$ 13.66 vs. 19.95 $\pm$ 13.88). In particular mutations affecting dimerization such as L86A/L87A and F121A strongly increased the B50 relative to UL44 dimerization (to ca. 90 and 70, respectively), but not those relative to UL54 binding (ca. 10 and 1, respectively). On the other hand, the I135A substitution within UL44 connector loop, essential for the UL44-UL54 interaction specifically increased the B50 relative to the UL44-UL54 interaction (ca. 80), but not relative to UL44 homodimerization (ca. 25). As expected, mutation of UL44 NLS, which selectively affects nuclear import of the protein, did not affect either UL44 dimerization (B_{50} = 11.18 $\pm$ 4.91 (4)) or binding to UL54 (B_{50} = 15.13 $\pm$ 5.43 (2)). Similar results were obtained for the UL44-Δloop mutant, which cannot efficiently bind to dsDNA in cells. Such mutant still efficiently dimerized (B_{50} = 11.31 $\pm$ 2.13 (2)) and bound UL54 B_{50} = 35.37 $\pm$ 12.93 (4). Importantly, all UL44 mutants impaired in DNA binding generated lower B_{max} values both in case of UL44 dimerization and UL54 binding, implying a potential conformational change of UL44 upon DNA binding (Table 4.3, Figure 4.13).

Overall the data shown suggest that BRET is a very fast, simple and semiquantitiative assay, which appears therefore ideal to be used for screening SM compounds able to interfere with UL44 dimerization.

6 Study of UL44 dimerization by GST-pull down *in vitro* method

In order to complete our study of the dimerization of UL44 we wanted to use another assay, an in vitro test.

The pull-down assay is an in vitro method used to determine a physical interaction between two or more proteins. Pull-down assays are useful for both confirming the existence of a protein-protein interaction predicted by other research techniques (e.g., co-immunoprecipitation) and as an initial screening assay for identifying previously unknown protein-protein interactions.

To do this, we performed an assay, using the recombinant proteins 6His-UL44(1-290), 6His-UL44(1-290)-L86/L87A dimerization impaired point mutant, GST-UL44 (1-290) and GST [75, 77]. We incubated the recombinant proteins (see§ 3.31) for 2h at RT in binding buffer (see appendix), using 0.03nmol of either GST or GST-UL44(1-290) fusion protein with 0.12nmol of either 6His-UL44(1-290), 6His-UL44(1-290)L86/L87A. After incubation, the complexes were loaded on glutathione specific columns. After extensive washes with NETN buffer, complexes where eluted with NETN+GSH buffer. Input, Wash and Eluted fractions were electrophoretically separated on 8.5% bis-tris acrylamide gels and analysed by Western Blotting (see §3.33) using a mouse monoclonal antibody anti-6His tag (see 3.34).

Importantly, we could detect a band of the expected molecular weight corresponding 6His-UL44(1-290) relative to the GST-UL44(1-290)/6His-UL44(1-290), complex, but not relative to the GST/6His-UL44(1-290) complex. Intriguingly, the 6His-UL44(1-290)-L86/L87A band, relative to the GST-UL44(1-290)/6His-UL44(1-290)L86/L87A complex was much less intense (Figure 4.14).

These results suggest that GST-pulldown is suitable to monitor UL44 dimerization in vitro and provides an alternative to the in cells methods described in the previous sections.

II Testing the effect of SMs on UL44 dimerization and assays optimization

We previously identified 18 small molecules potentially interfering with UL44 dimerization (see 1.12 . We decided to use our BRET assay to test the effect of such molecule on UL44 dimerization. We reasoned that stable cell lines would offer the advantage of more reliable assays, not being influenced by external factors such as transfection efficiency. Therefore we decided to generate cell lines that expressed stable levels of YFP-UL44.

7. Polyclonal and monoclonal cell lines YFP-UL44

To do so, it is ideal to work at a Y/R which results in a BRET ratio closed to the 50% of the Bmax. Under these conditions, the binding of YFP-UL44 to RLuc-UL44 would not result in saturation, thereby offering an ideal dynamic range to detect SMs decreasing or increasing dimerization. To allow generation of cell lines stably expressing the appropriate amount of YFP-UL44, we initially determined concentration the optimal selection agents (see §3.22). To this end, we seeded HEK293 A $1x10^5$ in 24 well plate and we treated with increasing concentration of each selection agent (puromycin, blasticidin and neomycin, see table §4.5) and cell viability assessed daily for 10 days. We noted that three selection agents acted with very different kinetics (see § figure 4.14 A). Cells treated in puromicyn or blaticidin started to die as early as one or two days post treatment, respectively, while cells treated in neomycin did not exhibit any cytotoxic effect until day 6. Based on our analysis, we chose the minimum concentration sufficient for killing all cells at a specific time point. In particular, for puromycin we chosen 1 µg/ml, for blasticidin 5 µg/ml and for neomycin 700 µg/ml (see § figure 4.15.)

7.1 Generation of stable cells line

We initially decided to generate different polyclonal cell line stably expressing YFP-UL44, with the aim of identifying cell lines expressing the appropriate amount of protein to generate a BRET ratio close to 50% of the B_{max} in the presence of RLuc-UL44. HEK293 A were transduced once, twice, or trice at 12 h intervals with lentiviral supernatant containing either lentivirus pWPI-YFP-UL44-PURO or empty pWPI-puro 48 hour after the transduced, puromycin (1µg/ml) was added to kill any un transduced cells, and cells passage (as describe§ 3.23) We treaded the cell with 1µg/ml of puromycin for 10 days.

7.2 Analysis of stable YFP-UL44 cell lines expression levels and BRET ratio in the presence of transiently expressed RLuc-UL44

In order to verify the right localization, we seeded $1x10^5$ HEK293 A-YFP-UL44 (68-1x, 68-2x, 68-3x) and HEK293 A-pWPI-puro (7-1x, 7-2x, 7-3x) in 24 well plates, and after 24 hour we checked the cells by inverted fluorescent microscope. Our data indicated that increasing the number of transduction rounds also increased proteins expression levels. Also, despite most of YFP-UL44 localized to the cell nuclei, in some cells its localization was mainly cytosolic (see figure § 4.16).

We also tested the expression and the ability to generate a BRET signal. To do this we seeded $1x10^5$ HEK293 A-YFP-UL44 (68-1x, 68-2x, 68-3x) and HEK293 A-pWPI-puro (7-1x, 7-2x, 7-3x) in 24 well plates in duplicate, and after 24 hour we transfected them with either UL44 (25 ng) or RLuc-UL44 (405-433) (12.5 ng) as a control, or pCDNA3 empty vector to calculate background. 48h later cells were processed for BRET analysis. Per each condition, the YFP fluorescent signal generated after excitation at 485 nm (YFP-Net, see §3.27) was recorded, and subsequently the YFP and RLuc

emission values relative to each condition was performed in luminometry, at 5 minutes after the addition of RLuc substrate CTZ (5 µM, see § 3.25).

Our results indicated that all HEK293 A-YFP-UL44 cells expressed the fusion protein to detectable levels, while cells transduced with empty vector did not. (see §4.17A). We also evaluated the BRET ratio at 45 minutes (see § 3.27) generated by the different stable cell lines. Transfections of pWPI-puro empty vector cell line with RLuc-UL44 or RLuc-UL44 (405-433) was used as the background BRET values to calculate BRET ratios. As expected transfection of HEK293 A YFP-UL44 stable cell lines with RLuc-UL44 but not with RLuc-UL44 (405-433) generated a detectable BRET ratio (see §4.17C). Importantly, HEK293 A YFP-UL44 3x generated the higher BRET ratio (0.17) According to our results, we decided to use the YFP-UL44 3x cell line to generate subsequent monoclonal lines.

7.3 Generation of monoclonal stable cell line YFP-UL44

Our data indicated that our polyclonal cell lines mediated the expression of a heterogeneous YFP-UL44 population with a detectable number of cells exhibiting aberrant localization. Therefore, we decided to generate monoclonal cell lines by performing limiting dilution assay (see § 3.23). To this end, we seeded polyclonal stable cells line and HEK293 A- YFP-UL44 (68-3x) 0.5 cells/well into 96 well plates. We monitored the cells and we select only the wells containing one colony. Once the cells reach confluent we transferred them into 24 well plates to be able to evaluate the expression and test their ability to generate a BRET signal. In fact, in accord with previous data we want to select one or more cell lines that generate a BRET signal similar to the B50.

In order to verify what was the monoclonal cell line that would express an optimal level of YFP, we performed an expression test on four monoclonal cell lines (called 1F6, 1B2, 2B3, 1F3), and as controls, we used the polyclonal cell line YFP-UL44 3x and a empty cell line. The first step we

evaluated the YFP levels. The resulted indicated that the YFP expression levels were different for each cells line.

In order to verify the BRET signal, we transfected the cells with RLuc-UL44 (25 ng, 50 ng and 100 ng) and 48h p.t. we analyzed RLuc activity and BRET ratio by plate reader (see § 3.27).

The data obtained show that the lines 1F6, 1B2 and 2B3 express, in terms of YFP levels, more than the polyclonal cell line, and that 1F3 line express much less than the other. For all monoclonal lines the best BRET signal is generated in combination with 25 ng of RLuc, (BRET ratio 45 minutes, 1F6= 0.18±0.06 , 12=0.23±0.00, 2B3=0.19±0.04, 1F3=0.20±0.00.

According to our results, we chose to use in subsequent assays the monoclonal cell line denominated 1B2 because it generates a BRET ratio equal to the B50 when we used 25 ng of RLuc-UL44 (see § Figure 4.18).

8 Probing the effect of DMSO on cell viability

Before testing the effect of SMs on the BRET ratio generated by the 1B2 cell line, we evaluated the effect of DMSO, the agent used for SM resuspension, cell viability by WST assay. In order to do so, we initially identified the optimal number of cells to be seeded by means of cell proliferation curves. To do this, we have seeded different concentrations of cells for 24h (0-10000 cells/well) and 48h (0-5000 cells/well). At the indicated time points post seeding WST substrate was added and plate analyzed using an ELISA plate reader to calculate the cell number. Our results indicate that the assay maintained a good linearity at 24h post seeding at all cell numbers tested. On the other hand, cells seeded for 48h seemed to maintain linearity between cell numbers and signal up to 2500 cells seeded Figure 4.19 A, C). . Therefore, we seeded HEK293 A in 96 well at 24h $1x10^4$ cells/well and $0.5x10^4$ cells/well for 48h and we treaded the cells with DMSO at different concentrations (10%, 1%, 0.1%, 0.01% and 0%). After 24h or 48h depending on the plate, we

added the WST-1 and analyzed the plate by ELISA plate reader. Our data indicated that HEK293 A cells well tolerated a DMSO of 1%, which was then set as the final solvent concentrations of our assay (Figure 4.19 B, D).

9 Probing the effect of DMSO 1% on BRET signal

We similarly tested the effect of the solvent (1% DMSO) on the BRET signal generated after transient transfection with RLuc-UL44 of a polyclonal and a monoclonal stable cell line, HEK293 A pWPI-puro was used as a control.

We seeded $1x10^5$ of cells in 24 well plate and 24h later we transfected polyclonal, monoclonal and HEK293 A-pPWI-puro cells line with RLuc-UL44 (25ng) and HEK293 A with RLuc-UL44 (25 ng) and YFP-UL44 (80 ng) and we used mock-untransfected cells were processed in parallel. 6h p.t. media was replaced with 1% DMSO or with fresh DMEM. 48h p.t. We evaluated the effect of 1% DMSO on YFP expression levels and RLuc activity, and the results indicated that DMSO does not have affect. We, also, evaluated the effect of 1% DMSO on BRET signal relative to each condition, at different time points after substrate addition. According to the results obtained, we can say that there was no difference between BRET signal obtained in DMEM and 1% DMSO. Furthermore, we wanted to verify the robustness of our assay as screening assay for our compounds. To do this, we calculated the Z' score § 3.26. Our results indicate that under every condition tested, DMSO had no negative impact on either BRET ratio or Z' factor, which reached a value > 0.5 starting from 15' post addition of CTZ, (Figure 4.20 C, D).

10 Assessment of Cell viability upon SMs treatment

Before testing the ability of SMs to inhibit UL44 homodimerization, we assessed their effect on cell viability, in order to determine the appropriate concentration to be used in subsequent experiments. To this end WST assays were performed at 48h. We seeded $0.5x10^4$ cells/well HEK293 A in 96 well plate, and we treated the cells with increasing concentrations of each SM (3-200 μM). After 48h of incubation with the SMs, cells were processed as described in §3.29,3.30.

For each SM, the CC_{50} (Cytotoxic Concentration to reduce cells viability by 50%) was calculated using GraphPad Prism software using either a linear regression (Figure 4.21) or with a sigmoidal 4PL logarithmic mode (Figure 4.22). In parallel cell viability was also visually inspections evaluated (see Figure 4.23 and 4.24). Our data showed very different toxicity levels associated to the tested SMs with CC_{50} ranging from c. 10 to > 200 μM (see Table 4.3). In order to screen SMs we chose two different concentration for each SMs (see Table 4.3).

11 Assessment of the Effect of SMs on UL44 dimerization by BRET using the stable YFP-UL44 1B2 cell line transiently transfected with RLuc-UL44

We decided to use the stable YFP-UL44 (1B2) cell line to study the effect of the effect of SMs identified by an *in silico* screening (see §1.12) on UL44 dimerization.

To do this, $1x10^5$ 1B2 stably expressing YFP-UL44 cells were seeded in 24 well plates cells and 24h later cells were transfected with 25 ng of RLuc-UL44 expression plasmid. HEK293A cells were seeded in parallel and transfected either with 25 ng of RLuc-UL44, to allow calculation of background BRET signal, or with both 25 ng of RLuc-UL44 and 40 ng of YFP-UL44, as a positive control. Based on previous experiments, we calculated that such combination of plasmids would result in a BRET ratio similar to 50% of the B_{max}. In order to subtract background due to cell

autoluminescence and autofluorescence, mock-transfected cells were processed in parallel. 6h p.t. media was changed and replaced with DMEM containing either DMSO1% or with two different final concentrations of each SM in 1% DMSO. Such concentrations were selected on the basis of the cytotoxicity assays (see § 3.30, (see Table 4.3). Samples were analysed 48h p.t. to calculate the BRET ratio relative to the Rluc-UL44/YFP-UL44 in the absence or in the presence of the SMs. Our results indicated that treatment with SMs did not cause large variations of BRET ratio. However, three compounds (A4, B6 and C6) at the highest concentration tested, generated a BRET ratio between 30% and 40% lower than the control (see § figure 4.25, Table 4.6).

These results suggested that our BRET assay could in principle detect variations in BRET ratio caused by SMs, but also that the assay in the current setup, might not be sensitive enough to allow identification of all relevant hits. Prompted by these results, we decided to optimize the assay, and re-evaluated the original experimental set up.

12 Optimization experimental set-up for BRET assay

We wanted to optimize our assay in order to have more chances to detect the inhibition of UL44 dimerization upon treatment with molecules. To do this we have re-evaluated the settings of our assay. As a first step, we decided to compare different systems mediating the expression of the BRET pairs and therefore, in addition to the mixed expressing platform tested previously, whereby YFP-UL44 was stably expressed and RLuc-UL44 was expressed transiently, we developed platforms enabling the expression of the BRET pair of interest either in a completely stable or in a completely transient fashion. In addition, we reasoned that increasing the ratio between SM and expressed proteins would have made easier the disruption of protein dimerization. This could be achieved by decreasing the amount of transfected plasmids encoding for RLuc and YFP fusions. However, this is not an easy task since the RLuc signal relative to RLuc-UL44 using our previous setup were already very close to the background, making the reduction of RLuc expressing

plasmids a potentially problematic. Such issue was avoided by decreasing the amount of transfected DNA and using a substrate that generates a RLuc signal ten times higher than CTZ, Coelenterazine-h (h-CTZ).

We also wanted to reduce the time between the treatment of the cells with molecules and their analysis, because we do not know the half-life of the small molecules. Indeed the time between SMs addition and sample processing was reduced from 48 hours p.t. to 24 hours p.t. Finally; we also included a control molecule, AL18 (see § 1.11), known to disrupt the UL54-UL44 interaction, as a positive control for our assay. We also tested the effect of SMs on the control protein RLuc-YFP to determine if the effect of the SMs was specific, as negative control.

12.1 Development of additional biological expression systems to study UL44 dimerization by BRET

In order to verify which biological expression system was the most appropriate to detect inhibition of UL44 dimerization, we decided to express our BRET pairs from three distinct expression systems. In addition to the transient/stable setting, whereby Rluc-UL44 was transiently expressed in a YFP-UL44 stably expressing cell line, we also generated cell lines stably expressing both RLuc-UL44 and YFP-UL44 (stable/stable expression system) and compared them to a transient/transient expression system, whereby RLuc-UL44 and YFP-UL44 are both transiently expressed. Such expression systems were then challenged in inhibition experiments, whereby the ability of an overexpressed, non-labelled competitor such as FLAG-UL44, to decrease the BRET ratio was tested. To do this we generating double monoclonal stable cells line expressed optimal levels of RLuc-UL44 and YFP-UL44.

12.1.1 Generation double stable cells line from 1B2

The generation of double stable cells line has been done starting from the HEK293A monoclonal cell line 1B2, stably expressing high levels of YFP-UL44. Such cell line was transfected with pre-linearized RLuc-UL44 in a 6 well plate (see §3.21), and cells expressing RLuc-UL44 were selected by treatment with neomycin (700 μg/ml). When cells reached confluence, they were expanded to a T25 flask. When the cells reached confluence they were subjected to limited dilution assays by being seeded at in 96 well plates described (SS).

After 14 days, we could select 13 wells that contained one colony per well. When cells became confluent their content was split to two independent wells. One well was used for subculturing, the other one was used to assay fluorimetric and luminometric signals as described in (§3.27), thus also allowing to monitor the BRET ratio generated, by using a plate reader 45' post CTZ (5 μM) addition.

The results obtained here indicate that the tested cell lines generated variable YFP fluorescent signal, despite originating from the monoclonal cell line 1B2 (Fig. 4.26 A). The luminometric RLuc signal was even more variable, and in four cases it was indistinguishable from the background (Fig. 4.26B). Importantly, six cell lines generate a BRET ratio higher than the background (see figure 4.26 C). Cell line G5A was selected for further analysis because generated a BRET signal very close to 50% of the Bmax previously calculated for the RLuc-UL44/YFP-UL44 BRET pair, in combination with low but detectable RLuc activity (see figure §4.26 B, C).

13 BRET inhibition experiments

In order to identify the most suitable biological expression system to allow selective screening, we compared all the systems generated in inhibition experiments. To do this, we seeded 1B2, G5A and HEK293 T $1x10^5$ in 24 well plates. 24 hours later, 1B2 cells were transfected using 25ng RLuc-

UL44, and HEK293T cells were transfected 25 ng of RLuc-UL44 and 40 YFP-UL44, combinations which - based on our previous experiments - result in a BRET ratio close to half of the Bmax. Since cell line G5A already express an optimal ratio of RLuc-UL44 and YFP-UL44, it was transfected with neither RLuc nor YFP-UL44 expression plasmids. All cell lines were also transfected with increasing amounts of a competitor expressing plasmid FLAG-UL44 (0-900 ng), which would be expected to disrupt the YFP-UL44/RLuc-UL44 complexes. As negative control, a parallel set of cells was transfected with increasing amounts of a plasmid expressing FLAG-UL42, the monomeric processivity factor of Herpes Simplex Virus-1 (§1.8). Samples were then processed for BRET measurements 48h p.t. as described in §3.27. Surprisingly, we could not detect any inhibition of the BRET ratio relative to G5A stable cell line (stable/stable expression system, Figure 4.27A), whereas clear inhibition was detected for both the transient/stable expression system (1B2 + Rluc UL44; Figure 4.27I) and for the transient/transient expression system (HEK293 T + RLucUL44 and YFP-UL44; Figure 4.27E). The latter system generated maximum observable inhibition (up to 70% reduction in BRET ratio) upon overexpression of FLAG-UL44. Much milder effects observed upon overexpression of FLAG-UL42. Importantly, both overexpression of UL44-FLAG and UL42-FLAG, similarly affected YFP-UL44 expression levels, stressing the specificity of the inhibition (Figure 4.7C, D, G, H, M, N). These results suggest that stable expressing systems are not ideal to detect the disruption of PPI in BRET assays, most likely because of the difficulty of disrupting a pre-existing protein-protein complex as compared to the prevention of the formation of a similar complex. According to our result, we have decided to use to screen for SMs inhibitors of the UL44-UL44 interaction a transient expression system.

14 Substitution of CTZ with h-CTZ allows to decrease plasmid amount required for BRET assays

Our previously performed BRET-based screening did not allow identification of SMs interfering with UL44 dimerization by more than 40% (see §5). Therefore, we reasoned that this could be the consequence of the high protein expression levels used in the assay. In such assay, cells were transfected with high amounts (25-100 ng) of RLuc expressing plasmids, required to generate a RLuc signal sufficiently higher from the background to perform the analysis. This would result in very high SMs amounts necessary to mediate PPI inhibition. In principle, lowering protein expression levels would also facilitate the disruption of a PPI by a given SM concentration. We therefore set out to decrease protein expression levels in our BRET assays. All previous BRET experiments were performed using Coelenterazine-n (CTZ) as a substrate for RLuc. RLuc can also use Coelenterazine-h (h-CTZ) as a substrate, which results in higher emission in comparison to CTZ. We therefore decided to test the possibility to use h-CTZ with the purpose of lowering the levels of expressed proteins in the context of the RLuc-UL44/YFP-UL44 and RLuc-UL54/YFP-UL44 BRET pairs expressing plasmids. To this end, we transfected HEK293 T cells with different amounts of RLuc-UL44, in triplicate and 24 h p.t. RLuc activity was quantified using a plate luminometer as described in §3.27. In order to subtract background due to cell autoluminescence, mock-transfected cells were processed in parallel. RLuc activity was then recorded at different time points after substrate addition, starting from 5 min. Since we expected incubation with h-CTZ to result in higher signal as compared to CTZ, we transfected lower amounts of plasmid as compared to what usually done for CTZ (25ng of RLuc-UL44).

Interestingly, h-CTZ derived luminescent signal appeared more stable over time as compared to that derived from CTZ. Indeed, h-CTZ generated RLuc signal peaked at 15 min post substrate addition, and being 100% of that obtained 5 min after substrate addition 30 min later. On the other hand, by that time, CTZ derived luminescent signal after 30 min was 70%, lower than showing a more rapid decay (Figure 4.28 A). In the subsequent analysis we therefore focused on RLuc signal generated at 15' post substrate addition.

We also studied the influence of h-CTZ concentration on signal intensity, and incubated cells with increasing amount of the substrate (5, 10 and 20 μM, respectively). Importantly, increasing concentrations of h-CTZ over a 5-20 μM range did not significantly affected RLuc signal (Figure 4.28 B). For this reason, we decided to use 5μM h-CTZ concentration for subsequent experiments. Importantly, we observed detectable signal already with 1 ng of RLuc-UL44, suggesting that it might be possible to significantly decrease the amount of plasmids for BRET studies (Figure 4.28 B).

We subsequently decided to evaluate the optimal amount of RLuc-UL44 and RLuc-UL54 plasmids to transfect in order to obtain a luminescent signal of about 4000 RLU. This, considering the expected inter-assay variability, would reasonably ensure to obtain a signal distinguishable from the background in future experiments. We performed an experiment transfecting HEK239 T cells with increasing amounts of RLuc-UL44 (1; 2.5 and 5 ng, respectively) and Rluc-UL54 (2.5; 5 and 10 ng respectively), and detected RLuc activity 24h and 48 h p.t. after the addition of 5μM h-CTZ. Both for the 24h and 48h pt. experiments, we measured optimal RLuc activity transfecting 2.5ng of RLuc-UL44 and 10ng of RLuc-UL54 expression plasmids (Figure 4.28C). These amounts are 10 times lower as compared from those required to generate similar signals using CTZ as substrate. Therefore, subsequent experiments were performed with such quantity of plasmid DNA.

14.1 BRET saturation curves

Once identified the optimal amount of the BRET donor (RLuc fusions) plasmids to be used in transfection assays, saturation experiments were performed in order to calculate Bmax and B50 values, which would then be used to determine the amount of BRET pair plasmids to be transfected for inhibition experiments. To this end a fixed amount of donor plasmids (2.5 ng for RLuc-UL44 and 10ng for RLuc-UL54) were transfected with increasing amounts of the acceptor plasmids (YFP-UL44; 0-180 ng) in HEK293 T cells. Experiments were performed five times. Briefly,

transfected cells were processed (see §3.27) to calculate BRET ratio and YFP/RLuc values relative to each condition, and generate BRET saturation curves, which then allowed to calculate Bmax and B50 values as described in §3.27.1.

Previously we calculated saturation curves using data obtained 45 min after CTZ addition. This was mainly because BRET signal at earlier time points was either too low or too variable (Di Antonio et al., unpublished). Since h-CTZ appears to generate a more stable RLuc signal over time as compared to CTZ (see Figure 4.29A), we firstly re-assessed the optimal time to calculate BRET ratio to be plotted for generation of saturation curves. We considered the variations over time of both RLuc and BRET ratio for both the RLuc-UL44/YFP-UL44 and RLuc-UL54/YFP-UL44 BRET pairs obtained using maximum amounts of acceptor plasmid (YFP-UL44 180 ng), relative to the h-CTZ substrate and compared them to those previously obtained for the CTZ substrate under similar conditions (YFP-UL44 900 ng) (Figure 4.29). Our results indicate that for both RLuc-UL44 and RLuc-UL54, h-CTZ allowed to reach a signal comparable to that obtained with CTZ, using 1/10 of donor plasmid (Figure 4.29 A, E). As mentioned earlier such signal was more stable over time as compared to CTZ (Figure 4.29 B, F). As compared to those observed for CTZ, BRET ratios appeared higher (Figure 4.29 C, G) and more stable (Figure 4.29 D, H), with stable signals already obtained 15 min post substrate addition. Therefore, we used data generated 15 min post substrate addition for further analysis, thus also reducing the experimental time required for the procedure for data acquisition from 45 to 15 min. In order to reduce inter assay variability, YFPnet/RLuc values were also normalized for those obtained for the control BRET expressing construct RLuc-YFP (15 min after h-CTZ addition). As expected, lowering the amount of transfected Rluc expression plasmid, the BRET signal reached saturation by transfecting lower amounts of YFP expression plasmids. For UL44-UL44 self-dimerization we calculated Bmax values of 0.49 ± 0.18 and of 0.76 ± 0.13 at 24h and 48h p.t. respectively. Similarly, we calculated B50 values of 2.47 ± 2.62 and of 7.52 ± 5.51 at 24h and 48h pt respectively (see Table 4.4 A, Figure 4.30). These values are consistent with a specific PPI. For the UL54-UL44 interaction we calculated Bmax values of 0.46 ±

0.07 and of 0.51 ± 0.16, at 24h and 48h p.t. respectively, and B50 values of 2.69 ± 1.72 and of 3.40 ± 2.19 at 24h and 48h p.t. respectively (see Table 4.5 B, Figure 4.30). Normalization of the YFP/RLuc values using that relative to the RLuc-YFP fusion control protein (see §3.27.2), offered the possibility to compare Bmax and B50 values calculated using h-CTZ and CTZ, which resulted almost identical (Table 4.5, Figure 4.30).

Since it is advisable to perform BRET inhibition assays using amounts of BRET expressing plasmids resulting in a YFP/Rluc value close to the B50 value, we identified the ng of acceptor plasmid required to fulfil this condition. According to our analysis, 40 ng and 22 ng of YFP-UL44 were selected for both pairing with RLuc-UL44 and RLuc-UL54 at 24h and 48h p.t., respectively.

14.1.1 BRET competition curves

We then decided to verify it our new BRET assay setup allowed to detect a reduction of BRET ratio for the UL44-UL44 and UL44-UL54 interaction upon overexpression of a competitor. To this end, HEK293 T cells were transfected using the identified BRET pair quantities (RLuc-UL44/YFP-UL44 2.5 ng + 40 ng; RLuc-UL54/YFP-UL44 10 ng + 40 ng), in the presence of increasing amounts of a competitor expressing plasmid FLAG-UL44 (0-180 ng). As negative control, a parallel set of cells was transfected with increasing amounts of a plasmid expressing UL42, the processivity factor of Herpes Simplex Virus-1 (FLAG-UL42). Samples were then processed for BRET measurements 48h pt as described in §3.27.3. We performed one experiment using h-CTZ (Figure 4.31) and we compared the results to those obtained using CTZ and cells transfected with higher amount of plasmids (Figure 4.30). As expected, overexpression of FLAG-UL44 resulted in a much stronger inhibition of the BRET signal, as compared to the control molecule FLAG-UL42. Importantly, both overexpression of UL44-FLAG and UL42-FLAG, similarly affected YFP-UL44 expression levels, stressing the specificity of the inhibition (Figure 4.31C, D, G, H). Overall the extent of inhibition was similar to that obtained using CTZ as substrate which however required

much higher amounts of competitor expressing plasmid to be transfected (Figure 4.30). Therefore, h-CTZ allowed to reach similar inhibition of BRET signal, using lower amounts of competitor expression plasmid. Consequently, we planned to use these new BRET assay setups to screen for SMs inhibitors of the UL44-UL44 interaction.

14.1.2 Effect of SMs on UL44 dimerization as assessed by BRET using h-CTZ

We then used our modified BRET setup to investigate the effect of our SM library to affect UL44 dimerization. To this end, $2x10^4$ 2HEK293 T cells were seeded into 24 well plates. Cells were transfected 24 h later with 2.5 ng of Rluc-UL44, alone or in the present of 40ng of YFP-UL44. In order to subtract background due to cell autoluminescence and autofluorescence, mock-transfected cells were processed in parallel. 8h p.t. media was changed and replaced with either DMEM containing either 1% DMSO or with two different final concentrations of each SM. Samples were analysed 24 h pt to calculate the BRET ratio relative to the Rluc-UL44/YFP-UL44 in the absence or in the presence of the SM. The addition of SMs only mildly affected the BRET ratio, with a small reduction relative to the B6 and C6 molecules (Figure 4.33). These results did not significantly differ from those obtained with the previous experimental set-up, implying that reduction of SM incubation time and amount of proteins expressed do not increase their inhibitory effect as assessed by BRET.

15 Analysis of the effect of SMs on BRET relative to the control RLuc-YFP fusion protein

We decided to investigate the specificity of the observed inhibition of BRET signal relative to UL44 dimerization. Indeed, a decrease of BRET signal upon treatment with SM can depend on several factors other than the disruption of the PPI of interest. This can be the result of light emission or fluorescence of the molecule that would alter the calculations of the BRET values, as

well as from interference of the molecule with the energy transfer due to conformational changes of the donor and acceptor moieties. We therefore tested the effect of treatment with the most promising compounds on the BRET ratio of the Rluc-YFP fusion control molecule. This is a fusion protein between RLuc and YFP and constitutively undergoes BRET as a consequence of energy transfer from RLuc to the neighbouring YFP.

To this end, we transfected HEK293 T cells with the appropriate amounts of RLuc-UL44 and YFP-UL44 expression plasmids, or of the RLuc-YFP control molecule. In order to subtract background due to cell autoluminescence, mock-transfected cells were processed in parallel. 8h pt media was replaced DMEM containing either DMSO1% or with two different final concentrations of the SMs A6, B6 and C6h. 24h pt cells were processed to calculate BRET ratio, YFPnet and RLuc activity relative to each condition. Subsequently we calculated the precent of inhibition relative to each sample due to treatment with the SMs (Figure 4.34). Our results indicate that treatment with SM A6 and C6 neither affected the BRET ratio relative to RLuc-UL44/YFP-UL44, nor that relative to RLuc-YFP. Surprisingly, treatment of cells with B6 decreased to similar extent the BRET ratio relative to RLuc-UL44/YFP-UL44, and that relative to RLuc-YFP. These data suggest that the observed inhibition of BRET ratio after treatment with B6 is likely not the effect of the inhibition of the UL44 homodimerization.

16 Effect of AL18 on the UL54-UL44 interaction as detected by BRET

We therefore wished to assess if our BRET assay was capable of detecting the disruption of a known PPI as mediated by a molecule known to interfere with such process. To this end we choose to test the effect of AL18, known to disrupt the UL54-UL44 interaction in vitro and to impair viral replication in cells (see Introduction §1.11). To this end, we transfected HEK293 T cells with the appropriate amounts of plasmids expressing RLuc-UL54 and YFP-UL44, as well as RLuc-UL44

and YFP-UL44, or the RLuc-YFP control molecule as controls. In order to subtract background due to cell autoluminescence, mock-transfected cells were processed in parallel. 6h p.t. media was replaced DMEM containing either DMSO1% or with two different final concentrations of AL18. 24h and 48h p.t. cells were processed to calculate BRET ratio, YFPnet and RLuc activity relative to each condition (§3.27). Subsequently, we calculated the precent of inhibition relative to each sample due to treatment with AL18. Our results indicate that AL18 does not interfere with the BRET ratio relative to the negative control at all time p.t. tested. However, at 24h p.t. no effect was observed on the BRET ratio relative to RLuc-UL54/YFP-UL44, while a mild, although dose dependent inhibition of the BRET ratio relative to RLuc-UL44/YFP-UL44 was detected (Figure 4.35). This scenario did not change much 48h later, with AL18 causing a 20% decrease of the BRET ratio relative to RLuc-UL54/YFP-UL44RLuc-YFP at the highest concentration tested (Figure 4.36), but inhibiting the BRET ratio relative to RLuc-UL54/YFP-UL44 to significantly higher extent in a dose dependent manner (up to 50%). These results suggest that our BRET set up might not be sensitive enough to be used as a screening tool to identify molecules disrupting protein-protein interactions.

17 Analysis of the effect of AL18 on the UL44/UL54 interaction as assessed by FRET acceptor photobleaching

After the validation of FRET acceptor photobleaching as a method to detect the interaction between FRET pairs (§3.28,) we verified its reliability for the screening of small molecules inhibiting specific PPI. Since FRET is extremely time consuming as compared to BRET, we decided to initially test the ability of small molecule AL18, which is known to impair the UL54-UL44 interaction (see Introduction §1.8), but which failed to specifically reduce the BRET ratio relative to RLuc-UL54/YFP-UL44, (see Figure 4.11) to selectively reduce FRET efficiency relative to CFP-

UL54/YFP-UL44. We therefore transfected HEK293 T cells with the fFRET pairs CFP-UL54/YFP-UL44, CFP-UL54/YFP-UL44-I135A, CFP-UL44/YFP-UL44, and CFP-YFP using condition A (Table 4.2), as well as with donor expression plasmids alone. Media was changed 8h p.t. and substituted with DMEM containing either DMSO 1% or AL18 at 3μM and 30 μM (in 1% DMSO final concentration). Samples were processed 48h p.t. for localization studies and FRET acceptor photobleaching (§3.28 and §3.28.2). Treatment with AL18 did not seem to significantly affect the subcellular localization of the proteins expressed, as assessed by CLSM analysis (Figure 4.37). Importantly, AL18 did not caused a specific inhibition of FRET efficiency relative to the CFP-UL54/YFP-UL44 FRET pair (Figure 4.38A). In addition, neither FRET efficiency of the control fusion protein CFP-YFP, nor of the CFP-UL44/YFP-UL44 and CFP-UL54/YFP-UL44-I135A FRET pairs, were affected by treatment by AL18 (Figure 4.37A). Likewise, AL18 treatment did not affect FRET relative to expression of CFP expressed alone (Figure 4.37B). Therefore, we reasoned that FRET acceptor photobleaching, similarly to BRET, probably it is not suitable to identify SMs able to interfere with PPI.

17.1 Analysis of YFP and CFP correlation with FRET efficiency upon AL18 treatment

As for previously analysed samples (§4.3.), we investigated if there was a correlation between the fluorophores expression levels and the FRET efficiency as after treatment of cells with AL18. The same frequency of correlation was found between FRET efficiency and YFP or CFP expression (19% of cases for both, Figure 4.19 and Figure 4.20). As expected, correlation between YFP and FRET efficiency was always positive (reaching maximum Pearson r value of 0.80), while that between CFP and FRET efficiency % was preferentially negative (reaching a minimum Pearson r value of -0.95). Subsequently, we investigated whether the decreased in FRET efficiency caused by treatment of cells expressing CFP-UL54/YFP-UL44 was due to an alteration of the expression

levels of the two proteins. To this end, we compared CFP (Figure 4.21B) and YFP (Figure 4.21A) expression levels of the different FRET pairs, in the presence or in the absence of AL18, and found no marked differences.

18 Identification of SMs inhibiting UL44 dimerization by GST-pull down

Since our BRET based assay failed to identify any molecule specifically inhibiting UL44 dimerization, and our FRET acceptor photobleaching assay failed to detect the effect of positive control molecule AL18 on UL44/UL54 interaction, we reasoned that an in vitro method might be better suitable to our aim. To this end we decided to test the effect of the 18 SMs identified as potentially important for UL44 dimerization by means of GST pull down assays. We initially tested the effect of DMSO on the ability of GST-UL44(1-290) to bind to 6His-UL44. To this end, recombinant proteins were incubated for 2h, either in binding buffer alone, or in binding buffer containing DMSO 1%, before being processed for GST-pull down analysis as described in (§ 3.31). Analysis of input, wash and elution fractions by Western blotting (see §3.34) using a mouse monoclonal antibody anti-6His tag (clone His-1, Sigma, 1:2500). We detected the immunocomplex by goat anti-mouse immunoglobulin Ab conjugated to horseradish peroxidase (HRP, Santa Cruz Biotech, 1:2000) and visualized them with using a Versadoc image station (Biorad). Our analysis revealed that DMSO negatively affected binding of GST-UL44(1-290) to 6His-UL44(1-290) (Figure 4.3). For this reason, we decided to test the effect of SMs on UL44 dimerization at the lowest DMSO concentration possible, i.e. 0.25%. We subsequently incubated the recombinant proteins for 2h in 0.25% DMSO, in the presence or in the absence of the SMs (50 μM), or of AL18 as a negative control, before proceeding with GST-pull down assays as described above. A first screening of indicated that some molecules, such as A6, B6, an AL18 appear to have positive effect on dimerization, while other molecules appeared to inhibit the formation of the complex (see Figure 4.4), in particular the most extreme inhibition was observed upon incubation of GST-UL44 (1-290)

and 6His-UL44(1-290) in the presence of SMs A4, B1, B2, B3, B4 and C6. A repetition of such experiment is currently being performed.

5. DISCUSSION

HCMV is a major human pathogen, whose genome is replicated via a rolling circle mechanism in the nucleus of infected cells by a number of cellular and viral proteins. Among them, the DNA polymerase holoenzyme is strictly required for viral genome replication. Such enzyme is composed by a catalytic subunit, UL54 and a processivity factor UL44, which tethers the holoenzyme to dsDNA. The latter protein functions as a dimer, and dimerization is essential for DNA binding. Since SMs have already been identified as capable of inhibiting HMCV replication by mediating disruption of the UL44/UL54 complex, we reasoned that it might be possible to identify compounds hindering viral replication by targeting the dimerization of UL44. This idea was fostered by the recent crystallization of UL44 N-terminal dimeric structure, which revealed a surface potentially amenable to drug targeting. Before the start of this thesis, a virtual screening had been performed to identify 137 SMs potentially targeting UL44 dimerization and elected the 18 ideal candidates by means of visual inspection.

In the current study we initially dedicated great efforts to the development of assays to monitor UL44 dimerization. In particular we develop two new in cell based assays which could confirm that UL44 dimerizes in a cellular context, further extending earlier results that showed that UL44(1-290) exists as a dimer *in vitro* [56], and that UL44 can dimerize in cells before nuclear translocation occurs [49, 61]. Indeed our study provides the first quantitative assays of UL44 dimerization in cells by means of FRET and BRET experiments (see Figs.). Furthermore, our assays performed with hCTZ as substrate showed dimerization of UL44 at very low protein expression levels, deriving by transfection with as low as 2.5 ng of plasmid DNA per a 24 well plate of HEK293-T cells, thus suggesting that UL44 is very likely to dimerize in the context of the viral infection, where it is expressed to very high levels.

Furthermore our BRET assays calculated very similar B50 values for the UL44/UL54 interaction and for UL44 dimerization (CTZ:, hCTZ: normalized CTZ, normalized hCTZ). This interesting because these data suggest that the dissociation constant (Kd) of the UL44 homodimerization in living cells is very similar to that of the UL54-UL44 interaction. Since the UL54-UL44 interaction has been successfully disrupted by the SM AL18, which is capable of interfering with HCMV replication [71] it is therefore hypothesaziable that the UL44 dimerization could be similarly disrupted. It should be noted that the Kd calculated for the UL54/UL44 interaction (700 nM) and for UL44 dimerization (243 nM) *in vitro*, are almost three times different uM [56, 78]. This difference is in apparent contrast with the data reported here, and most likely depend on the fact that different methods were used to analyze UL44/UL54 interaction and UL44 dimerization *in vitro*. In particular the binding between UL44 and UL54 was studied using, isotermal titration calorimetry and UL44 dimerization was studied using gel filtration. In addition, it should be mentioned that in vitro studies were performed using UL44(1-290) a C-terminal deletion mutant devoid of UL44 C-terminal 143 aa. Furthermore, our BRET assays revealed that several UL44 point mutants unable to bind DNA, but still capable of both binding to UL54 and dimerizing, such as UL44-Δloop, and UL44ΔNLS, exhibited reduced B_{max} values, without significant changes in B_{50} when challenged for binding to UL54 or for dimerization. Such findings are of interest because they might suggest that UL44 can change conformation upon DNA binding, thus resulting in a change in efficiency of energy transfer. Consistently it has been shown that UL44 dimeric conformation changes upon binding to UL54 [59], and that UL44 can be efficiently sumoylated on multiple residues only upon DNA binding [54].

By generating cell lines stably expressing YFP-UL44 as well as YFP-UL44 in the presence of RLuc-UL44 to levels very similar to those needed to generate a BRET ratio similar to 50% of the Bmax, and comparing the ability of such systems to undergo a reduction in BRET ratio after overexpression of a competing FLAG-tagged version of UL44, we could show that transiently

expressing YFP-UL44/RLuc-UL44 cells were more prone to inhibition of stably expressing cell lines. This is probably due to the difficulty of disrupting a pre formed complex [79].

Unfortunately, the in cells assays developed in this study were not sensitive enough to enable the discovery of SMs inhibiting UL44 dimerization. This is further highlighted by the failure of such assays to detect any inhibition of the UL54/UL44 interaction as mediated by the positive control molecule AL18, a well-known inhibitor of HCV DNA polymerase holoenzyme formation.

While in the case of FRET-based assay such phenomenon can be explained by the high expression levels required to generate a positive signal, in the case of BRET this could not be the exploitation. Indeed, extensive assay optimization lead to the possibility to detect UL44 dimerization at very low protein concentrations. The reason for such failure might depend on the fact that some compounds might interfere with RLuc mediated luminescence or with YFP fluorescence, thus masking the potential disruption of the interaction by creating art factual BRET measurements. For these reasons, in the last part of our study we started to adopt an in vitro assay, based on previously described GST-pull-down approach, to monitor UL44 dimerization *in vitro*. By performing a first screening of the SMs we could identify several potential candidates potentially interfering with UL44 dimerization. GST-pull down assays have been previously adopted to monitor the disruption of PPI [77]. We are currently re-testing the effect of SMs on UL44 dimerization by means of GST-pull down assays.

6. RESULTS TABLES AND FIGURES

Table 4.1

FRET plasmids		Conditions (ng) A	B
CFP-UL44		250	
CFP-UL44	+ YFP-UL44	125 + 125	60 + 60
CFP-UL44-L86/L87A	+ YFP-UL44-L86/L87A	450 + 450	250 + 250
CFP-UL54		250	
CFP-UL54	+ YFP-UL44	125 + 125	500 + 125
CFP-UL54	+ YFP-UL44-I135A	125 + 125	500 + 125
CFP + YFP		125 + 125	
CFP-YFP		250	
CFP		250	

Table 4.2

	YFP			CFP		
SETTING	Laser 514nm	Gain	Offset	Laser 458nm	Gain	Offset
1	20%	616	-2	31%	629	-2
2	13%	671	-2	15%	658	-2
2 BIS	5%	574	-2	15%	614	-1
3	5%	574	-2	45%	614	-2
4	11%	607	-2	31%	629	-2
5	12%	561	-1	45%	614	-2
6	11%	607	-2	40%	629	-2
7	60%	596	-1	33%	605	-2
8	20%	565	-2	45%	614	-2
9	5%	574	-2	9%	601	-2
10	9%	574	-2	12%	601	-2

Table 4.3

Table 1.1 Effect of point mutations of UL44 on indicated properties

UL44 mutant	UL54 binding		UL44 dimerization		DNA binding		Viral DNA replication[7]	Localization in Transfected cells[8]
	in vitro[1]	*in cells*[2,3]	*in vitro*[4,5]	*in cells*[1,3]	*in vitro*[4,5]	*in cells*[6]		
wild-type	0.7 μM	yes, 0.52±0.15, 19.96±13.88 (5)	dimer, 243 nM	dimer, 0.64±0.09; 19.04±13.66 (8)	yes, 1 nM	yes	yes	nuclear, speckled
F121A	0.7 μM	yes, 0.24±0.01, 0.97±0.24 (2)	monomer, ND	monomer, 0.59±14; 91.20±47.76 (8)	weak, 8-10 nM	NA	no	nuclear, mainly diffuse
L866/L867A	0.7 μM	yes, 0.24±0.07, 11.47±9.75 (4)	monomer, ND	monomer, 0.26±0.11; 73.64±25.72 (6)	very weak, 80-100 nM	weak	no	nuclear, diffuse
I135A	no	no, 0.14±0.02, 81.17±24.34 (3)	NA	dimer, 0.77±0.15, 25.45±15.37 (5)	yes	NA	no	nuclear, speckled
ΔFL-loop	NA	yes, 0.31±0.09, 35.37±12.93 (4)	NA	dimer, 0.45±0.06; 11.31±2.13 (2)	NA	weak	no (TDN)	nuclear, diffuse
wt/ΔFL-loop	NA			NA, 0.48±0.07, 30.40±7.66 (6)				
ΔNLS	NA	yes, 0.23±0.02, 15.13±5.43 (2)	NA	dimer, 0.44±0.06, 11.18±4.91 (4)	NA	NA	NA	cytosolic

Table 4.4

A

	CC50	R^2	concentration tested (μM)
A1	80.54[1]	0.98	50/25
A2	>200[2]	0.06	200/100
A3	200[2]	0.84	50/25
A4	8.36[1]	0.99	4/2
A6	138.52[2]	0.86	75/25
B1	248.73[2]	0.7	100/50
B2*	56.13[2]	0.82	25/12.5
B3	210.89[2]	0.85	50/25
B4	40.99[1]	0.99	20/10
B5	>200[2]	ND	100/50
B6	12.85[1]	0.96	6/3
B7	36.47[1]	0.99	12/6
B8	212[1]	0.91	40/20
C1	>200[2]	ND	50/12.5
C2	240.77[2]	0.79	50/25
C3	766.43	0.95	100/50
C4	225[2]	0.57	25/12.5
C6	24.2[2]	0.67	100/50
AL18	121.915±1.5[2]	0.94-0.92	30/3

B

	CC50	R^2	concentration tested (μM)
A1	57.02[1]	0.69	50/25
A2	ND[2]	0.15	200/100
A3	41.52[2]	0.81	50/25
A4	3.83[1]	0.61	4/2
A6	316.60[2]	0.79	75/25
B1	ND[2]	ND	100/50
B2*	74.65[2]	0.65	25/12.5
B3	35.87[2]	0.76	50/25
B4	40.06[1]	0.85	20/10
B5	ND[2]	ND	100/50
B6	12.76[1]	0.75	6/3
B7	29.39.47[1]	0.90	12/6
B8	ND[1]	ND	40/20
C1	26.18[1]	0.62	50/12.5
C2	269.60[1]	0.79	50/25
C3	393.44[2]	0.16	100/50
C4	189.94[2]	0.30	25/12.5
C6	240.2[1]	0.67	100/50
AL18	51.25[2]	0.49	30/3

Table 4.5

A

RLuc-UL44/YFP-UL44		
CTZ (25/0-900 ng)		
	Raw	Normalized
Bmax	0.64 ± 0.11 (6)	0.72 ± 0.18 (3)
B50	24.06 ± 12.55 (6) *	14.87 ± 9.63 (3)
h-CTZ (2.5/0-180 ng)		
	Raw	Normalized
Bmax	0.76 ± 0.13 (5)	0.80 ± 0.14 (5)
B50	7.52 ± 5.51 (5) *	20.96 ± 14.14 (5)

B

RLuc-UL54/YFP-UL44		
CTZ (100/0-900 ng)		
	Raw	Normalized
Bmax	0.62 ± 0.10 (6)	0.47 ± 0.02 (2)
B50	29.31 ± 9.64 (6) *	11.2 ± 7.83 (2)
h-CTZ (10/0-180 ng)		
	Raw	Normalized
Bmax	0.51 ± 0.16 (5)	0.54 ± 0.19 (5)
B50	3.40 ± 2.19 (5) *	13.50 ± 8.55 (5)

Table 4.6

NEOMICIN (µg/ml)					
0	50	100	200	300	400
500	600	700	800	1000	2000
PUROMICIN (µg/ml)					
0	0.3	0.4	0.5	0.6	0.7
0.8	0.9	1	2	3	6
BLASTICIDIN (µg/ml)					
0	0.6	0.7	0.8	0.9	1
2	3	4	5	10	20

Table 4.7

Name	Concentration	BRET retio
A1	50 μM	0,19
	25 μM	0,23
A2	75 μM	0,22
	25 μM	0,25
A3	75 μM	0,25
	25 μM	0,27
A4	6.12 μM	0,24
	3.12 μM	0,24
A6	75μM	0,18
	25μM	0,25
B1	75μM	0,23
	25μM	0,24
B2	75μM	0,22
	25μM	0,26
B3	75 μM	0,22
	25 μM	0,24
B4	50μM	0,25
	25μM	0,23
B5	75μM	0,26
	25μM	0,22
B6	75μM	0,13
	25μM	0,21
B7	75μM	0,20
	25μM	0,28
B8	50μM	0,24
	25μM	0,25
C1	75μM	0,23
	25μM	0,26
C2	75μM	0,26
	25μM	0,25
C3	75μM	0,26
	25μM	0,25
C4	25 μM	0,25
	12.5 μM	0,23
C6	50μM	0,24
	25μM	0,18

Figure 4.1

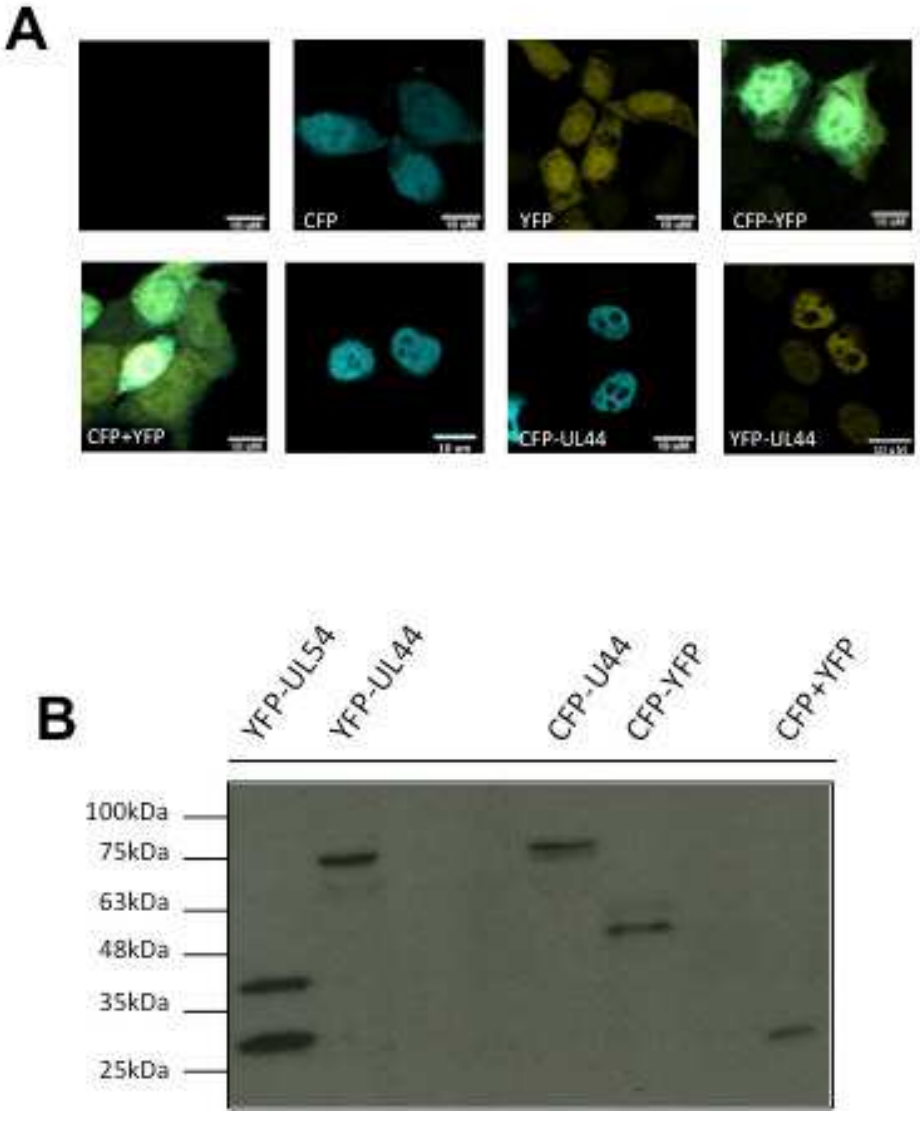
A
CFP
YFP
CFP-YFP
CFP+YFP
CFP-UL44
YFP-UL44
B
YFP-UL54
YFP-UL44
CFP-U44
CFP-YFP
CFP+YFP
100kDa
75kDa
63kDa
48kDa
35kDa
25kDa

Figure 4.2

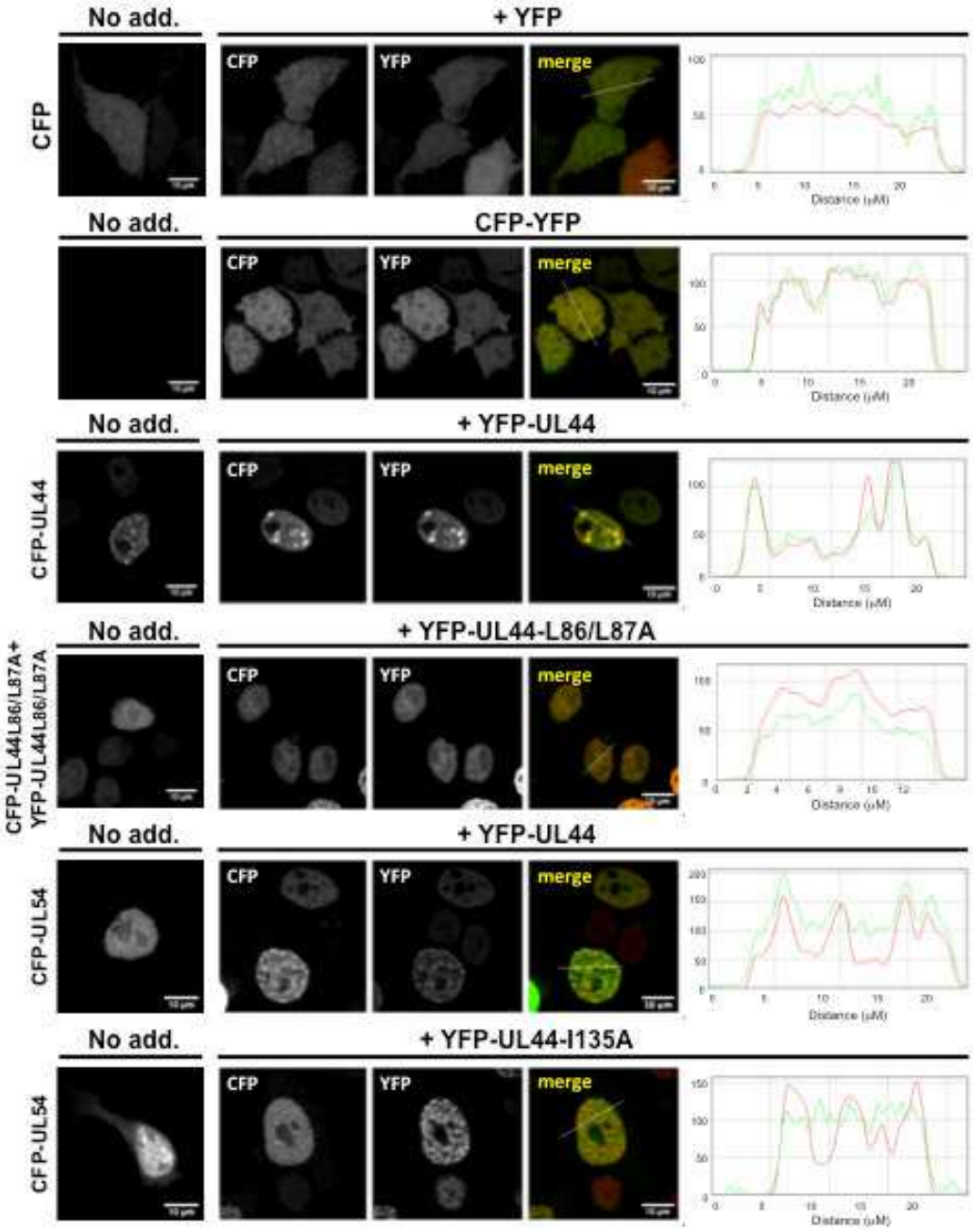
No add.
+ YFP
CFP
CFP
YFP
merge
Distance (μM)
No add.
CFP-YFP
CFP
YFP
merge
Distance (μM)
No add.
+ YFP-UL44
CFP-UL44
CFP
YFP
merge
Distance (μM)
No add.
+ YFP-UL44-L86/L87A
CFP-UL44L86/L87A+ YFP-UL44L86/L87A
CFP
YFP
merge
Distance (μM)
No add.
+ YFP-UL44
CFP-UL54
CFP
YFP
merge
Distance (μM)
No add.
+ YFP-UL44-I135A
CFP-UL54
CFP
YFP
merge
Distance (μM)

Figure 4.3

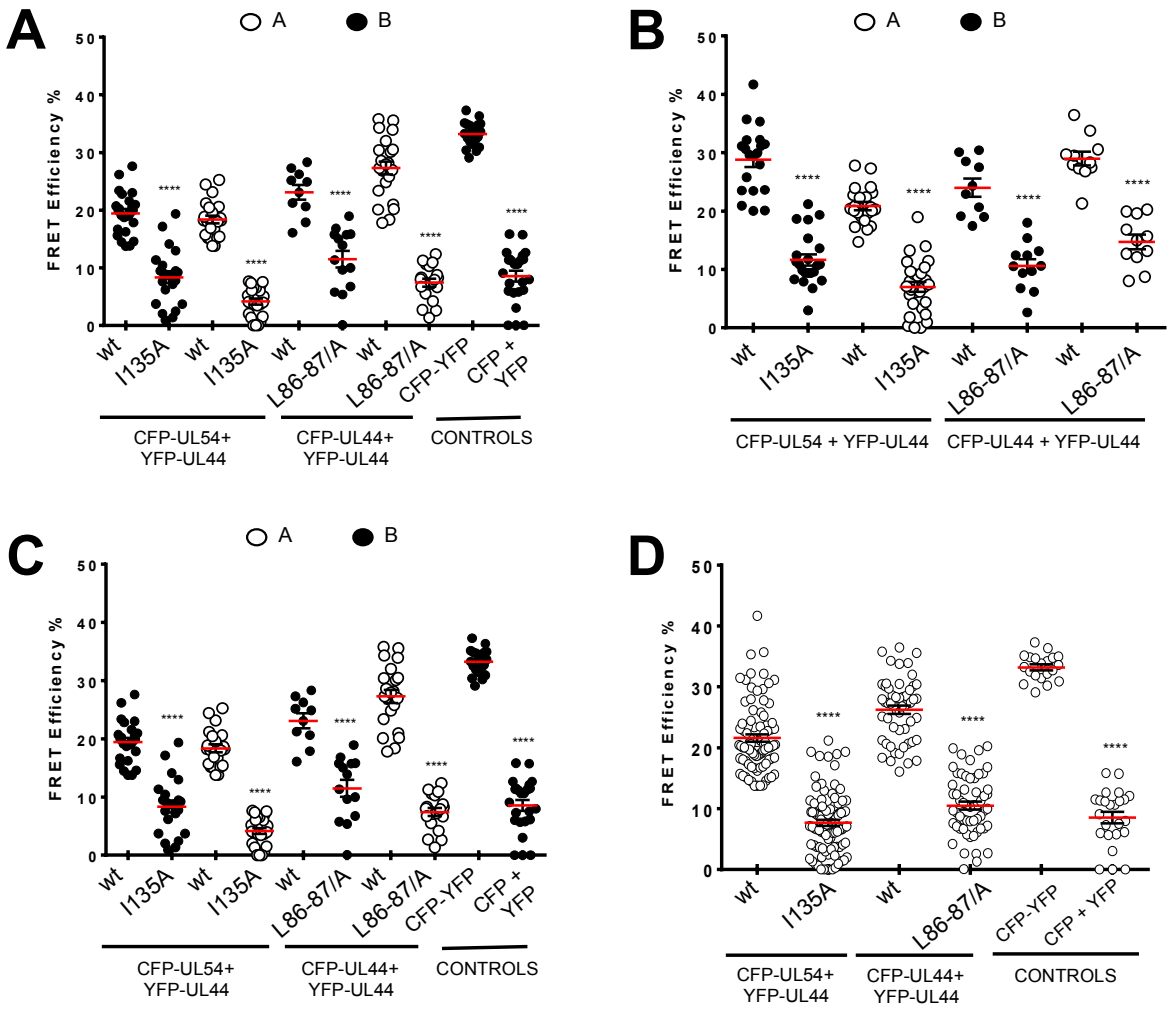
A
B
C
D
FRET Efficiency %
wt
I135A
L86-87/A
CFP-YFP
CFP + YFP
CFP-UL54+ YFP-UL44
CFP-UL44+ YFP-UL44
CONTROLS
CFP-UL54 + YFP-UL44
CFP-UL44 + YFP-UL44
****

Figure 4.4

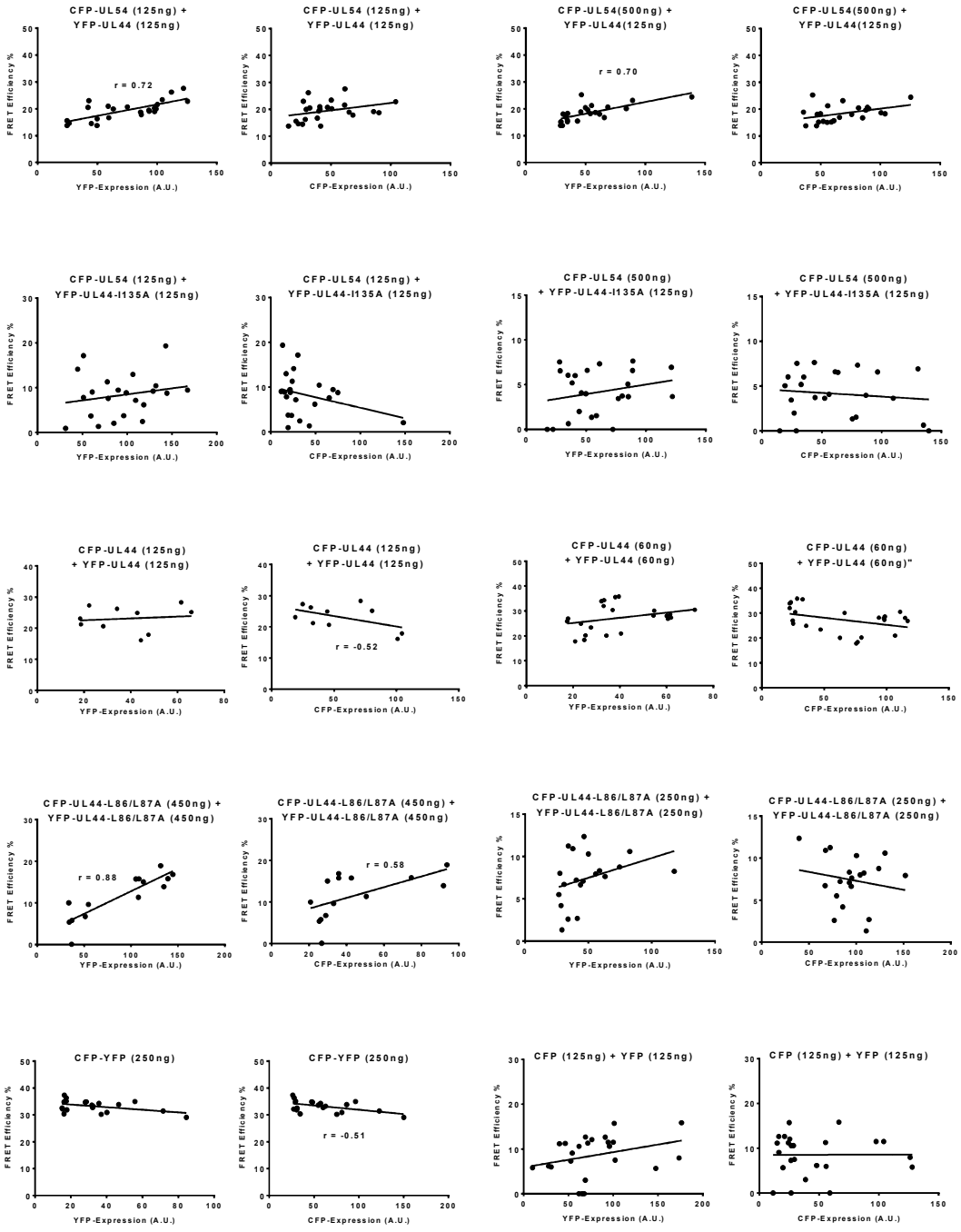
CFP-UL54 (125ng) + YFP-UL44 (125ng)
r = 0.72
FRET Efficiency %
YFP-Expression (A.U.)
CFP-UL54 (125ng) + YFP-UL44 (125ng)
FRET Efficiency %
CFP-Expression (A.U.)
CFP-UL54(500ng) + YFP-UL44(125ng)
r = 0.70
FRET Efficiency %
YFP-Expression (A.U.)
CFP-UL54(500ng) + YFP-UL44(125ng)
FRET Efficiency %
CFP-Expression (A.U.)
CFP-UL54 (125ng) + YFP-UL44-I135A (125ng)
FRET Efficiency %
YFP-Expression (A.U.)
CFP-UL54 (125ng) + YFP-UL44-I135A (125ng)
FRET Efficiency %
CFP-Expression (A.U.)
CFP-UL54 (500ng) + YFP-UL44-I135A (125ng)
FRET Efficiency %
YFP-Expression (A.U.)
CFP-UL54 (500ng) + YFP-UL44-I135A (125ng)
FRET Efficiency %
CFP-Expression (A.U.)
CFP-UL44 (125ng) + YFP-UL44 (125ng)
FRET Efficiency %
YFP-Expression (A.U.)
CFP-UL44 (125ng) + YFP-UL44 (125ng)
r = -0.52
FRET Efficiency %
CFP-Expression (A.U.)
CFP-UL44 (60ng) + YFP-UL44 (60ng)
FRET Efficiency %
YFP-Expression (A.U.)
CFP-UL44 (60ng) + YFP-UL44 (60ng)"
FRET Efficiency %
CFP-Expression (A.U.)
CFP-UL44-L86/L87A (450ng) + YFP-UL44-L86/L87A (450ng)
r = 0.88
FRET Efficiency %
YFP-Expression (A.U.)
CFP-UL44-L86/L87A (450ng) + YFP-UL44-L86/L87A (450ng)
r = 0.58
FRET Efficiency %
CFP-Expression (A.U.)
CFP-UL44-L86/L87A (250ng) + YFP-UL44-L86/L87A (250ng)
FRET Efficiency %
YFP-Expression (A.U.)
CFP-UL44-L86/L87A (250ng) + YFP-UL44-L86/L87A (250ng)
FRET Efficiency %
CFP-Expression (A.U.)
CFP-YFP (250ng)
FRET Efficiency %
YFP-Expression (A.U.)
CFP-YFP (250ng)
r = -0.51
FRET Efficiency %
CFP-Expression (A.U.)
CFP (125ng) + YFP (125ng)
FRET Efficiency %
YFP-Expression (A.U.)
CFP (125ng) + YFP (125ng)
FRET Efficiency %
CFP-Expression (A.U.)

Figure 4.5

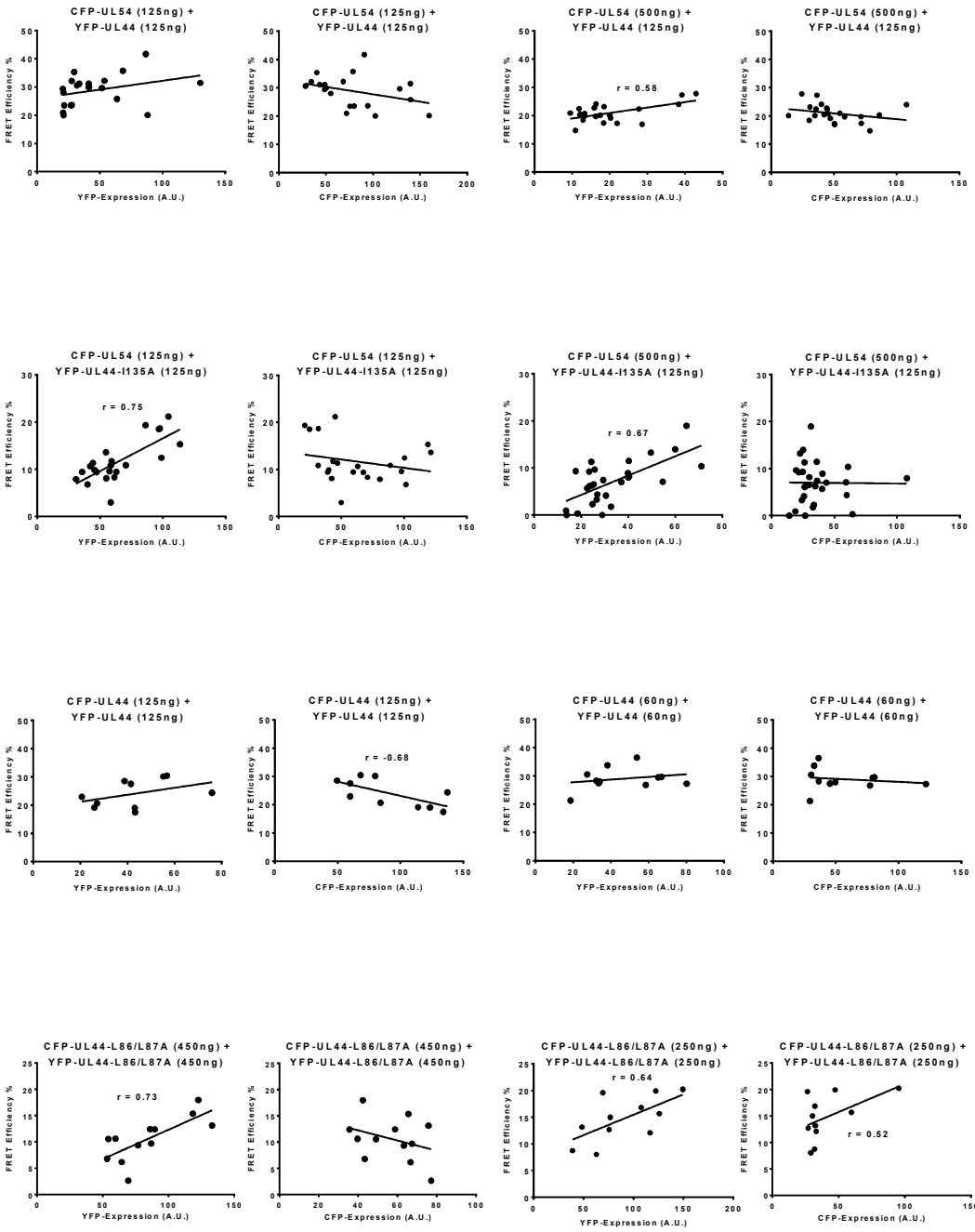
CFP-UL54 (125ng) + YFP-UL44 (125ng)
FRET Efficiency %
YFP-Expression (A.U.)
CFP-UL54 (125ng) + YFP-UL44 (125ng)
FRET Efficiency %
CFP-Expression (A.U.)
CFP-UL54 (500ng) + YFP-UL44 (125ng)
r = 0.58
FRET Efficiency %
YFP-Expression (A.U.)
CFP-UL54 (500ng) + YFP-UL44 (125ng)
FRET Efficiency %
CFP-Expression (A.U.)
CFP-UL54 (125ng) + YFP-UL44-I135A (125ng)
r = 0.75
FRET Efficiency %
YFP-Expression (A.U.)
CFP-UL54 (125ng) + YFP-UL44-I135A (125ng)
FRET Efficiency %
CFP-Expression (A.U.)
CFP-UL54 (500ng) + YFP-UL44-I135A (125ng)
r = 0.67
FRET Efficiency %
YFP-Expression (A.U.)
CFP-UL54 (500ng) + YFP-UL44-I135A (125ng)
FRET Efficiency %
CFP-Expression (A.U.)
CFP-UL44 (125ng) + YFP-UL44 (125ng)
FRET Efficiency %
YFP-Expression (A.U.)
CFP-UL44 (125ng) + YFP-UL44 (125ng)
r = -0.68
FRET Efficiency %
CFP-Expression (A.U.)
CFP-UL44 (60ng) + YFP-UL44 (60ng)
FRET Efficiency %
YFP-Expression (A.U.)
CFP-UL44 (60ng) + YFP-UL44 (60ng)
FRET Efficiency %
CFP-Expression (A.U.)
CFP-UL44-L86/L87A (450ng) + YFP-UL44-L86/L87A (450ng)
r = 0.73
FRET Efficiency %
YFP-Expression (A.U.)
CFP-UL44-L86/L87A (450ng) + YFP-UL44-L86/L87A (450ng)
FRET Efficiency %
CFP-Expression (A.U.)
CFP-UL44-L86/L87A (250ng) + YFP-UL44-L86/L87A (250ng)
r = 0.64
FRET Efficiency %
YFP-Expression (A.U.)
CFP-UL44-L86/L87A (250ng) + YFP-UL44-L86/L87A (250ng)
r = 0.52
FRET Efficiency %
CFP-Expression (A.U.)

Figure 4.6

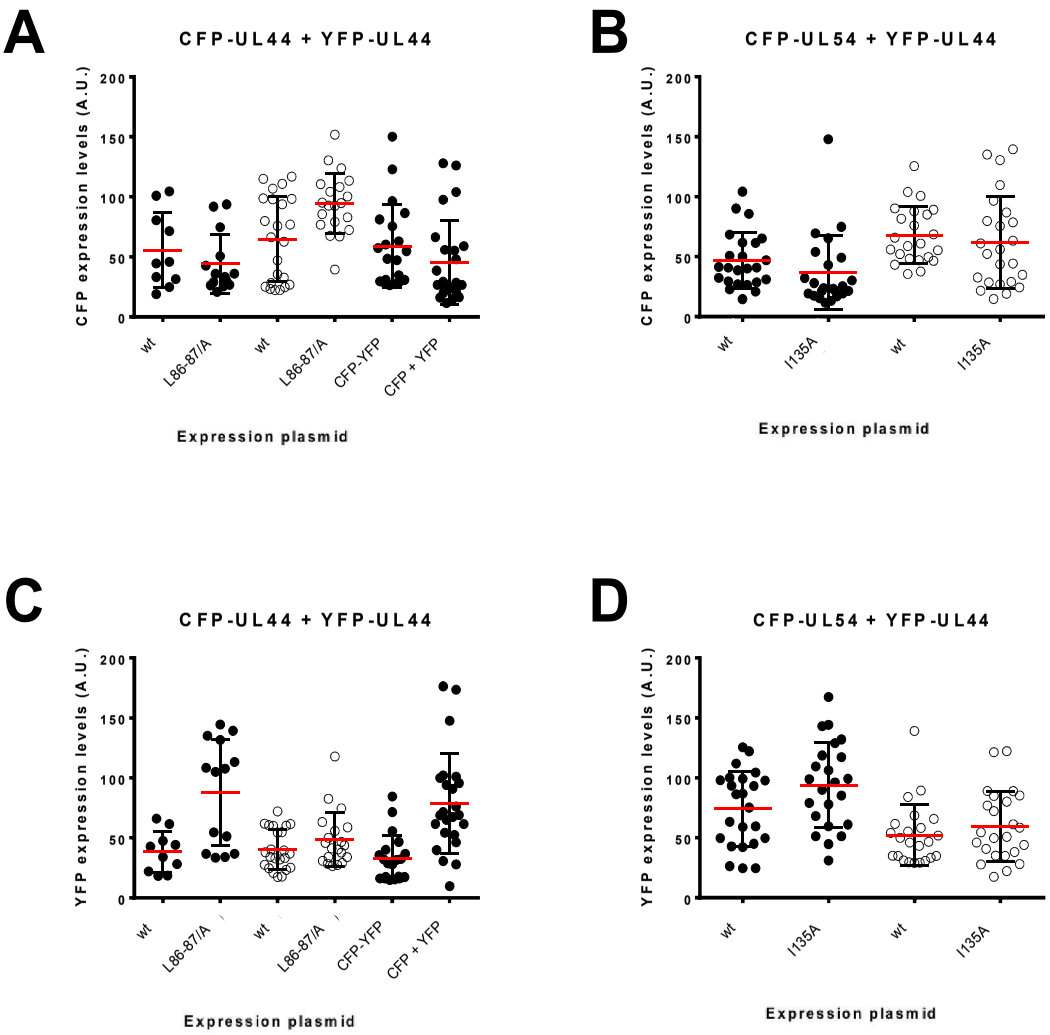
A
CFP-UL44 + YFP-UL44
CFP expression levels (A.U.)
200
150
100
50
0
wt
L86-87/A
wt
L86-87/A
CFP-YFP
CFP + YFP
Expression plasmid
B
CFP-UL54 + YFP-UL44
CFP expression levels (A.U.)
200
150
100
50
0
wt
I135A
wt
I135A
Expression plasmid
C
CFP-UL44 + YFP-UL44
YFP expression levels (A.U.)
200
150
100
50
0
wt
L86-87/A
wt
L86-87/A
CFP-YFP
CFP + YFP
Expression plasmid
D
CFP-UL54 + YFP-UL44
YFP expression levels (A.U.)
200
150
100
50
0
wt
I135A
wt
I135A
Expression plasmid

Figure 4.7

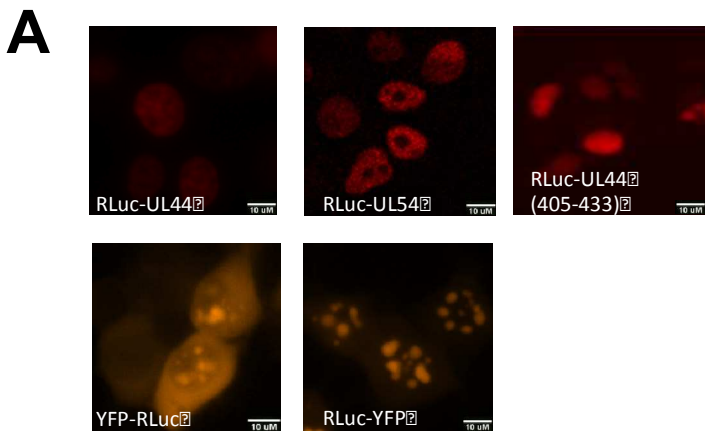
A
RLuc-UL44
RLuc-UL54
RLuc-UL44
(405-433)
YFP-RLuc
RLuc-YFP

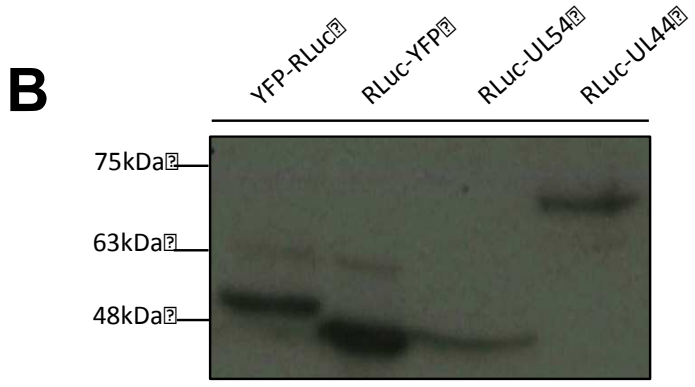
B
YFP-RLuc
RLuc-YFP
RLuc-UL54
RLuc-UL44
75kDa
63kDa
48kDa

Figure 4.8

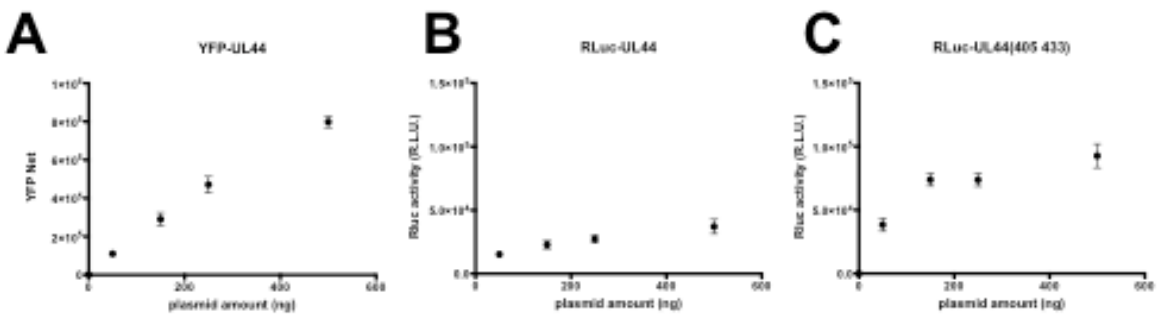

Figure 4.9

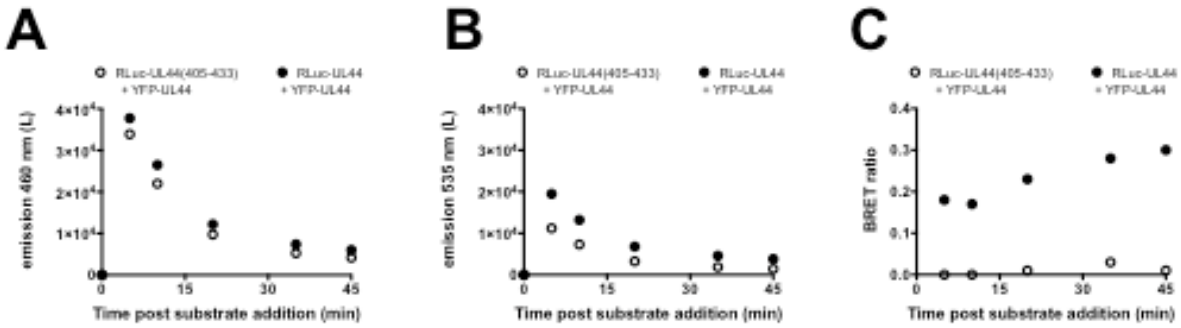

Figure 4.10

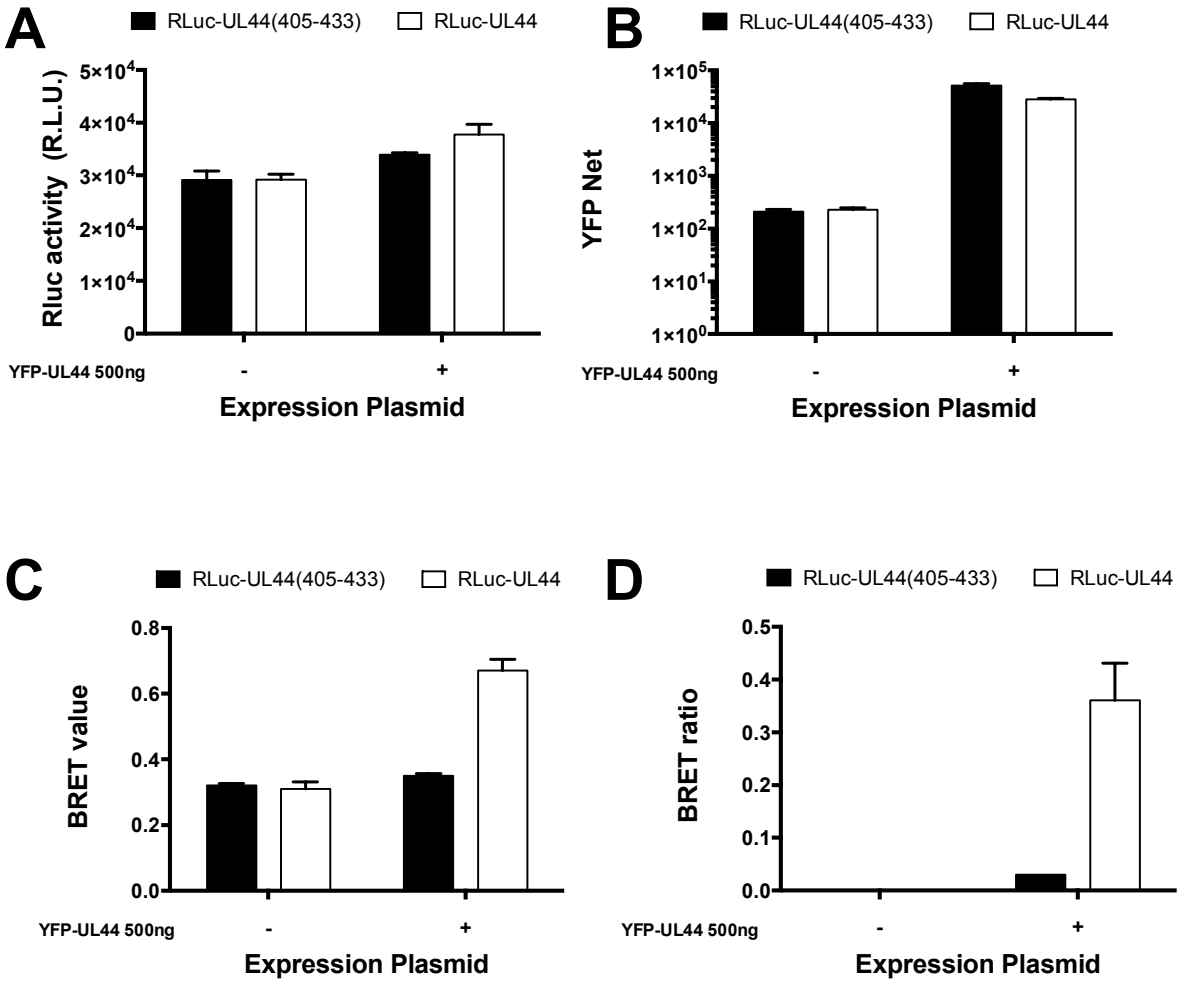
A
RLuc-UL44(405-433)
RLuc-UL44
Rluc activity (R.L.U.)
5×10^4
4×10^4
3×10^4
2×10^4
1×10^4
0
YFP-UL44 500ng
-
+
Expression Plasmid
B
RLuc-UL44(405-433)
RLuc-UL44
YFP Net
1×10^5
1×10^4
1×10^3
1×10^2
1×10^1
1×10^0
YFP-UL44 500ng
-
+
Expression Plasmid
C
RLuc-UL44(405-433)
RLuc-UL44
BRET value
0.8
0.6
0.4
0.2
0.0
YFP-UL44 500ng
-
+
Expression Plasmid
D
RLuc-UL44(405-433)
RLuc-UL44
BRET ratio
0.5
0.4
0.3
0.2
0.1
0.0
YFP-UL44 500ng
-
+
Expression Plasmid

Figure 4.11

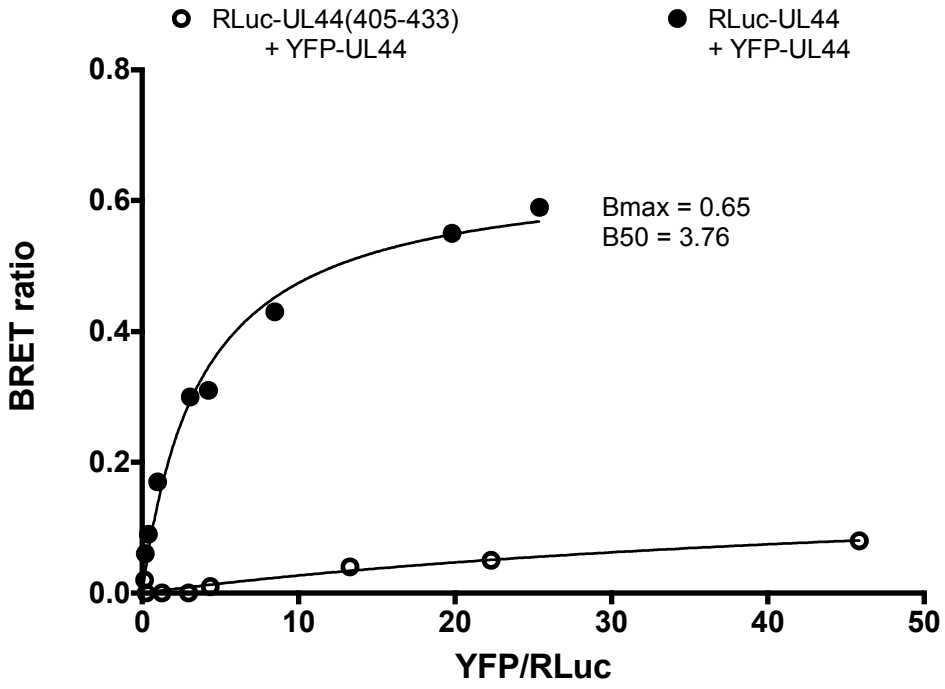
RLuc-UL44(405-433)
+ YFP-UL44
RLuc-UL44
+ YFP-UL44
Bmax = 0.65
B50 = 3.76
BRET ratio
0.0
0.2
0.4
0.6
0.8
0
10
20
30
40
50
YFP/RLuc

Figure 4.12

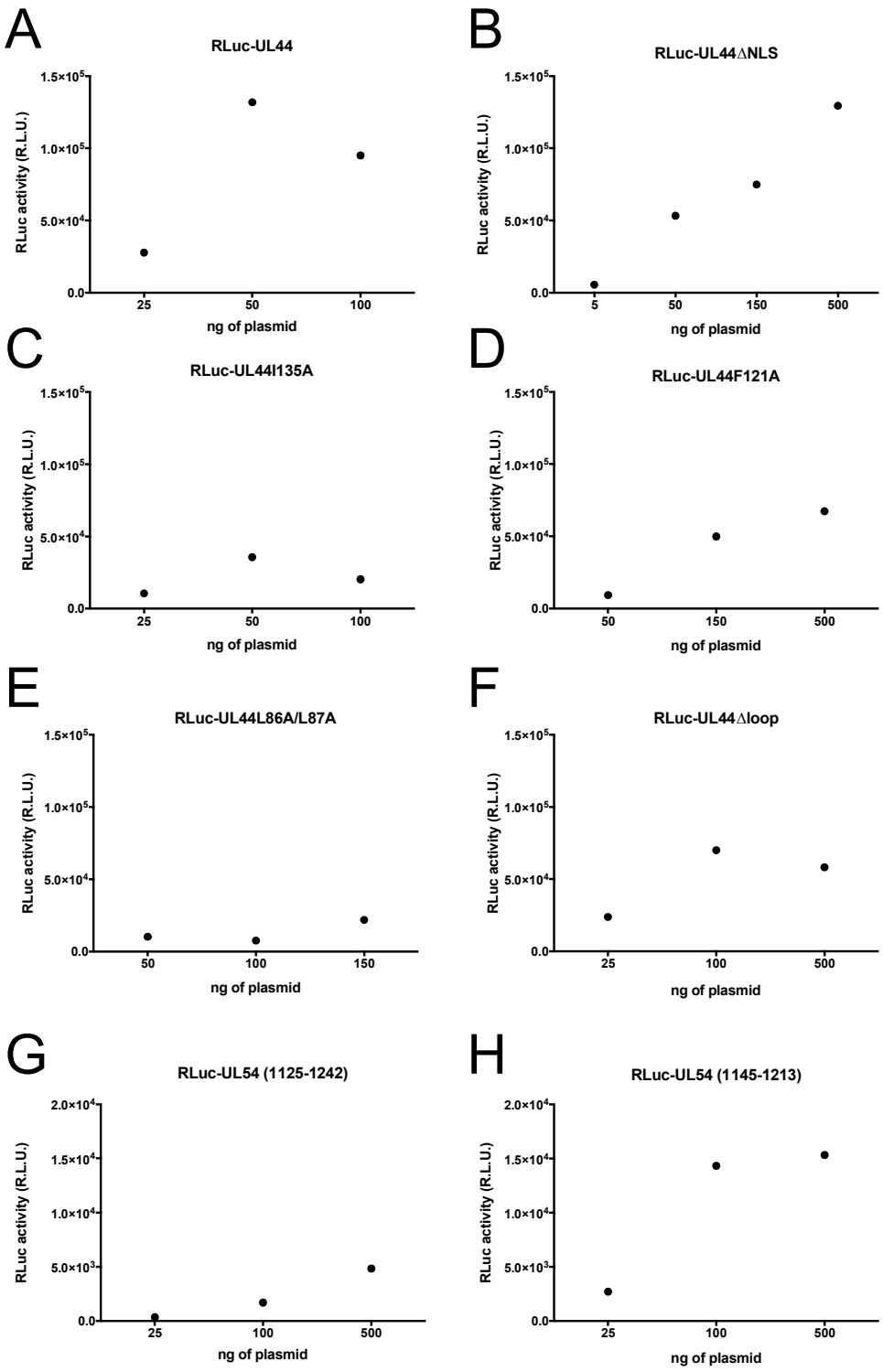
A
RLuc-UL44
RLuc activity (R.L.U.)
1.5×10^5
1.0×10^5
5.0×10^4
0.0
25
50
100
ng of plasmid
B
RLuc-UL44ΔNLS
RLuc activity (R.L.U.)
1.5×10^5
1.0×10^5
5.0×10^4
0.0
5
50
150
500
ng of plasmid
C
RLuc-UL44I135A
RLuc activity (R.L.U.)
1.5×10^5
1.0×10^5
5.0×10^4
0.0
25
50
100
ng of plasmid
D
RLuc-UL44F121A
RLuc activity (R.L.U.)
1.5×10^5
1.0×10^5
5.0×10^4
0.0
50
150
500
ng of plasmid
E
RLuc-UL44L86A/L87A
RLuc activity (R.L.U.)
1.5×10^5
1.0×10^5
5.0×10^4
0.0
50
100
150
ng of plasmid
F
RLuc-UL44Δloop
RLuc activity (R.L.U.)
1.5×10^5
1.0×10^5
5.0×10^4
0.0
25
100
500
ng of plasmid
G
RLuc-UL54 (1125-1242)
RLuc activity (R.L.U.)
2.0×10^4
1.5×10^4
1.0×10^4
5.0×10^3
0.0
25
100
500
ng of plasmid
H
RLuc-UL54 (1145-1213)
RLuc activity (R.L.U.)
2.0×10^4
1.5×10^4
1.0×10^4
5.0×10^3
0.0
25
100
500
ng of plasmid

Figure 4.13

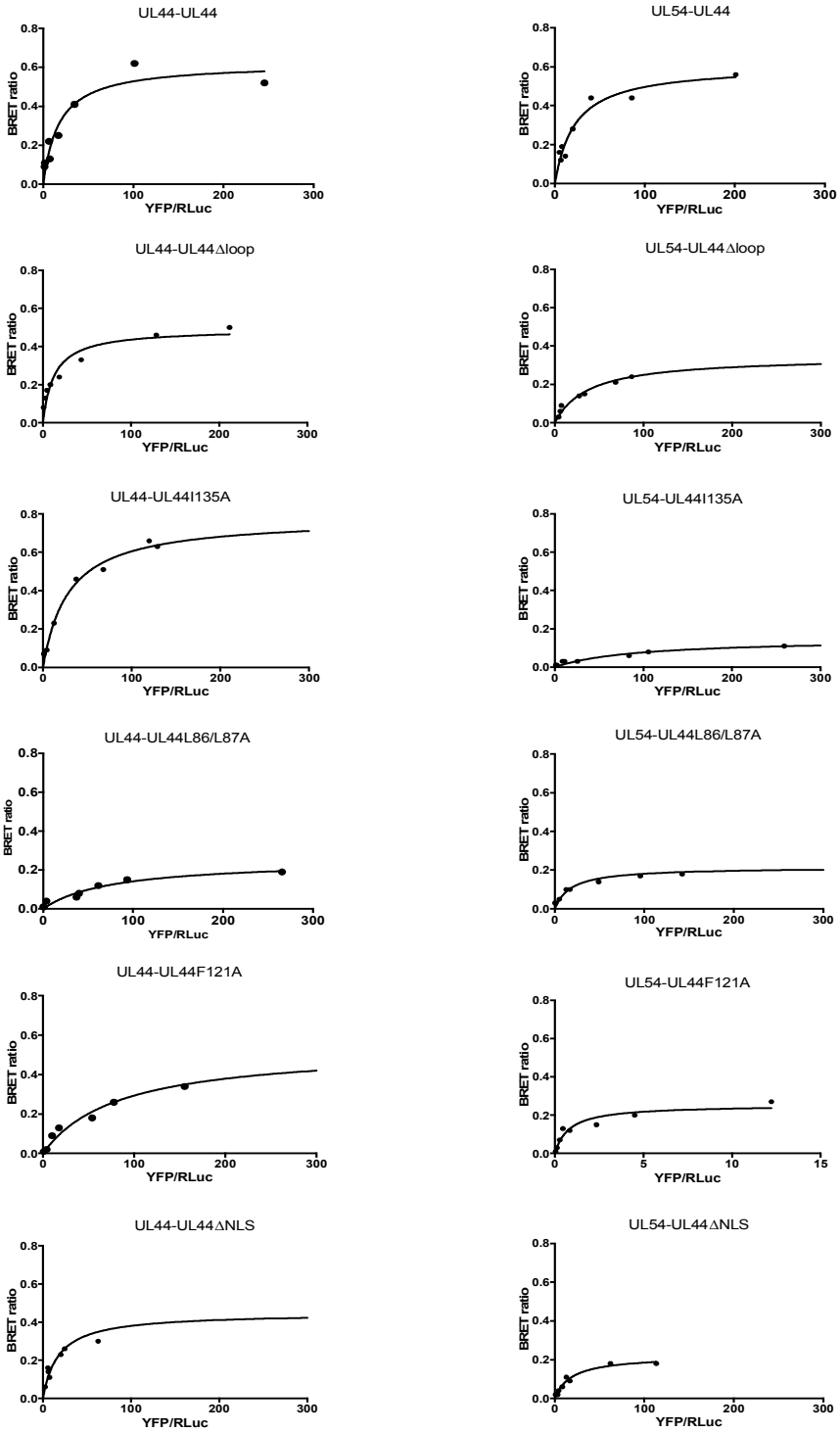
UL44-UL44
UL54-UL44
UL44-UL44Δloop
UL54-UL44Δloop
UL44-UL44I135A
UL54-UL44I135A
UL44-UL44L86/L87A
UL54-UL44L86/L87A
UL44-UL44F121A
UL54-UL44F121A
UL44-UL44ΔNLS
UL54-UL44ΔNLS
BRET ratio
YFP/RLuc

Figure 4.14


GST-
His6-UL44
GST-UL44-
His6-UL44
GST-UL44-
His6-UL44-L86/L87A
I
W
E2
E3
I
W
E2
E3
I
W
E2
E3
55
36
28

Figure 4.15

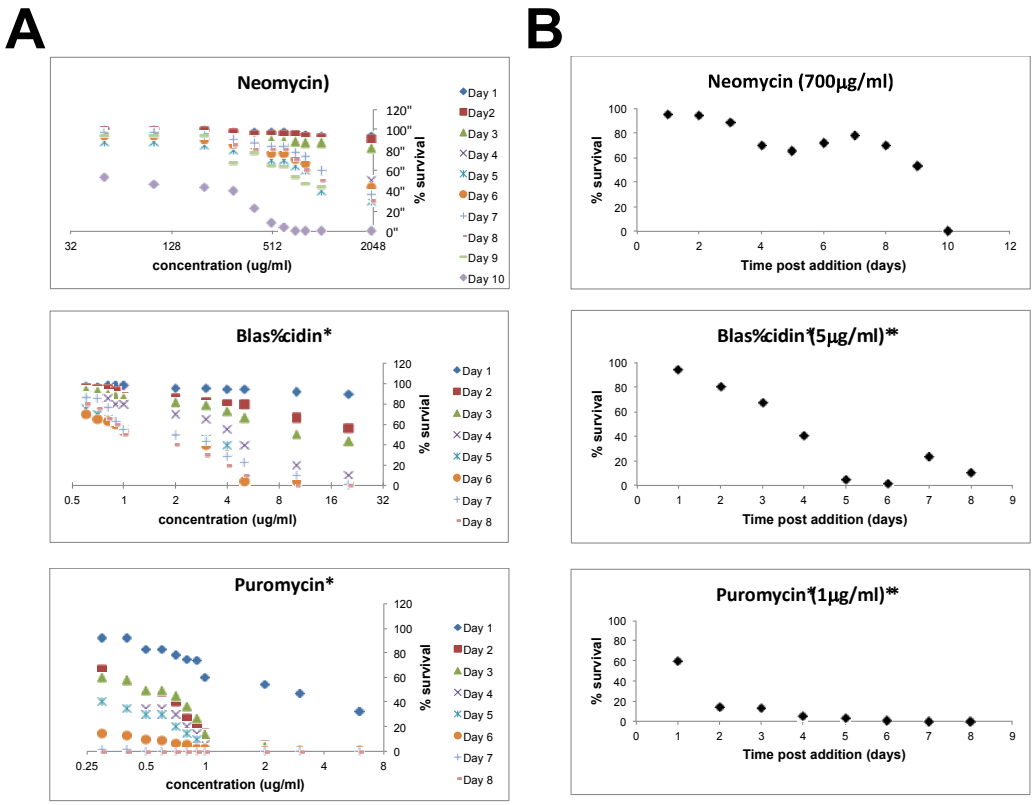
A
B
Neomycin)
% survival
concentration (ug/ml)
Day 1
Day2
Day 3
Day 4
Day 5
Day 6
Day 7
Day 8
Day 9
Day 10
Neomycin (700µg/ml)
% survival
Time post addition (days)
Blas%cidin*
% survival
concentration (ug/ml)
Blas%cidin*(5µg/ml)**
% survival
Time post addition (days)
Puromycin*
% survival
concentration (ug/ml)
Puromycin*(1µg/ml)**
% survival
Time post addition (days)

Figure 4.16

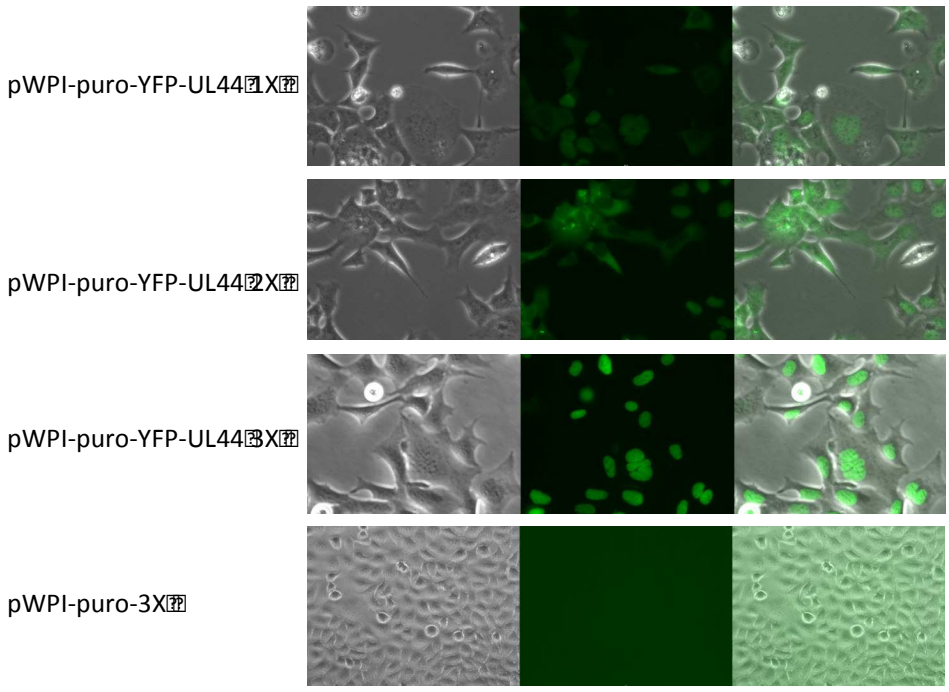
pWPI-puro-YFP-UL44 1X
pWPI-puro-YFP-UL44 2X
pWPI-puro-YFP-UL44 3X
pWPI-puro-3X

Figure 4.17

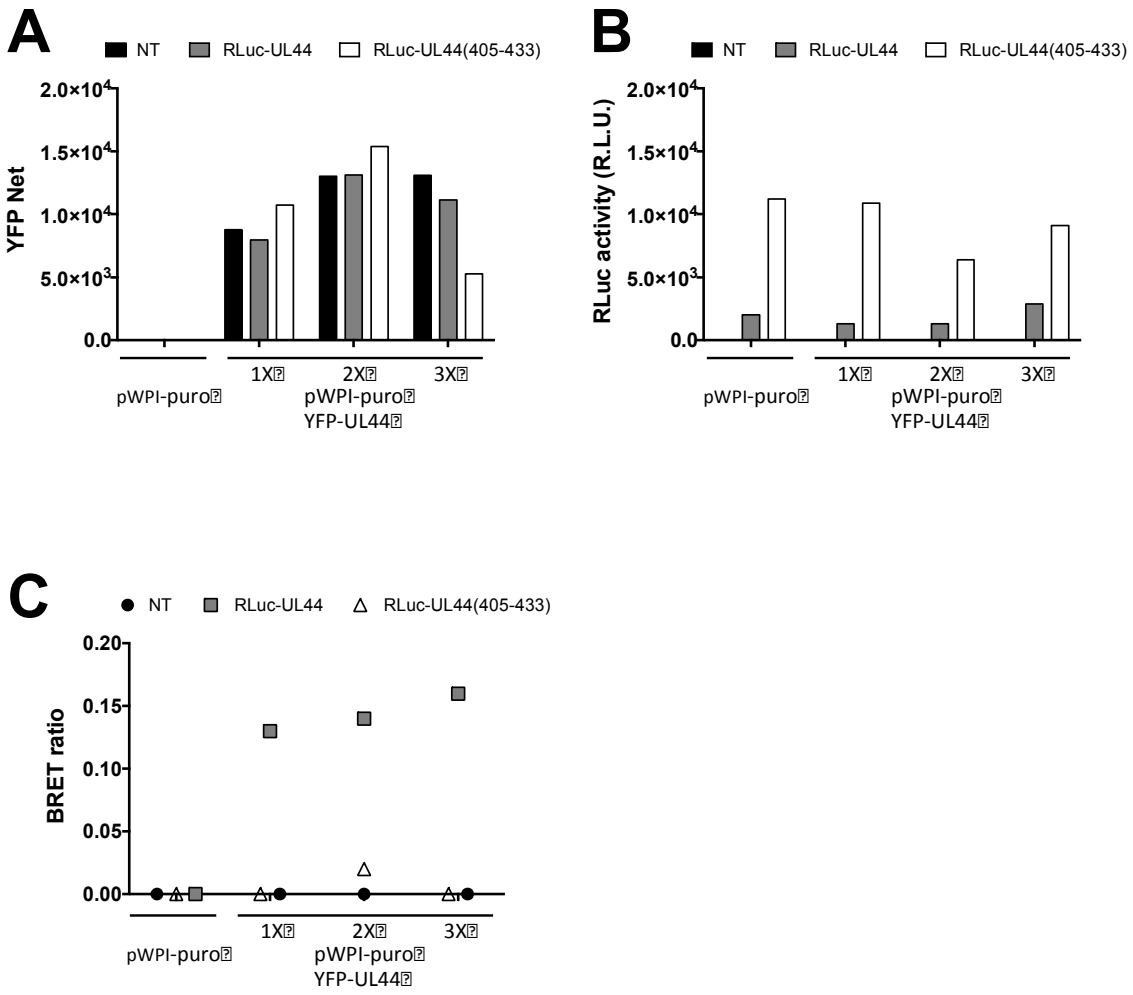
A
NT
RLuc-UL44
RLuc-UL44(405-433)
YFP Net
2.0×10^4
1.5×10^4
1.0×10^4
5.0×10^3
0.0
1X
2X
3X
pWPI-puro
pWPI-puro YFP-UL44
B
NT
RLuc-UL44
RLuc-UL44(405-433)
RLuc activity (R.L.U.)
2.0×10^4
1.5×10^4
1.0×10^4
5.0×10^3
0.0
1X
2X
3X
pWPI-puro
pWPI-puro YFP-UL44
C
NT
RLuc-UL44
RLuc-UL44(405-433)
BRET ratio
0.20
0.15
0.10
0.05
0.00
1X
2X
3X
pWPI-puro
pWPI-puro YFP-UL44

Figure 4.18

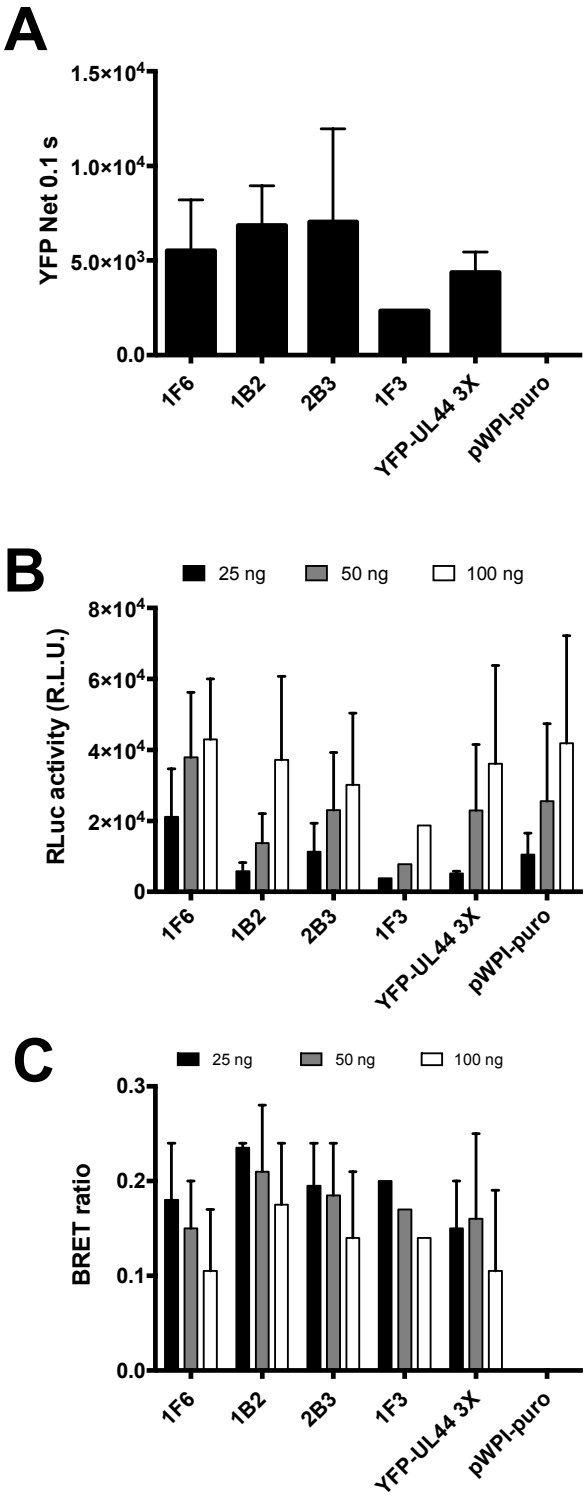
A
YFP Net 0.1 s
1.5×10^4
1.0×10^4
5.0×10^3
0.0
1F6
1B2
2B3
1F3
YFP-UL44 3X
pWPI-puro
B
25 ng
50 ng
100 ng
RLuc activity (R.L.U.)
8×10^4
6×10^4
4×10^4
2×10^4
0
1F6
1B2
2B3
1F3
YFP-UL44 3X
pWPI-puro
C
25 ng
50 ng
100 ng
BRET ratio
0.3
0.2
0.1
0.0
1F6
1B2
2B3
1F3
YFP-UL44 3X
pWPI-puro

Figure 4.19

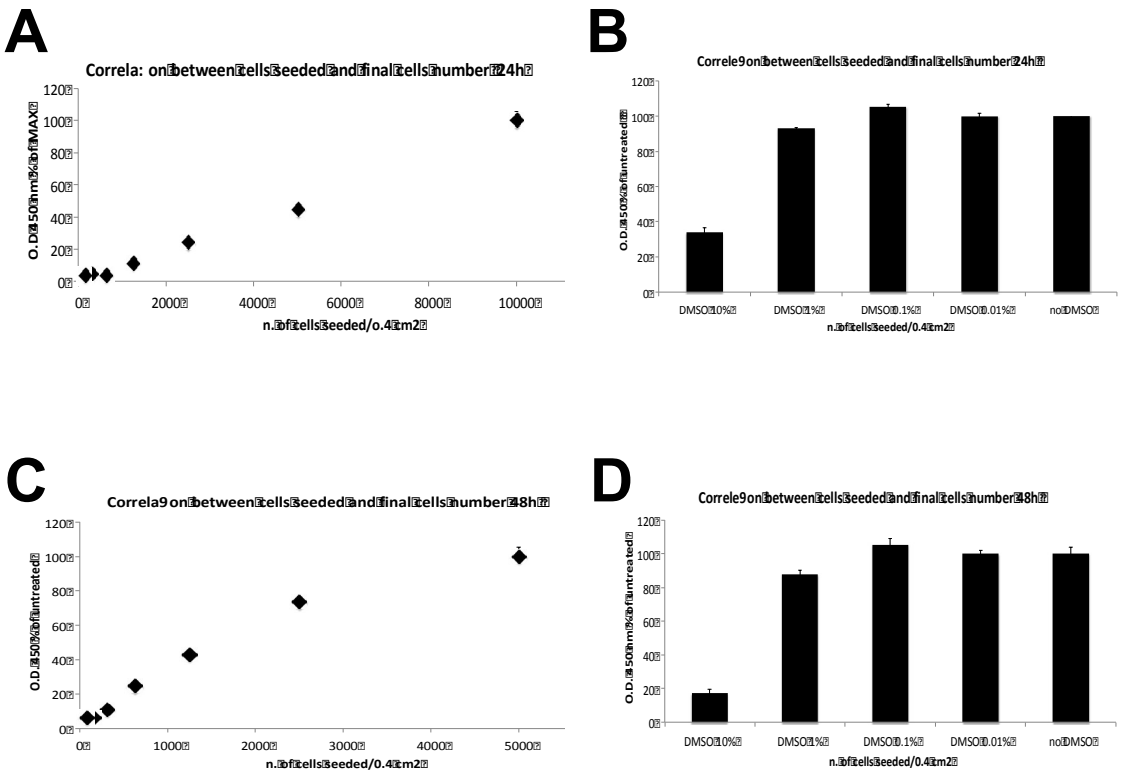
A
Correla: on between cells seeded and final cells number 24h
O.D. 450nm % of MAX
n. of cells seeded/0.4cm2
B
Correle9on between cells seeded and final cells number 24h
O.D. 450% of untreated
DMSO 10%
DMSO 1%
DMSO 0.1%
DMSO 0.01%
no DMSO
n. of cells seeded/0.4cm2
C
Correla9on between cells seeded and final cells number 48h
O.D. 450% of untreated
n. of cells seeded/0.4cm2
D
Correle9on between cells seeded and final cells number 48h
O.D. 450nm % of untreated
DMSO 10%
DMSO 1%
DMSO 0.1%
DMSO 0.01%
no DMSO
n. of cells seeded/0.4cm2

Figure 4.20

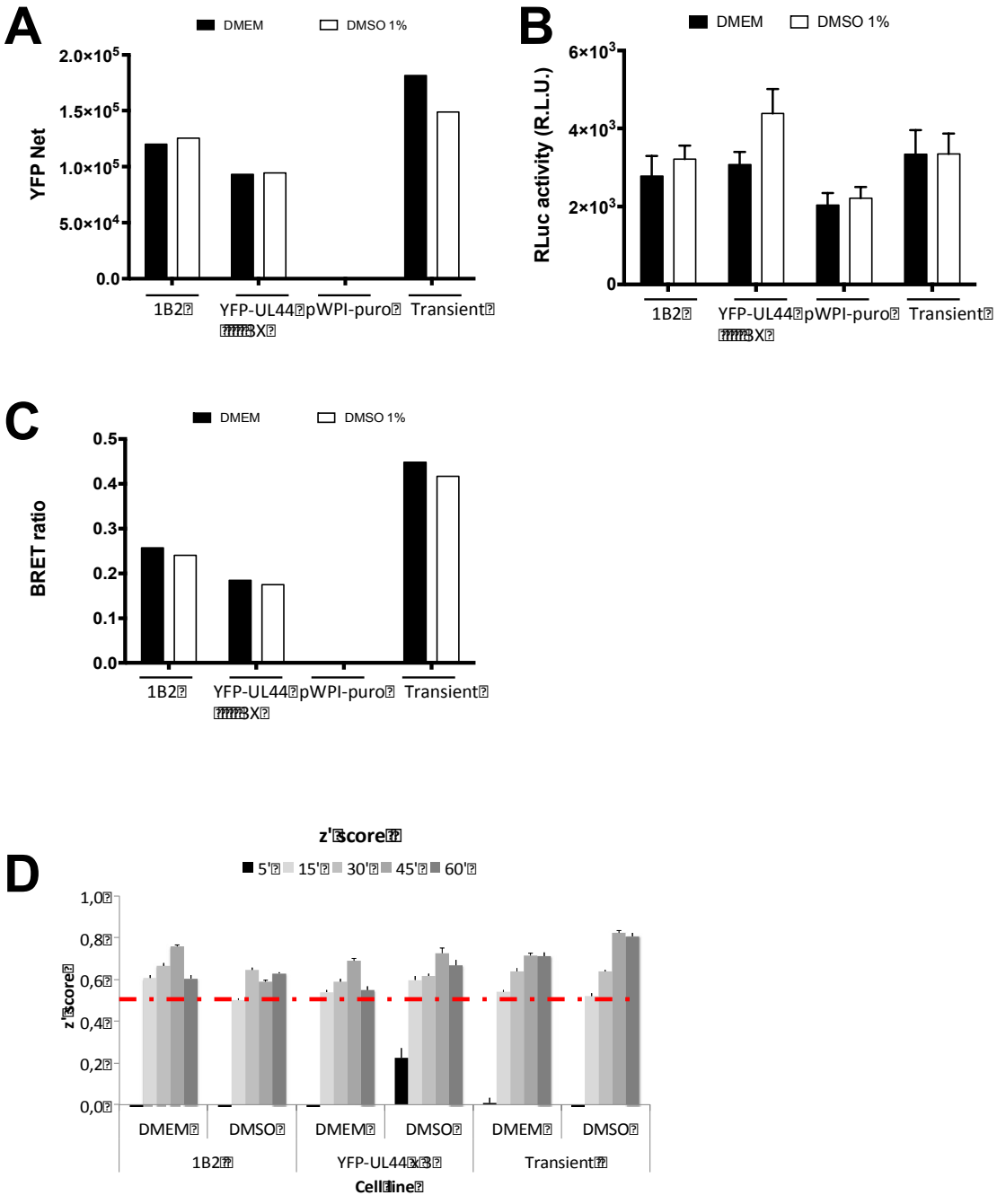
A
DMEM
DMSO 1%
YFP Net
2.0×10^5
1.5×10^5
1.0×10^5
5.0×10^4
0.0
1B2
YFP-UL44
pWPI-puro
Transient
B
DMEM
DMSO 1%
RLuc activity (R.L.U.)
6×10^3
4×10^3
2×10^3
0
1B2
YFP-UL44
pWPI-puro
Transient
C
DMEM
DMSO 1%
BRET ratio
0.5
0.4
0.3
0.2
0.1
0.0
1B2
YFP-UL44
pWPI-puro
Transient
D
z'-score
5'
15'
30'
45'
60'
1,0
0,8
0,6
0,4
0,2
0,0
z'-score
DMEM
DMSO
DMEM
DMSO
DMEM
DMSO
1B2
YFP-UL44
Transient
Cell line

Figure 4.21

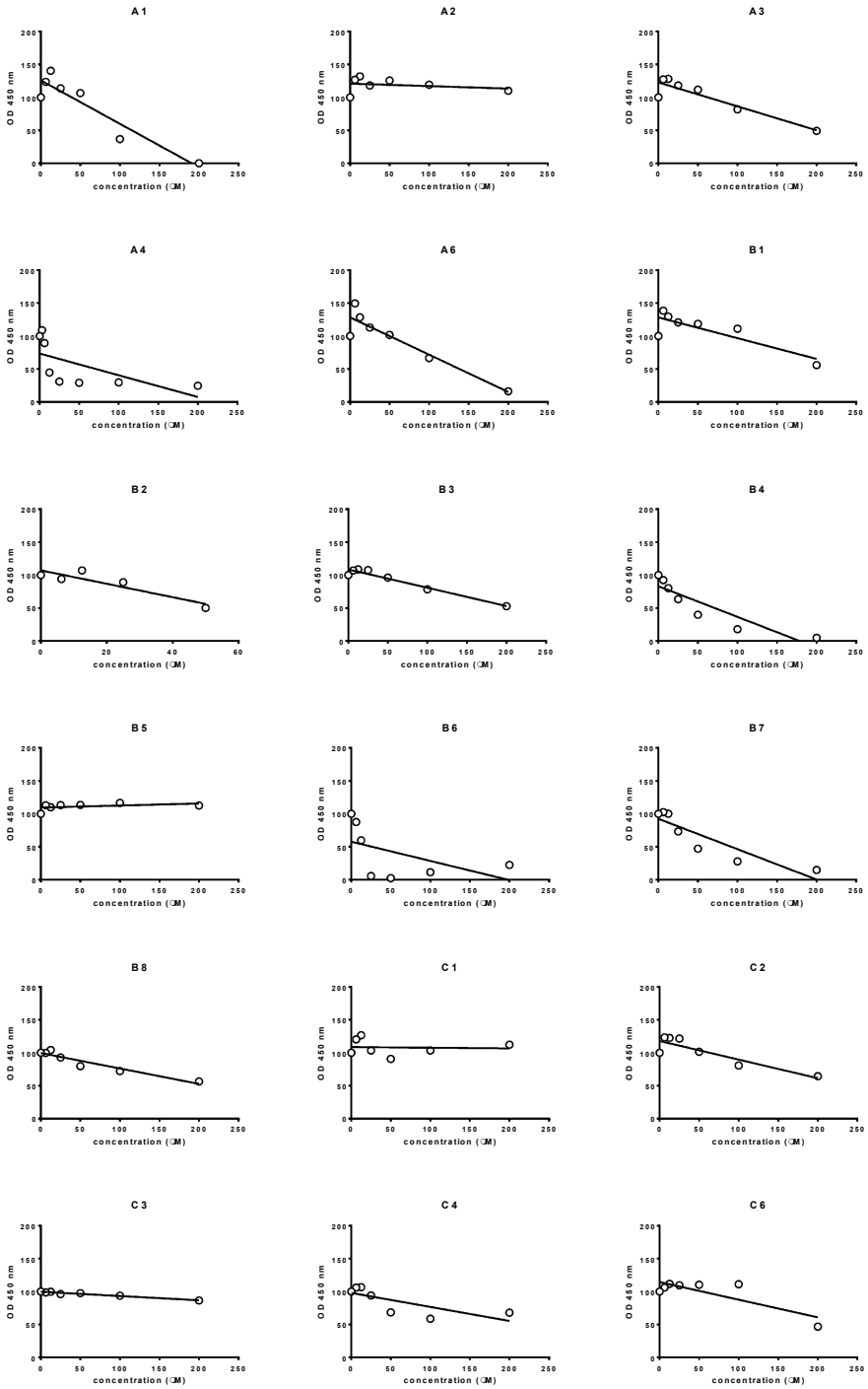
A1
A2
A3
A4
A6
B1
B2
B3
B4
B5
B6
B7
B8
C1
C2
C3
C4
C6
OD 450 nm
concentration (□M)

Figure 4.22

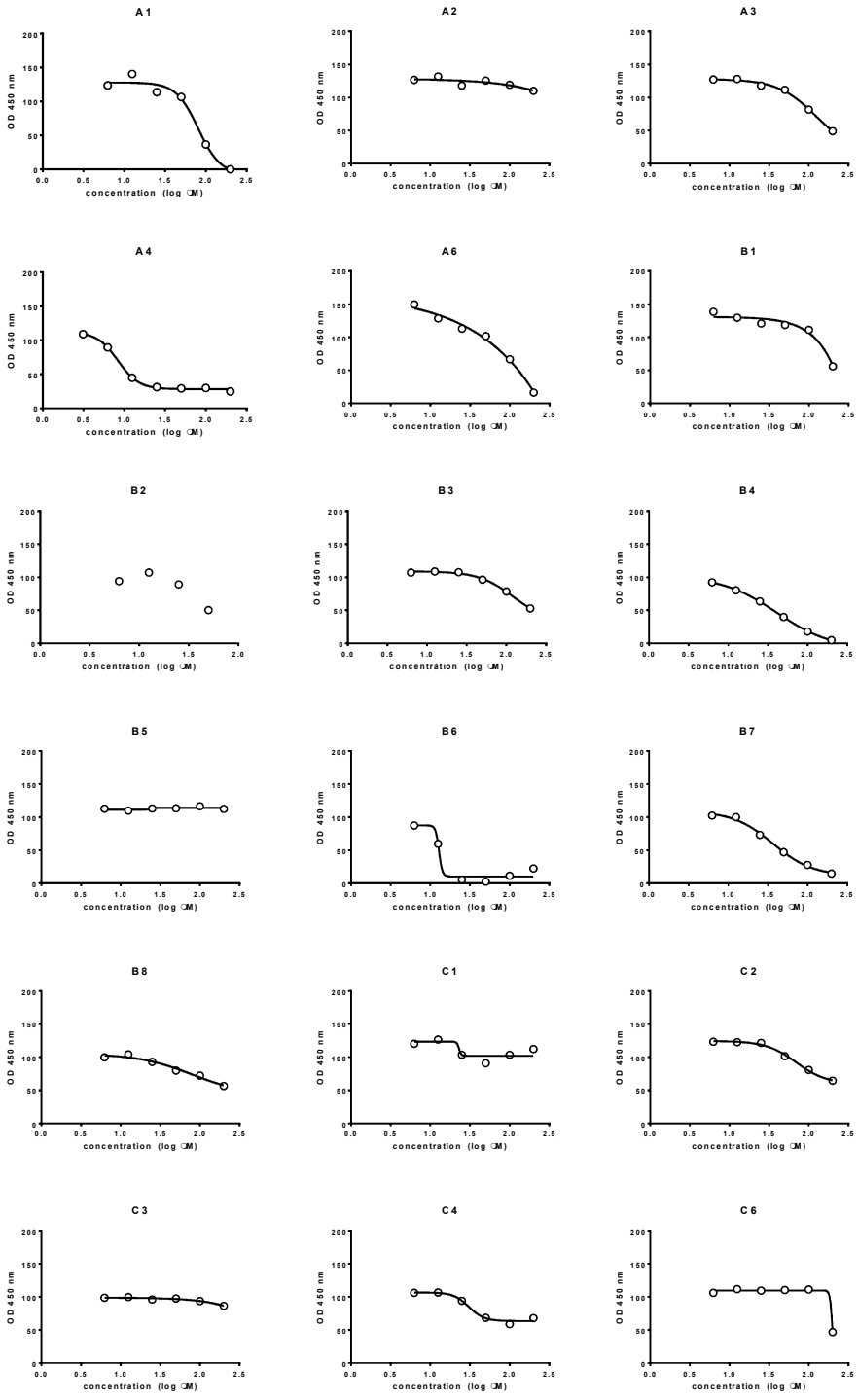
A1
A2
A3
A4
A6
B1
B2
B3
B4
B5
B6
B7
B8
C1
C2
C3
C4
C6
OD 450 nm
concentration (log ☐M)

Figure 4.23

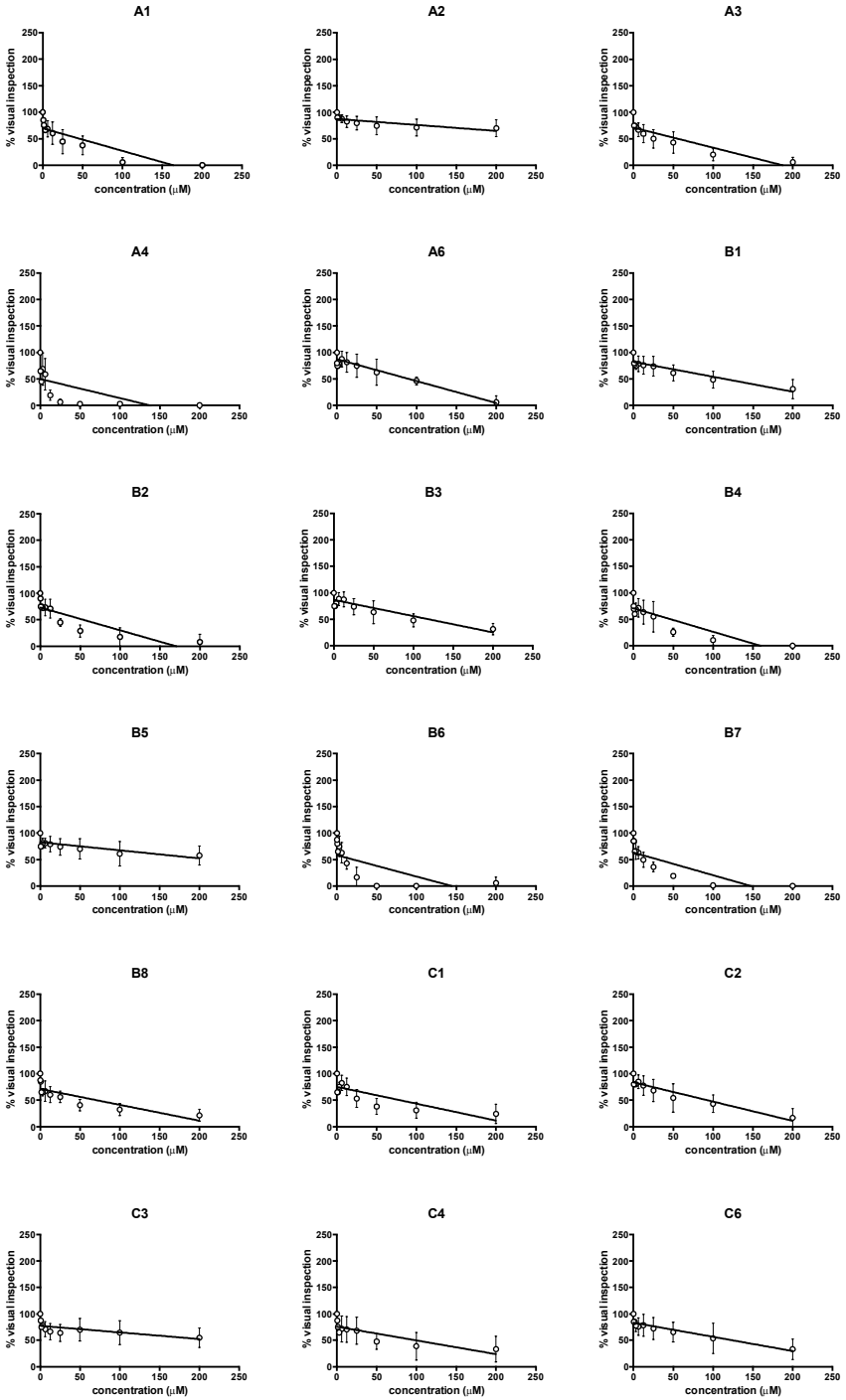
A1
A2
A3
A4
A6
B1
B2
B3
B4
B5
B6
B7
B8
C1
C2
C3
C4
C6
% visual inspection
concentration (μM)
0
50
100
150
200
250

Figure 4.24

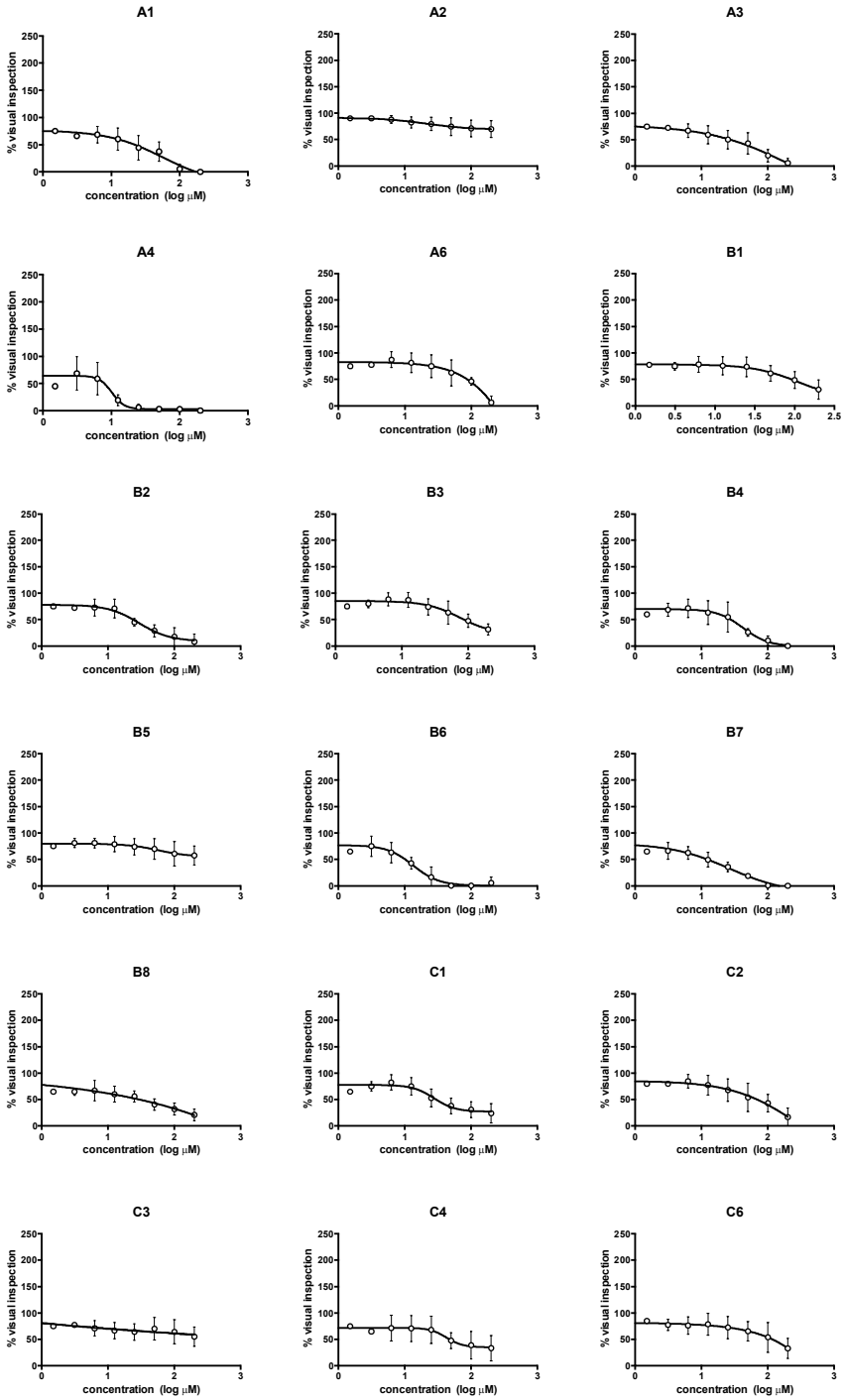
A1
A2
A3
A4
A6
B1
B2
B3
B4
B5
B6
B7
B8
C1
C2
C3
C4
C6
% visual inspection
concentration (log μM)

Figure 4.25

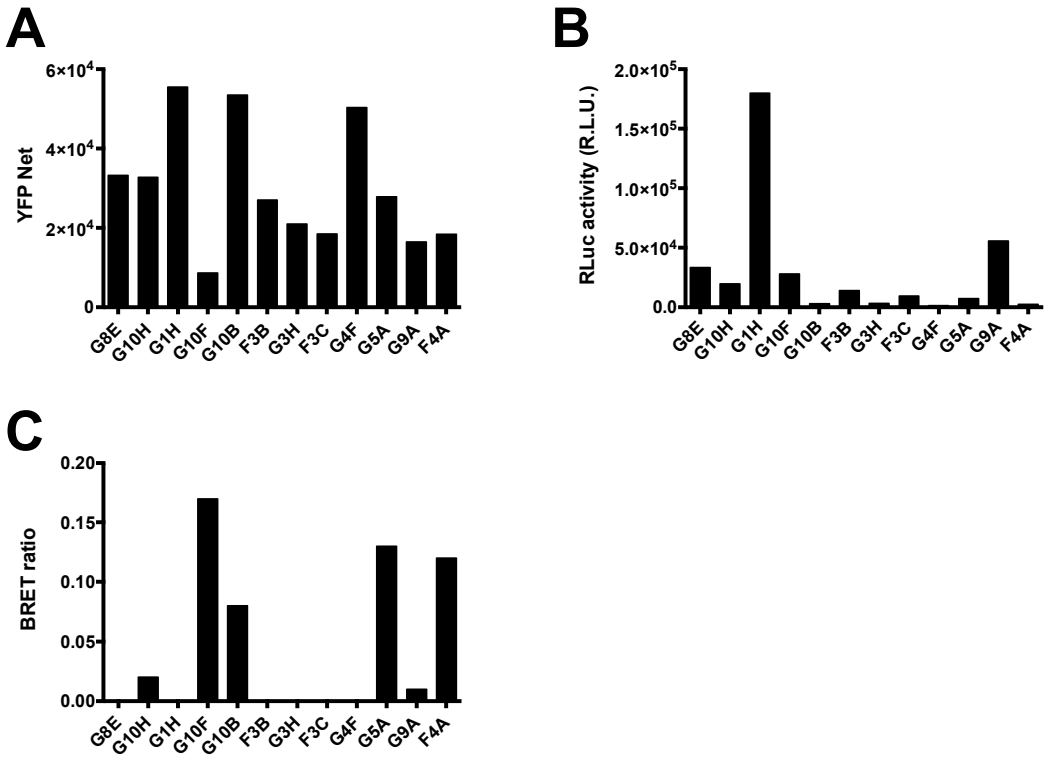
A
YFP Net
6×10^4
4×10^4
2×10^4
0
G8E
G10H
G1H
G10F
G10B
F3B
G3H
F3C
G4F
G5A
G9A
F4A
B
RLuc activity (R.L.U.)
2.0×10^5
1.5×10^5
1.0×10^5
5.0×10^4
0.0
G8E
G10H
G1H
G10F
G10B
F3B
G3H
F3C
G4F
G5A
G9A
F4A
C
BRET ratio
0.20
0.15
0.10
0.05
0.00
G8E
G10H
G1H
G10F
G10B
F3B
G3H
F3C
G4F
G5A
G9A
F4A

Figure 4.26

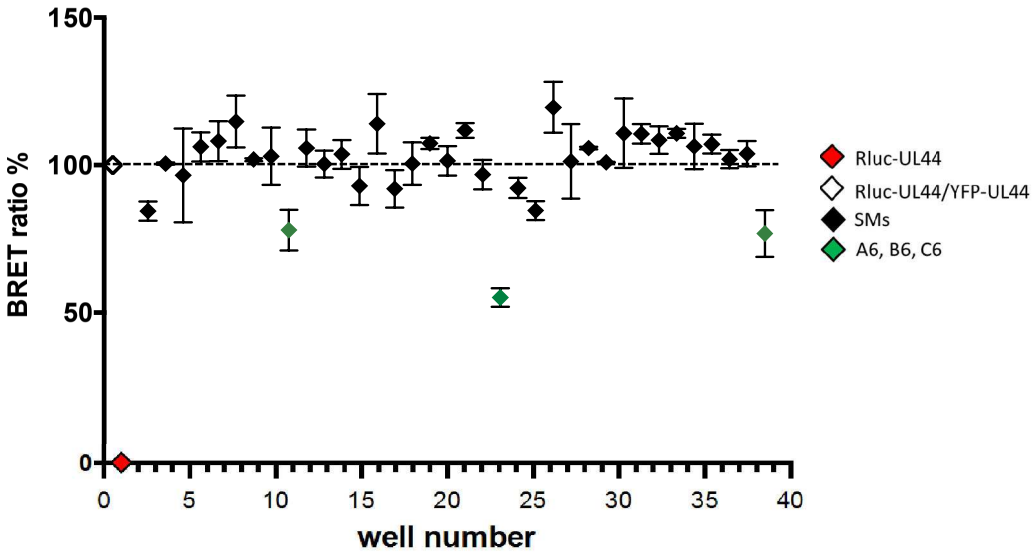
150
100
50
0
BRET ratio %
0
5
10
15
20
25
30
35
40
well number
Rluc-UL44
Rluc-UL44/YFP-UL44
SMs
A6, B6, C6

Figure 4.27

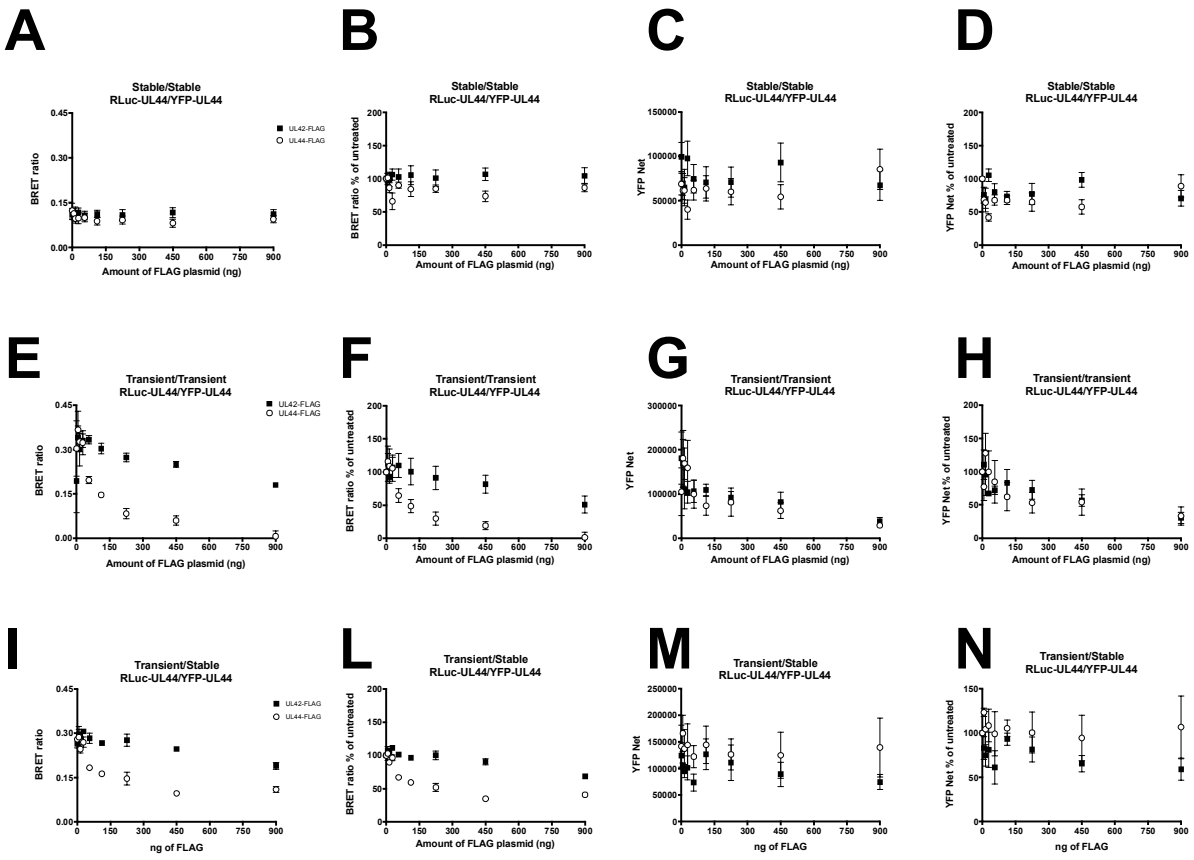
A
Stable/Stable
RLuc-UL44/YFP-UL44
BRET ratio
Amount of FLAG plasmid (ng)
UL42-FLAG
UL44-FLAG
B
Stable/Stable
RLuc-UL44/YFP-UL44
BRET ratio % of untreated
Amount of FLAG plasmid (ng)
C
Stable/Stable
RLuc-UL44/YFP-UL44
YFP Net
Amount of FLAG plasmid (ng)
D
Stable/Stable
RLuc-UL44/YFP-UL44
YFP Net % of untreated
Amount of FLAG plasmid (ng)
E
Transient/Transient
RLuc-UL44/YFP-UL44
BRET ratio
Amount of FLAG plasmid (ng)
UL42-FLAG
UL44-FLAG
F
Transient/Transient
RLuc-UL44/YFP-UL44
BRET ratio % of untreated
Amount of FLAG plasmid (ng)
G
Transient/Transient
RLuc-UL44/YFP-UL44
YFP Net
Amount of FLAG plasmid (ng)
H
Transient/transient
RLuc-UL44/YFP-UL44
YFP Net % of untreated
Amount of FLAG plasmid (ng)
I
Transient/Stable
RLuc-UL44/YFP-UL44
BRET ratio
ng of FLAG
UL42-FLAG
UL44-FLAG
L
Transient/Stable
RLuc-UL44/YFP-UL44
BRET ratio % of untreated
Amount of FLAG plasmid (ng)
M
Transient/Stable
RLuc-UL44/YFP-UL44
YFP Net
ng of FLAG
N
Transient/Stable
RLuc-UL44/YFP-UL44
YFP Net % of untreated
ng of FLAG

Figure 4.28

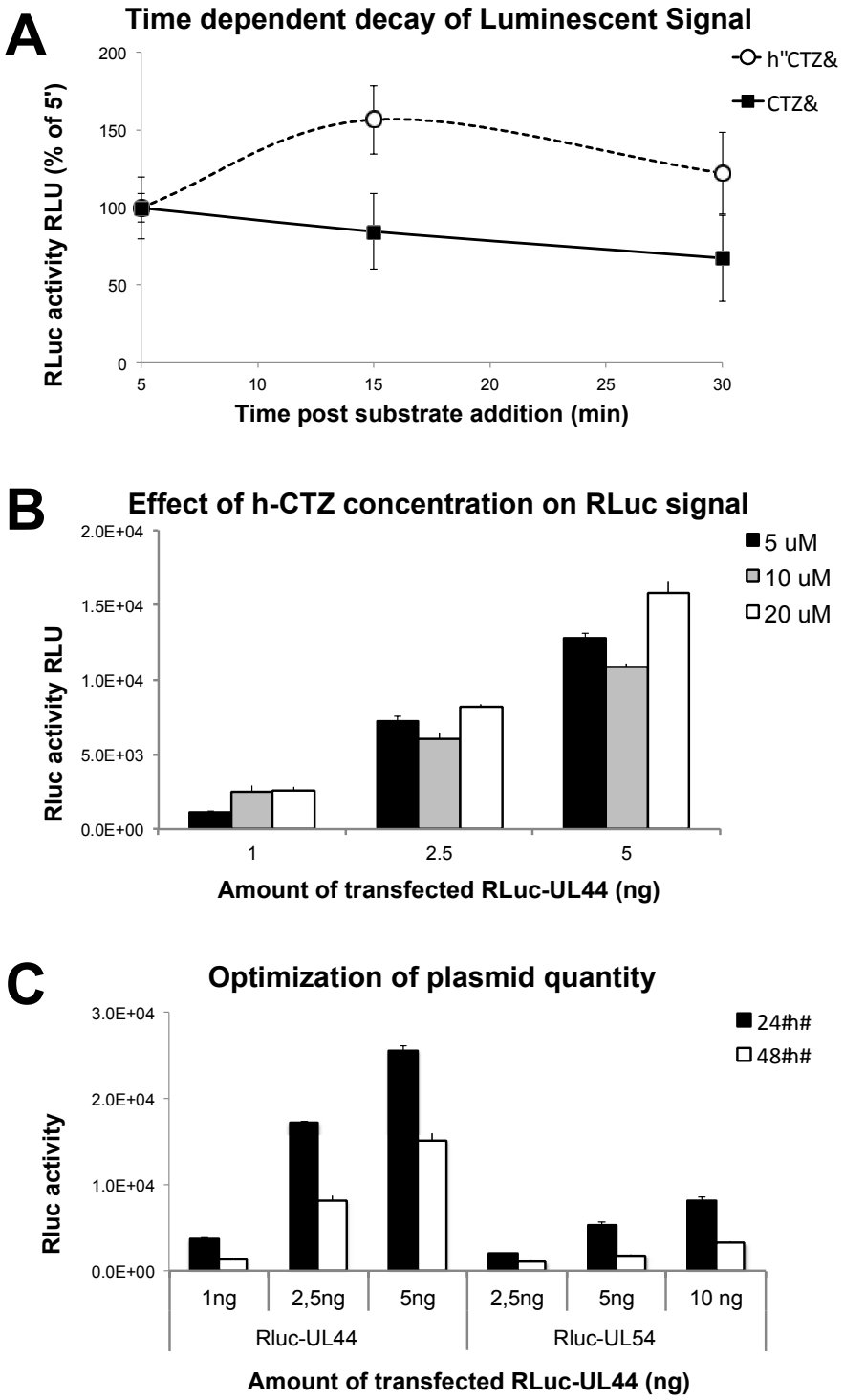
A
Time dependent decay of Luminescent Signal
h"CTZ&
CTZ&
RLuc activity RLU (% of 5')
200
150
100
50
0
5
10
15
20
25
30
Time post substrate addition (min)
B
Effect of h-CTZ concentration on RLuc signal
5 uM
10 uM
20 uM
Rluc activity RLU
2.0E+04
1.5E+04
1.0E+04
5.0E+03
0.0E+00
1
2.5
5
Amount of transfected RLuc-UL44 (ng)
C
Optimization of plasmid quantity
24#h#
48#h#
Rluc activity
3.0E+04
2.0E+04
1.0E+04
0.0E+00
1ng
2,5ng
5ng
2,5ng
5ng
10 ng
Rluc-UL44
Rluc-UL54
Amount of transfected RLuc-UL44 (ng)

Figure 4.29

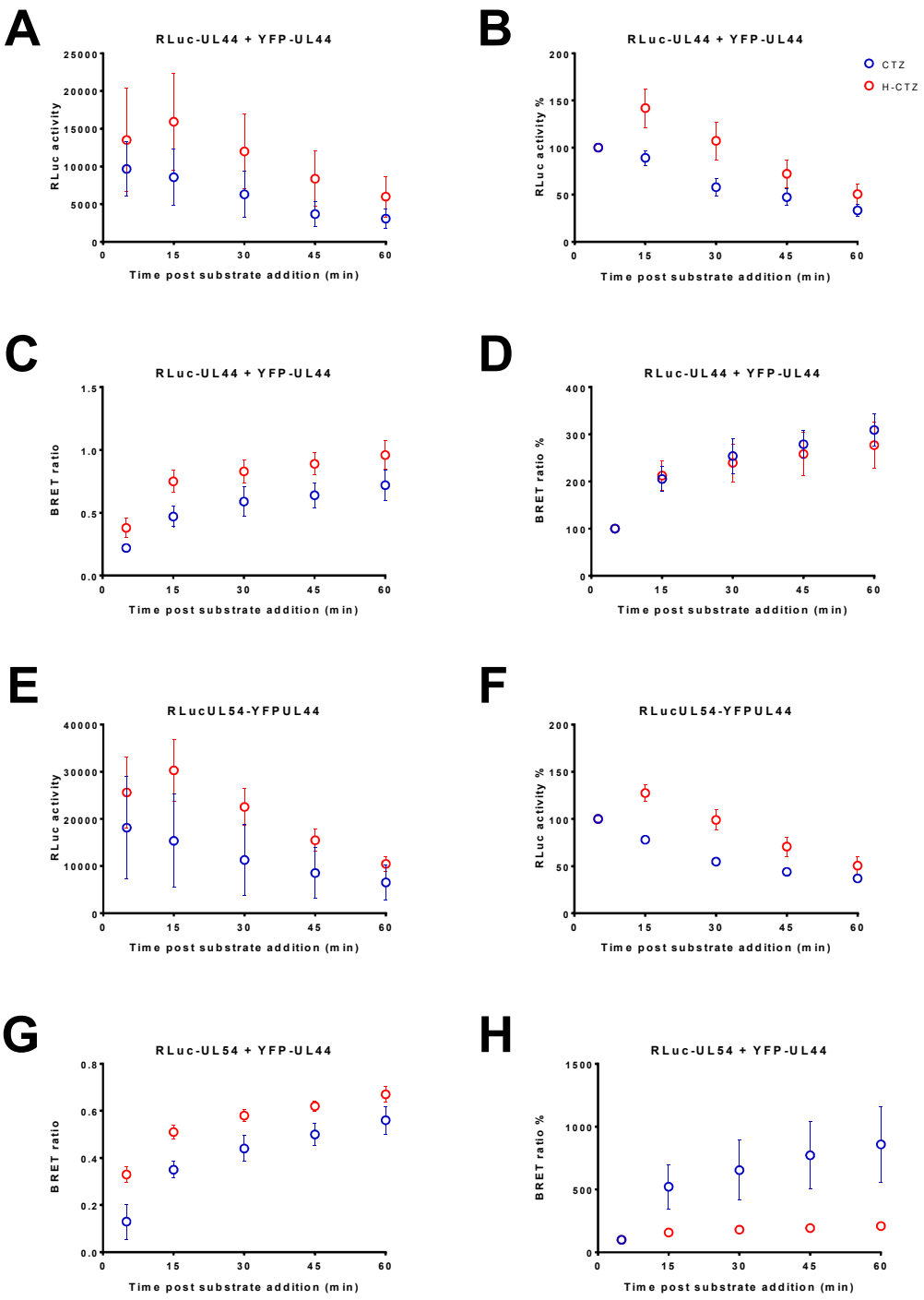
A
RLuc-UL44 + YFP-UL44
RLuc activity
Time post substrate addition (min)
B
RLuc-UL44 + YFP-UL44
RLuc activity %
CTZ
H-CTZ
Time post substrate addition (min)
C
RLuc-UL44 + YFP-UL44
BRET ratio
Time post substrate addition (min)
D
RLuc-UL44 + YFP-UL44
BRET ratio %
Time post substrate addition (min)
E
RLucUL54-YFPUL44
RLuc activity
Time post substrate addition (min)
F
RLucUL54-YFPUL44
RLuc activity %
Time post substrate addition (min)
G
RLuc-UL54 + YFP-UL44
BRET ratio
Time post substrate addition (min)
H
RLuc-UL54 + YFP-UL44
BRET ratio %
Time post substrate addition (min)

Figure 4.30

Rluc-UL44/YFP-UL44 **Rluc-UL54/YFP-UL44**

CTZ

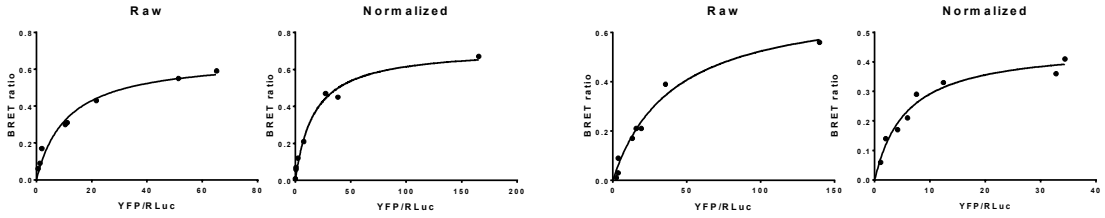

h-CTZ

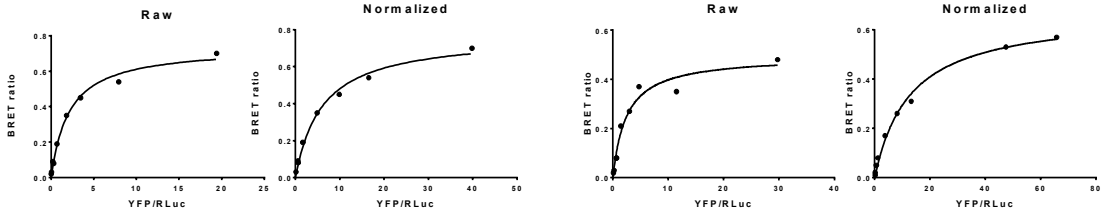

Figure 4.31

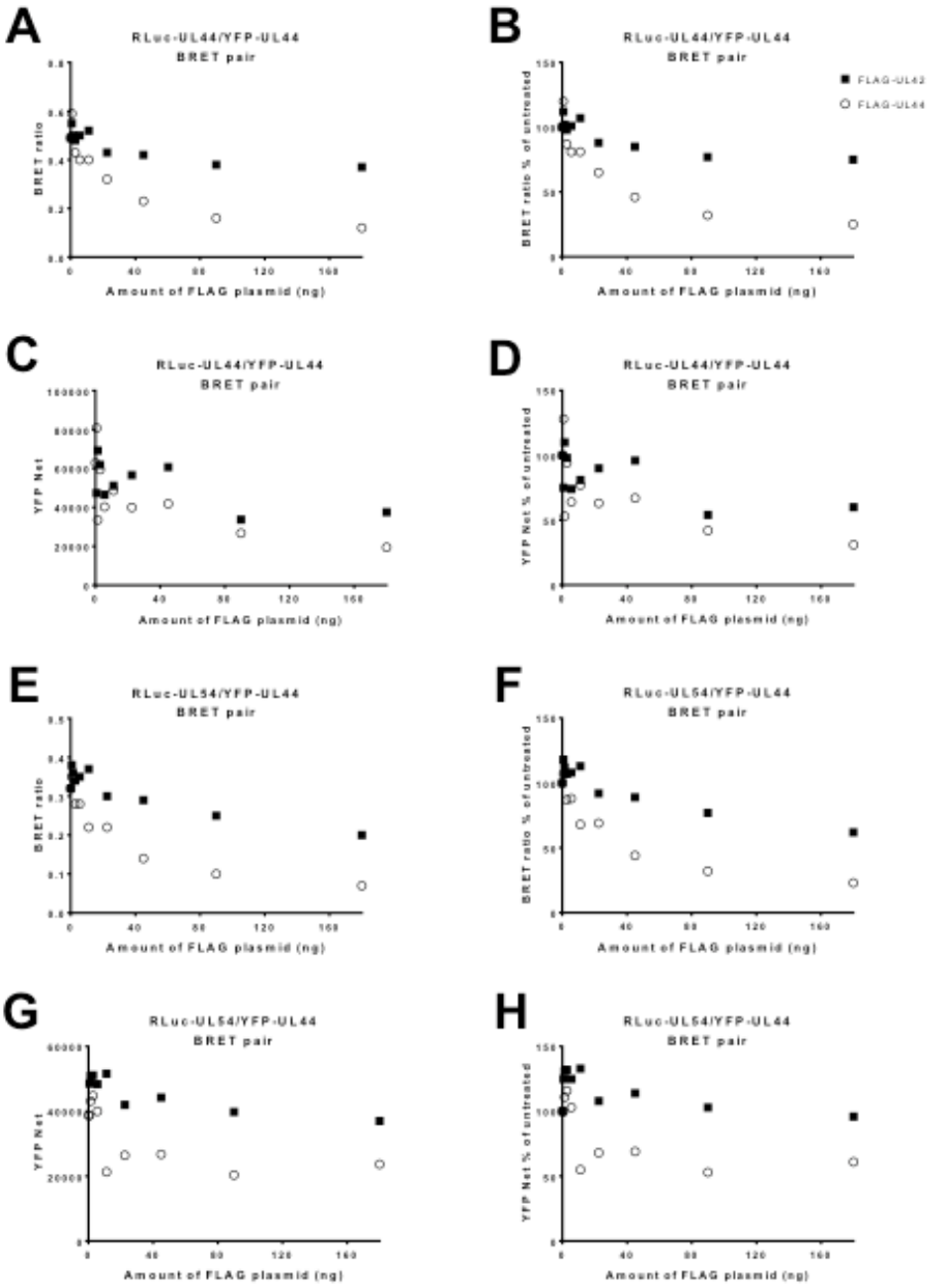
A
RLuc-UL44/YFP-UL44
BRET pair
BRET ratio
Amount of FLAG plasmid (ng)
B
RLuc-UL44/YFP-UL44
BRET pair
FLAG-UL43
FLAG-UL44
BRET ratio % of untreated
Amount of FLAG plasmid (ng)
C
RLuc-UL44/YFP-UL44
BRET pair
YFP Net
Amount of FLAG plasmid (ng)
D
RLuc-UL44/YFP-UL44
BRET pair
YFP Net % of untreated
Amount of FLAG plasmid (ng)
E
RLuc-UL54/YFP-UL44
BRET pair
BRET ratio
Amount of FLAG plasmid (ng)
F
RLuc-UL54/YFP-UL44
BRET pair
BRET ratio % of untreated
Amount of FLAG plasmid (ng)
G
RLuc-UL54/YFP-UL44
BRET pair
YFP Net
Amount of FLAG plasmid (ng)
H
RLuc-UL54/YFP-UL44
BRET pair
YFP Net % of untreated
Amount of FLAG plasmid (ng)

Figure 4.32

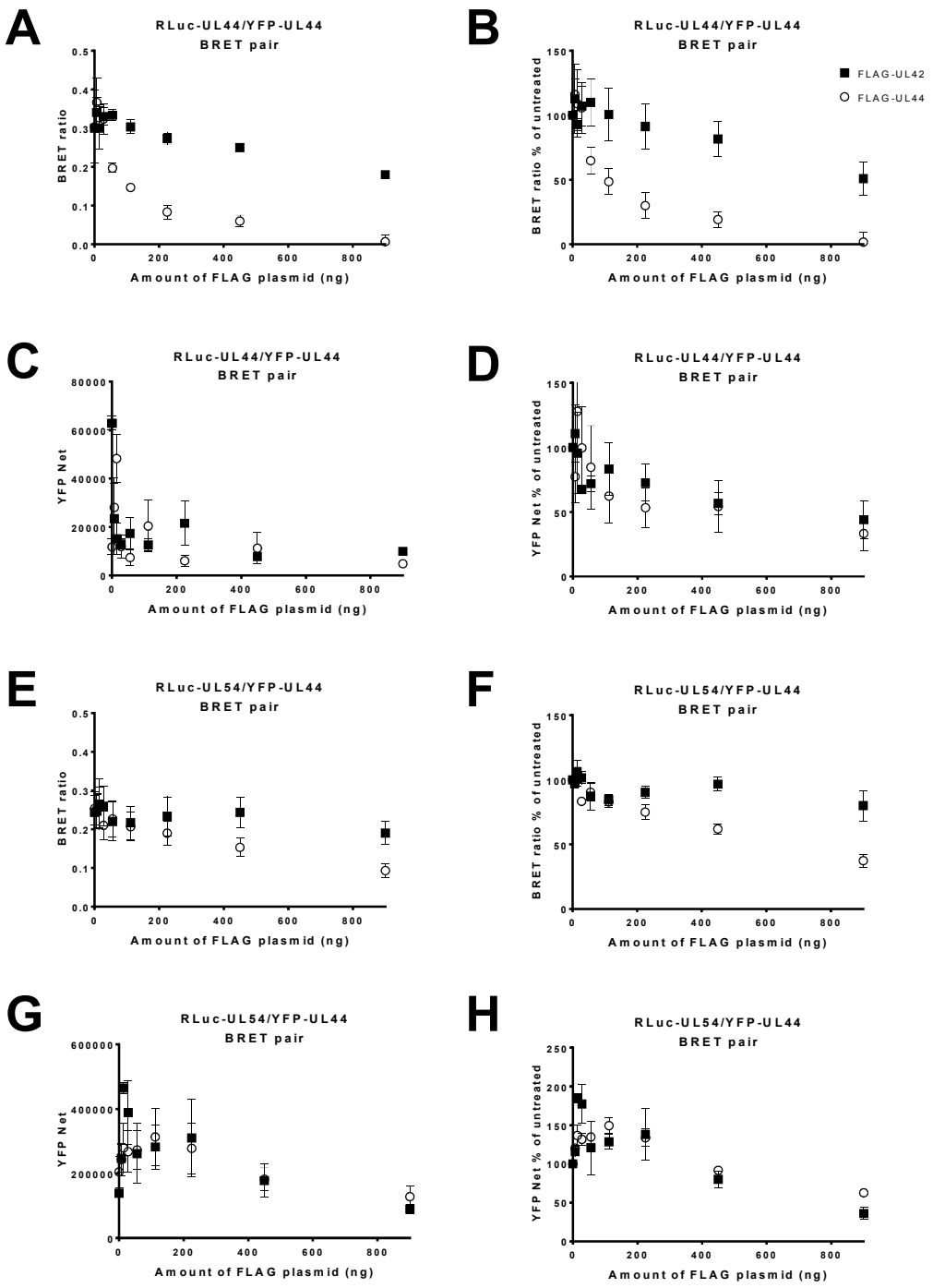
A
RLuc-UL44/YFP-UL44
BRET pair
BRET ratio
Amount of FLAG plasmid (ng)
B
RLuc-UL44/YFP-UL44
BRET pair
BRET ratio % of untreated
FLAG-UL42
FLAG-UL44
Amount of FLAG plasmid (ng)
C
RLuc-UL44/YFP-UL44
BRET pair
YFP Net
Amount of FLAG plasmid (ng)
D
RLuc-UL44/YFP-UL44
BRET pair
YFP Net % of untreated
Amount of FLAG plasmid (ng)
E
RLuc-UL54/YFP-UL44
BRET pair
BRET ratio
Amount of FLAG plasmid (ng)
F
RLuc-UL54/YFP-UL44
BRET pair
BRET ratio % of untreated
Amount of FLAG plasmid (ng)
G
RLuc-UL54/YFP-UL44
BRET pair
YFP Net
Amount of FLAG plasmid (ng)
H
RLuc-UL54/YFP-UL44
BRET pair
YFP Net % of untreated
Amount of FLAG plasmid (ng)

Figure 4.33

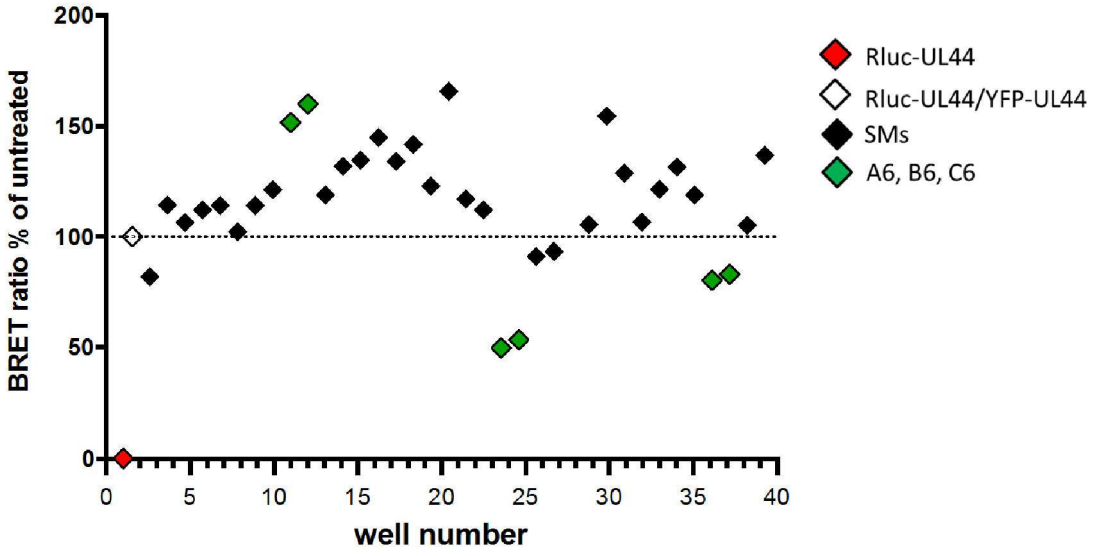
BRET ratio % of untreated
200
150
100
50
0
0
5
10
15
20
25
30
35
40
well number
Rluc-UL44
Rluc-UL44/YFP-UL44
SMs
A6, B6, C6

Figure 4.34

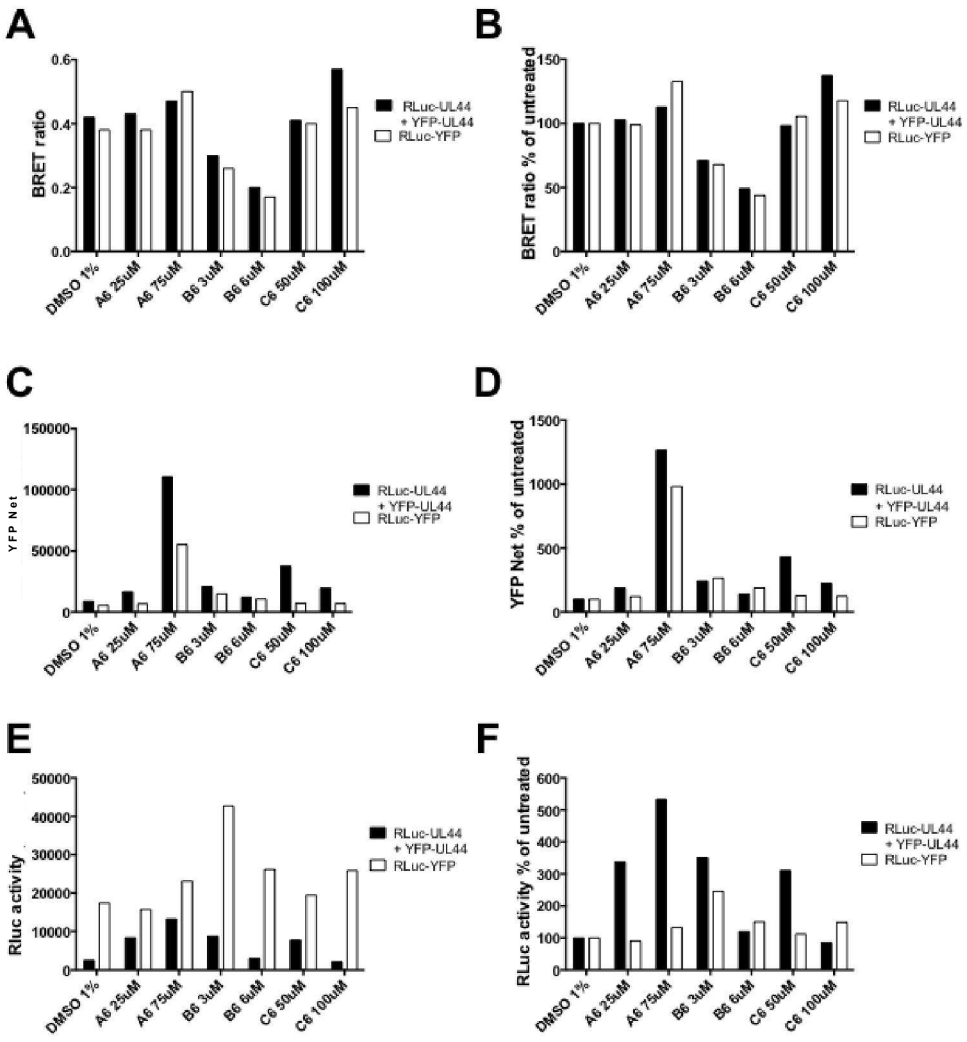
A
BRET ratio
0.6
0.4
0.2
0.0
RLuc-UL44
+ YFP-UL44
RLuc-YFP
DMSO 1%
A6 25uM
A6 75uM
B6 3uM
B6 6uM
C6 50uM
C6 100uM
B
BRET ratio % of untreated
150
100
50
0
C
YFP Net
150000
100000
50000
0
D
YFP Net % of untreated
1500
1000
500
0
E
Rluc activity
50000
40000
30000
20000
10000
0
F
RLuc activity % of untreated
600
500
400
300
200
100
0

Figure 4.35

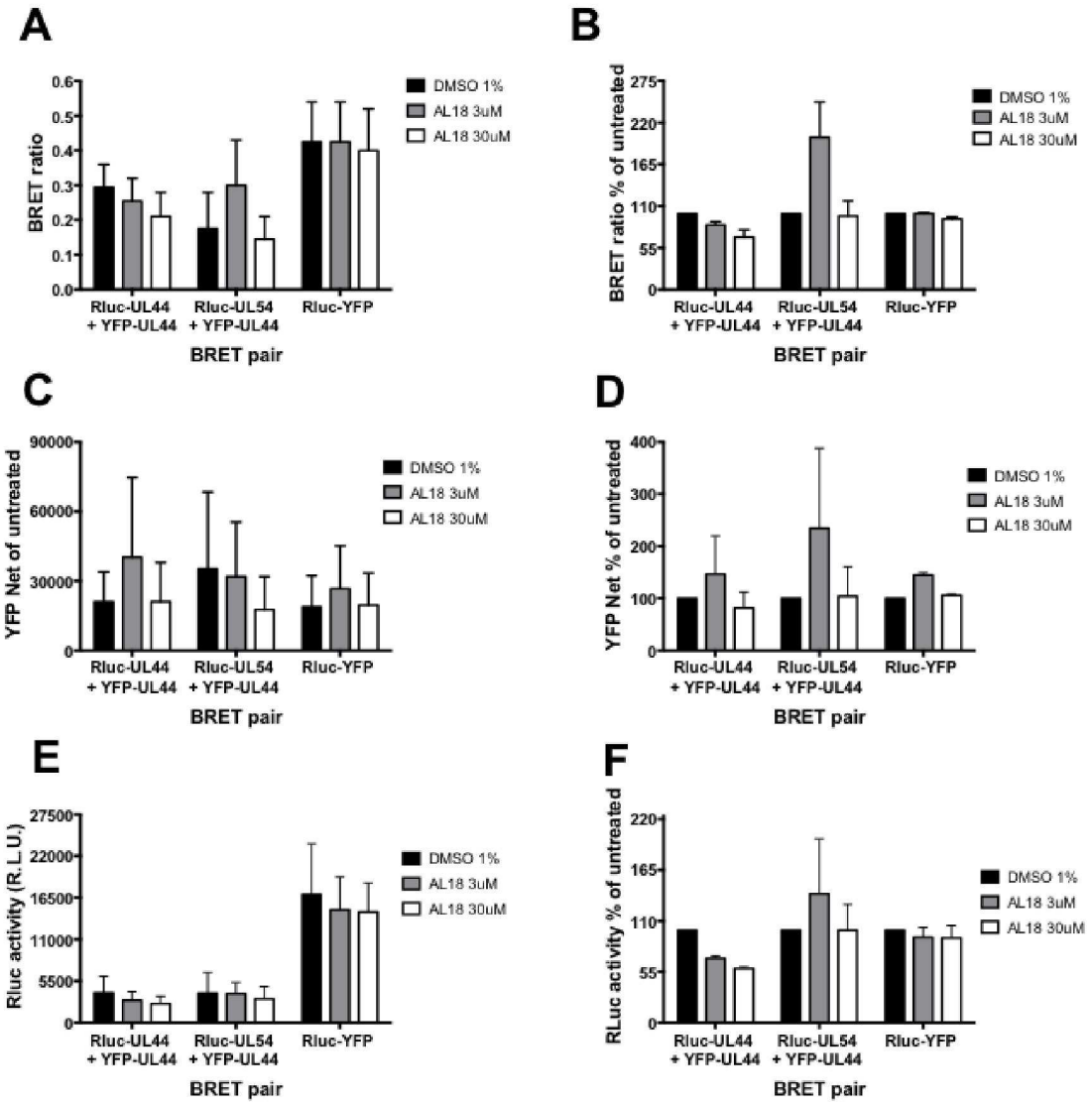
A
BRET ratio
0.6
0.5
0.4
0.3
0.2
0.1
0.0
DMSO 1%
AL18 3uM
AL18 30uM
Rluc-UL44 + YFP-UL44
Rluc-UL54 + YFP-UL44
Rluc-YFP
BRET pair
B
BRET ratio % of untreated
275
220
165
110
55
0
DMSO 1%
AL18 3uM
AL18 30uM
Rluc-UL44 + YFP-UL44
Rluc-UL54 + YFP-UL44
Rluc-YFP
BRET pair
C
YFP Net of untreated
90000
60000
30000
0
DMSO 1%
AL18 3uM
AL18 30uM
Rluc-UL44 + YFP-UL44
Rluc-UL54 + YFP-UL44
Rluc-YFP
BRET pair
D
YFP Net % of untreated
400
300
200
100
0
DMSO 1%
AL18 3uM
AL18 30uM
Rluc-UL44 + YFP-UL44
Rluc-UL54 + YFP-UL44
Rluc-YFP
BRET pair
E
Rluc activity (R.L.U.)
27500
22000
16500
11000
5500
0
DMSO 1%
AL18 3uM
AL18 30uM
Rluc-UL44 + YFP-UL44
Rluc-UL54 + YFP-UL44
Rluc-YFP
BRET pair
F
RLuc activity % of untreated
220
165
110
55
0
DMSO 1%
AL18 3uM
AL18 30uM
Rluc-UL44 + YFP-UL44
Rluc-UL54 + YFP-UL44
Rluc-YFP
BRET pair

Figure 4.36

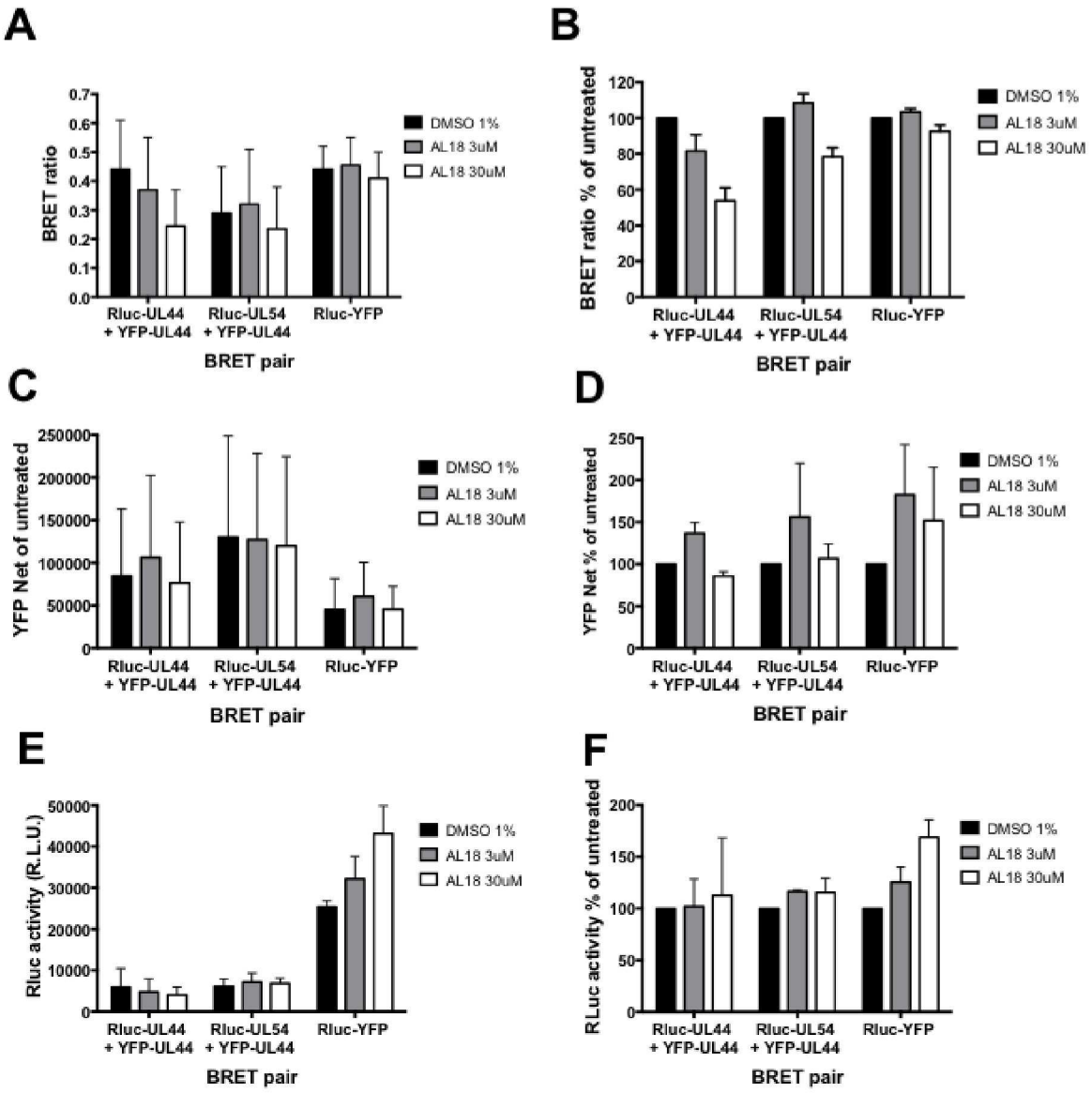
A
BRET ratio
0.7
0.6
0.5
0.4
0.3
0.2
0.1
0.0
DMSO 1%
AL18 3uM
AL18 30uM
Rluc-UL44 + YFP-UL44
Rluc-UL54 + YFP-UL44
Rluc-YFP
BRET pair
B
BRET ratio % of untreated
120
100
80
60
40
20
0
DMSO 1%
AL18 3uM
AL18 30uM
Rluc-UL44 + YFP-UL44
Rluc-UL54 + YFP-UL44
Rluc-YFP
BRET pair
C
YFP Net of untreated
250000
200000
150000
100000
50000
0
DMSO 1%
AL18 3uM
AL18 30uM
Rluc-UL44 + YFP-UL44
Rluc-UL54 + YFP-UL44
Rluc-YFP
BRET pair
D
YFP Net % of untreated
250
200
150
100
50
0
DMSO 1%
AL18 3uM
AL18 30uM
Rluc-UL44 + YFP-UL44
Rluc-UL54 + YFP-UL44
Rluc-YFP
BRET pair
E
Rluc activity (R.L.U.)
50000
40000
30000
20000
10000
0
DMSO 1%
AL18 3uM
AL18 30uM
Rluc-UL44 + YFP-UL44
Rluc-UL54 + YFP-UL44
Rluc-YFP
BRET pair
F
RLuc activity % of untreated
200
150
100
50
0
DMSO 1%
AL18 3uM
AL18 30uM
Rluc-UL44 + YFP-UL44
Rluc-UL54 + YFP-UL44
Rluc-YFP
BRET pair

Figure 4.37

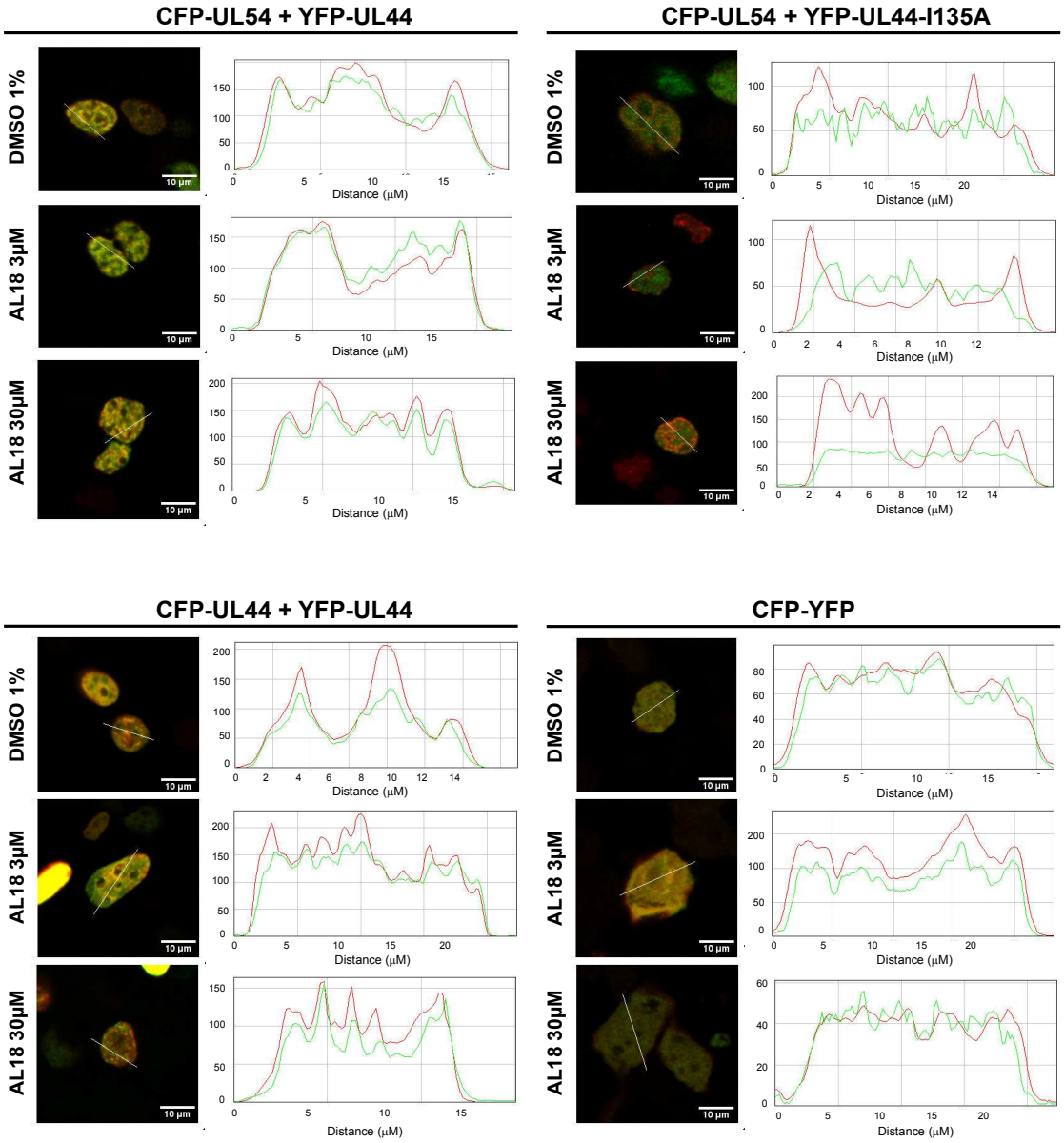
CFP-UL54 + YFP-UL44
CFP-UL54 + YFP-UL44-I135A
CFP-UL44 + YFP-UL44
CFP-YFP
DMSO 1%
AL18 3µM
AL18 30µM
10 µm
Distance (µM)

Figure 4.38

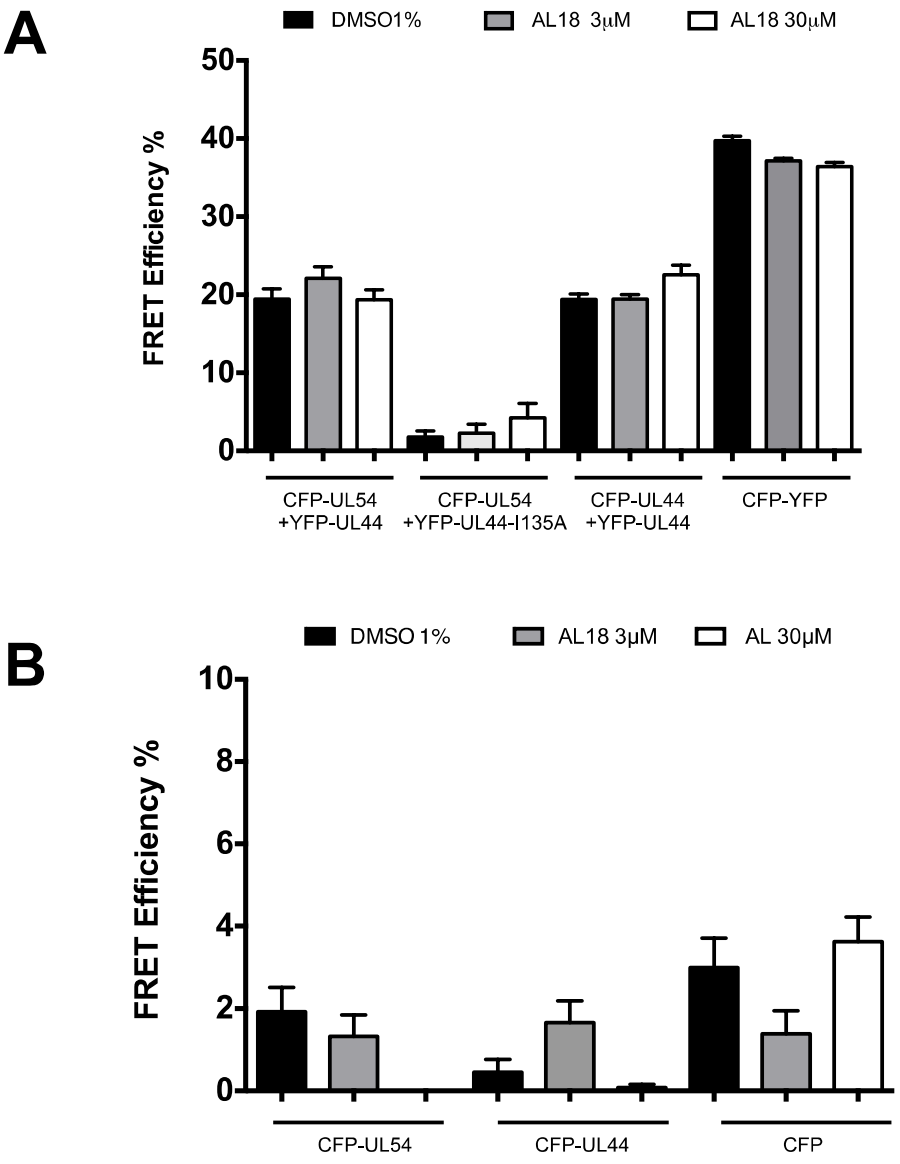
A
DMSO1%
AL18 3μM
AL18 30μM
FRET Efficiency %
50
40
30
20
10
0
CFP-UL54 +YFP-UL44
CFP-UL54 +YFP-UL44-I135A
CFP-UL44 +YFP-UL44
CFP-YFP
B
DMSO 1%
AL18 3μM
AL 30μM
FRET Efficiency %
10
8
6
4
2
0
CFP-UL54
CFP-UL44
CFP

Figure 4.39

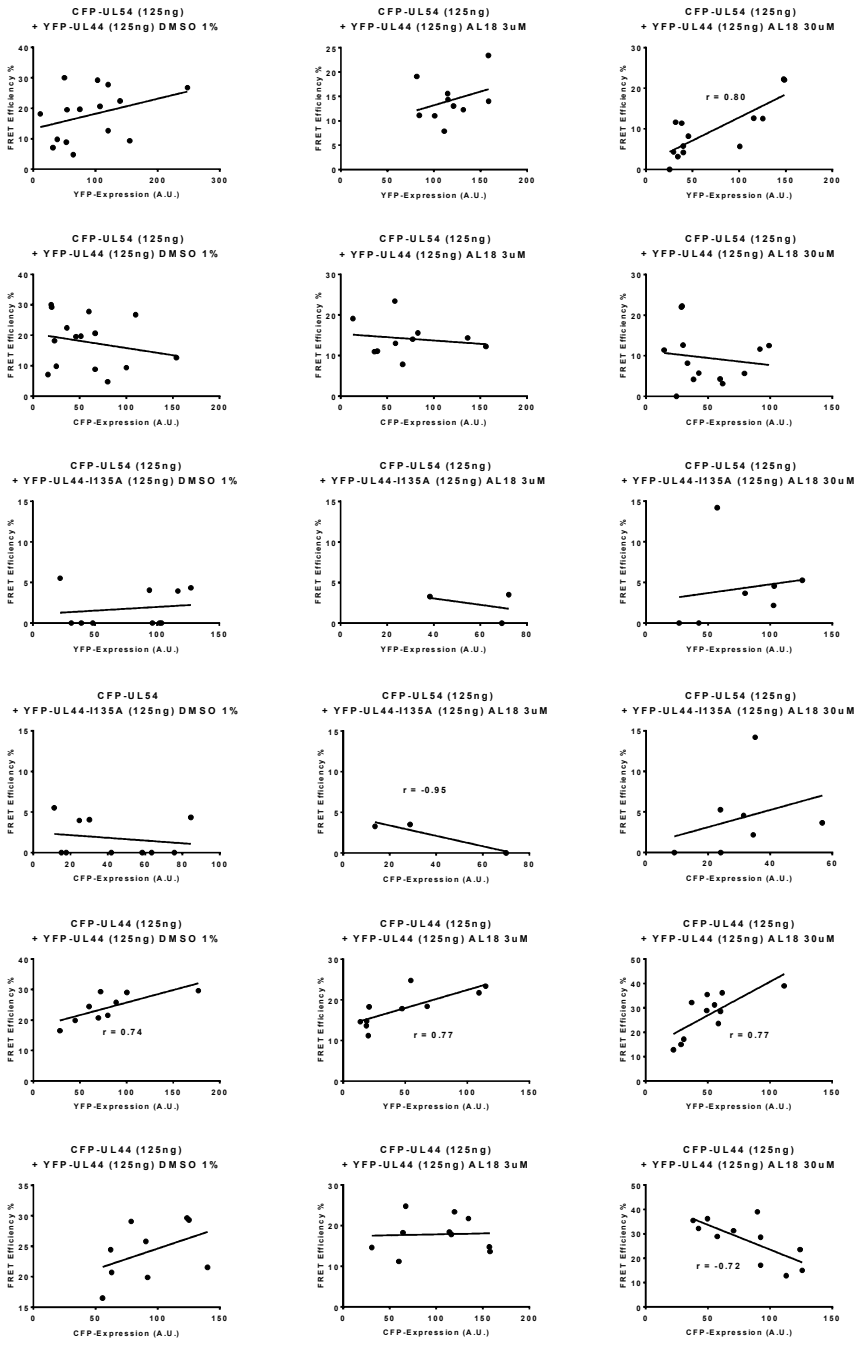
CFP-UL54 (125ng)
+ YFP-UL44 (125ng) DMSO 1%
CFP-UL54 (125ng)
+ YFP-UL44 (125ng) AL18 3uM
CFP-UL54 (125ng)
+ YFP-UL44 (125ng) AL18 30uM
r = 0.80
CFP-UL54 (125ng)
+ YFP-UL44 (125ng) DMSO 1%
CFP-UL54 (125ng)
+ YFP-UL44 (125ng) AL18 3uM
CFP-UL54 (125ng)
+ YFP-UL44 (125ng) AL18 30uM
CFP-UL54 (125ng)
+ YFP-UL44-I135A (125ng) DMSO 1%
CFP-UL54 (125ng)
+ YFP-UL44-I135A (125ng) AL18 3uM
CFP-UL54 (125ng)
+ YFP-UL44-I135A (125ng) AL18 30uM
CFP-UL54
+ YFP-UL44-I135A (125ng) DMSO 1%
CFP-UL54 (125ng)
+ YFP-UL44-I135A (125ng) AL18 3uM
r = -0.95
CFP-UL54 (125ng)
+ YFP-UL44-I135A (125ng) AL18 30uM
CFP-UL44 (125ng)
+ YFP-UL44 (125ng) DMSO 1%
r = 0.74
CFP-UL44 (125ng)
+ YFP-UL44 (125ng) AL18 3uM
r = 0.77
CFP-UL44 (125ng)
+ YFP-UL44 (125ng) AL18 30uM
r = 0.77
CFP-UL44 (125ng)
+ YFP-UL44 (125ng) DMSO 1%
CFP-UL44 (125ng)
+ YFP-UL44 (125ng) AL18 3uM
CFP-UL44 (125ng)
+ YFP-UL44 (125ng) AL18 30uM
r = -0.72
FRET Efficiency %
YFP-Expression (A.U.)
CFP-Expression (A.U.)

Figure 4.40

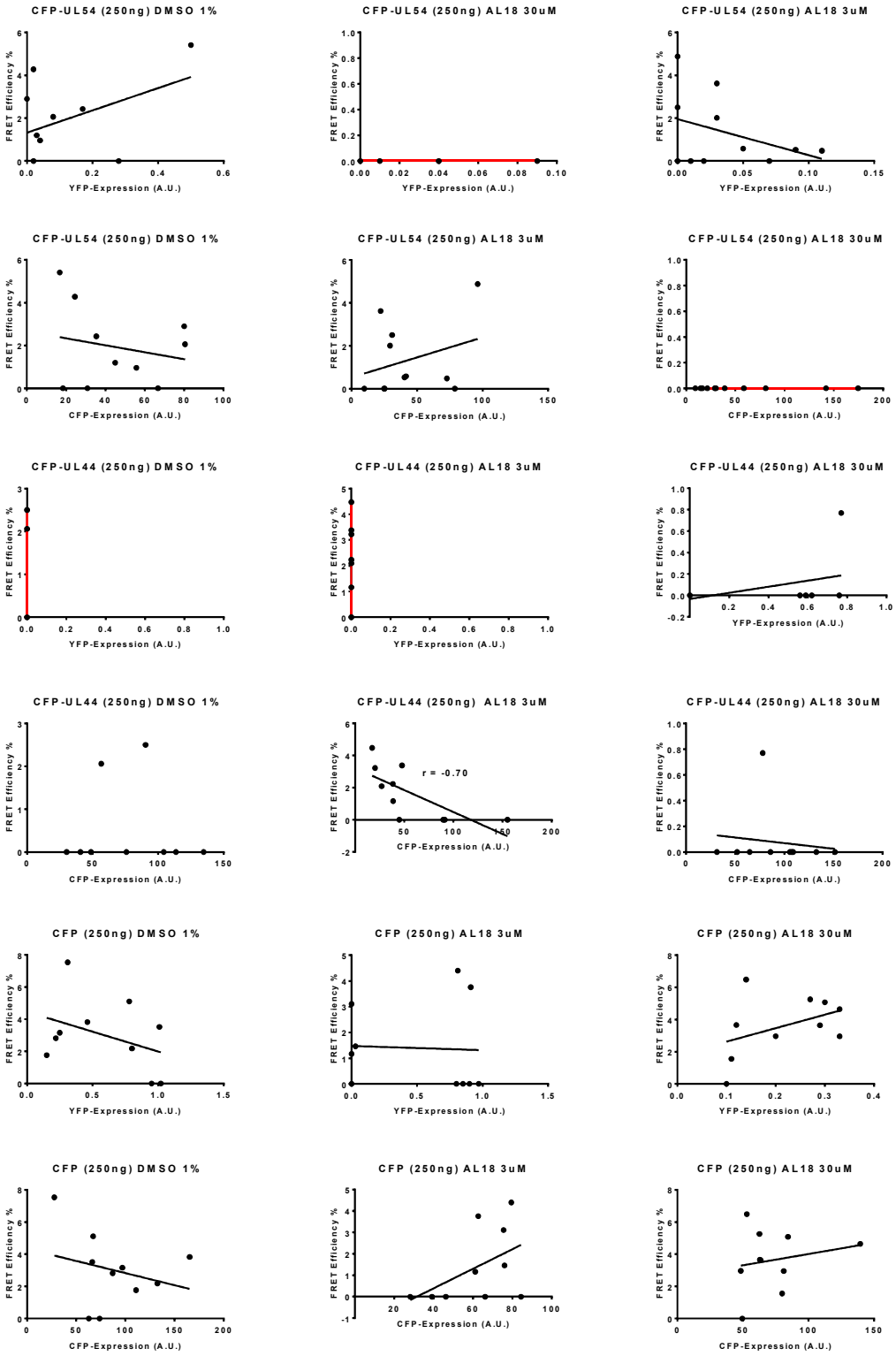
CFP-UL54 (250ng) DMSO 1%
FRET Efficiency %
YFP-Expression (A.U.)
CFP-UL54 (250ng) AL18 30uM
FRET Efficiency %
YFP-Expression (A.U.)
CFP-UL54 (250ng) AL18 3uM
FRET Efficiency %
YFP-Expression (A.U.)
CFP-UL54 (250ng) DMSO 1%
FRET Efficiency %
CFP-Expression (A.U.)
CFP-UL54 (250ng) AL18 3uM
FRET Efficiency %
CFP-Expression (A.U.)
CFP-UL54 (250ng) AL18 30uM
FRET Efficiency %
CFP-Expression (A.U.)
CFP-UL44 (250ng) DMSO 1%
FRET Efficiency %
YFP-Expression (A.U.)
CFP-UL44 (250ng) AL18 3uM
FRET Efficiency %
YFP-Expression (A.U.)
CFP-UL44 (250ng) AL18 30uM
FRET Efficiency %
YFP-Expression (A.U.)
CFP-UL44 (250ng) DMSO 1%
FRET Efficiency %
CFP-Expression (A.U.)
CFP-UL44 (250ng) AL18 3uM
r = -0.70
FRET Efficiency %
CFP-Expression (A.U.)
CFP-UL44 (250ng) AL18 30uM
FRET Efficiency %
CFP-Expression (A.U.)
CFP (250ng) DMSO 1%
FRET Efficiency %
YFP-Expression (A.U.)
CFP (250ng) AL18 3uM
FRET Efficiency %
YFP-Expression (A.U.)
CFP (250ng) AL18 30uM
FRET Efficiency %
YFP-Expression (A.U.)
CFP (250ng) DMSO 1%
FRET Efficiency %
CFP-Expression (A.U.)
CFP (250ng) AL18 3uM
FRET Efficiency %
CFP-Expression (A.U.)
CFP (250ng) AL18 30uM
FRET Efficiency %
CFP-Expression (A.U.)

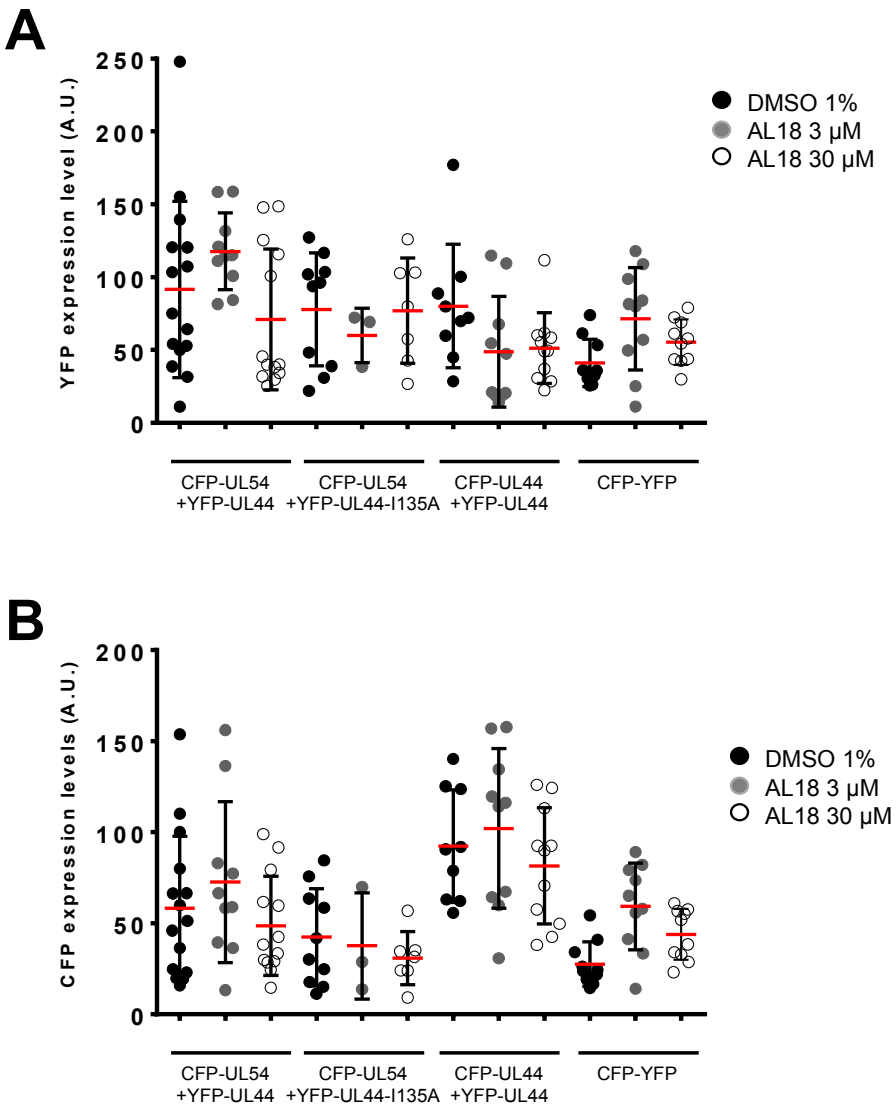
A
YFP expression level (A.U.)
250
200
150
100
50
0
DMSO 1%
AL18 3 µM
AL18 30 µM
CFP-UL54 +YFP-UL44
CFP-UL54 +YFP-UL44-I135A
CFP-UL44 +YFP-UL44
CFP-YFP
B
CFP expression levels (A.U.)
200
150
100
50
0
DMSO 1%
AL18 3 µM
AL18 30 µM
CFP-UL54 +YFP-UL44
CFP-UL54 +YFP-UL44-I135A
CFP-UL44 +YFP-UL44
CFP-YFP

Figure 4.42
Figure 4.41

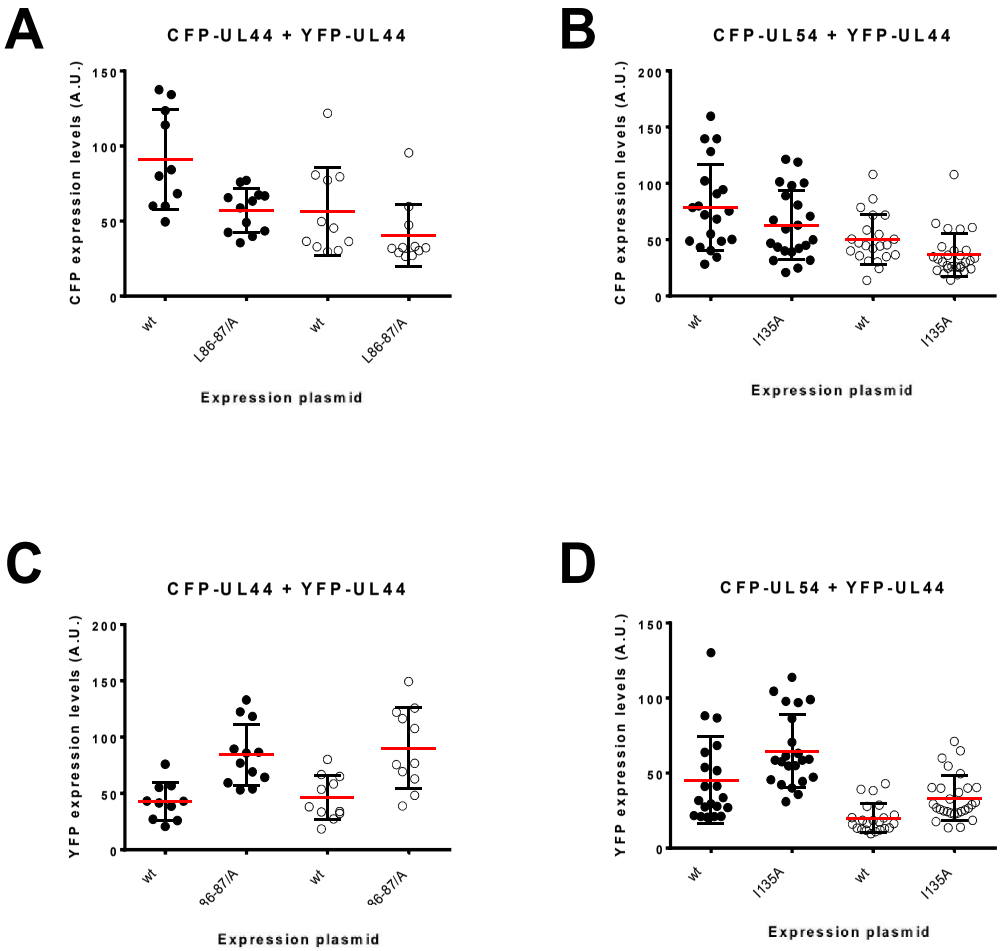

Figure 4.43

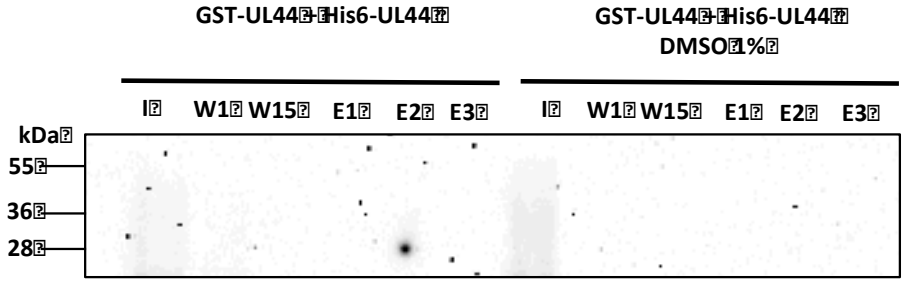
GST-UL44 + His6-UL44
GST-UL44 + His6-UL44
DMSO 1%
I
W1
W15
E1
E2
E3
I
W1
W15
E1
E2
E3
kDa
55
36
28

Figure 4.44

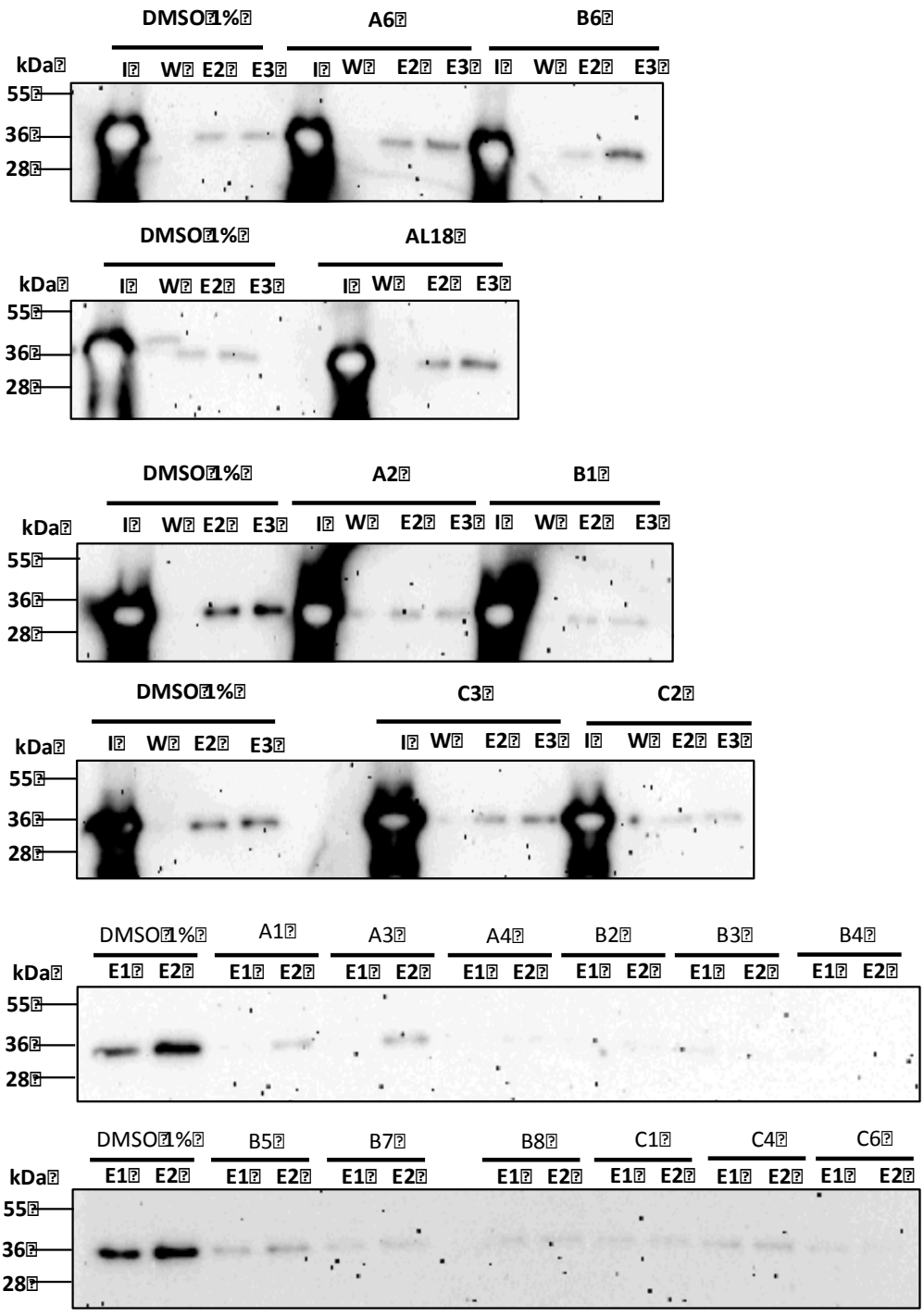
DMSO 1%
A6
B6
kDa
I W E2 E3 I W E2 E3 I W E2 E3
55
36
28
DMSO 1%
AL18
kDa
I W E2 E3 I W E2 E3
55
36
28
DMSO 1%
A2
B1
kDa
I W E2 E3 I W E2 E3 I W E2 E3
55
36
28
DMSO 1%
C3
C2
kDa
I W E2 E3 I W E2 E3 I W E2 E3
55
36
28
DMSO 1%
A1
A3
A4
B2
B3
B4
kDa
E1 E2 E1 E2 E1 E2 E1 E2 E1 E2 E1 E2 E1 E2
55
36
28
DMSO 1%
B5
B7
B8
C1
C4
C6
kDa
E1 E2 E1 E2 E1 E2 E1 E2 E1 E2 E1 E2 E1 E2
55
36
28

7. Table and figures legends

Table 4.1. FRET transfection conditions. Table reports all FRET plasmids used during this study with the relative amounts used to transfect HEK 293-T cells, related to conditions A and B.

Table 4.2. Laser and PMT settings used for FRET acceptor photobleaching analysis. Settings used (Laser power, Gain and Offset) for samples acquisition of pre and post-beaching images are indicated.

Table 4.3. Effect of point mutations of UL44 on indicated properties.

1: Isotermal titration calorimetry; bacterially expressed UL44 (CD290) 5-10 uM + 22 C-terminal peptide of UL54 100-250 uM [56, 78], when available, Kd is shown.

2: Subcellular re-localization assay [61, 62].

3: BRET assays using CTZ, Di Antonio et al., unpublished. Bmax and B50 are shown.

4: Analytical gel filtration using 20-25 uM of bacterially expressed UL44 (CD290) [56].

5: Analytical ultracentrifugation usingbacterially expressed UL44 (CD290) [56].

6: Cellular permeabilization assays [62].

7: OriLyt transcomplementation assay [61, 62].

8: Confocal microscopy [61, 62].

Table 4.4.Toxicity and solubility of SMs. The CC50 calculated for each of the indicated compounds in shown along with the maximum concentration at which precipitates were not observed. The concentration used for SMs screening in BRET assays is shown on the right. A, indicated the CC50 calculated by WST assay; B indicated the CC50 calculated by visual inspections. [1] Parameter Logistic Equation (Sigmoidal) method; [2]linear regression method; *massive precipitation at higher concentrations.

Table 4.5.BRET parameters related to the indicated BRET pairs obtained using CTZ or h-CTZ as substrates. BRET saturation curves such as those shown in Figure 4.5 were used as described in §3.28.1, to calculate Bmax and B50 values. Data indicated are mean values of different independent experiments, along with the S.D. of the mean and sample size. Values calculated based on raw YFP/RLuc values are shown on the left, whereas values calculated based on YFP/RLuc values normalized to that of the RLuc-YFP control molecule are shown on the right. (*) Indicates statistically significant difference between values obtained with CTZ and h-CTZ (t student, $p < 0.05$).

Table 4.6. Scheme Scheme of the concentrations used for the cell viability assay.

Table 4.7. **Effect of SMs on UL44 dimerization by BRET using the stable YFP-UL44 1B2 cell line .** $1x10^5$ 1B2 stably expressing YFP-UL44 cells were seeded in 24 well plates cells and 24h later cells were transfected with 25ng of RLuc-UL44 expression plasmid. HEK293A cells were seeded in parallel and transfected either with 25ng of RLuc-UL44, to allow calculation of background BRET signal, or with both 25ng of RLuc-UL44 and 40ng of YFP-UL44, as a positive control. Based on previous experiments, we calculated that such combination of plasmids would result in a BRET ratio similar to 50% of the B_{max}

Figure 4.1. Analysis of subcellular localization and molecular weight of expressed proteins. Plasmids were transfected in HEK293 T cells $5x10^4$ containing poly-lysinated glass coverslips and their subcellular localization investigated by CLSM 48h p.t. CFP, YFP and CFP-YFP homogenously distributed throughout the cells with a diffuse pattern (A).Fusion of UL44 to either CFP or YFP resulted in strong nuclear localization and fusion to UL54 (1125-1242) resulted in proteins mainly localized to the cell nuclei with a diffuse pattern due to the presence of a NLS, but the lack of any DNA binding domain in UL54 C-terminus. (B), YFP and CFP-UL44 fusions could be detected as 70 kDa discrete bands, whereas UL54 (1125-1242) fusions (apparent MW of 37 kDa) migrated slower than CFP and YFP as individually expressed (MW c. 27 kDa), but slightly faster than the CFP-YFP fusion protein (MW c. 54 kDa).

Figure 4.2 Subcellular localization of fusion proteins used for FRET experiments. HEK 293 T cells were seeded on glass coverslips and transfected with the indicated expression plasmids . 48h pt, cells were fixed and processed for IF, before being analyzed by CLSM to investigate the subcellular localization of the indicated fusion proteins. The subcellular localization of CFP fusions as expressed alone (*left panels*) or in the presence of YFP fusions (*middle panels*) is shown, together with the correspondent RGB profiles (*right panels*).

Figure 4.3. Detection of dimerization of UL44 and its interaction with UL54 by means of FRET acceptor photobleaching. Cells described in Figure 4.2, were subjected to FRET acceptor photobleaching to calculate FRET efficiency (

§3.19.2). FRET efficiency relative to the indicated proteins in cells were media was changed 8h pt or 16 pt is shown in panel A or B, respectively. *Filled circles*, condition A*, Empty* circles, condition B (see Table 4.2). Data obtained after pooling all cells from *panel A* and *B* are reported in *panel C*. *Filled circles*, condition A*, Empty* circles, condition B (see Table 4.2). *Panel D* reports data from *panel C* where conditions A and B are pooled.

Figure 4.4. Correlation between FRET efficiency % and fluorophores expression levels. YFP and CFP pre-bleaching expression levels, relative to images, such those shown in Figure 4.13A, are plotted against FRET efficiency. Pearson r values relative to correlations higher than 0.5 or lower than -0.5 are reported on the correspondent graph

Figure 4.5. Correlation between FRET efficiency % and fluorophores expression levels. YFP and CFP pre-bleaching expression levels, relative to images, such those shown in Figure 4.13A, are plotted against FRET efficiency. Pearson r values relative to correlations higher than 0.5 or lower than -0.5 are reported on the correspondent graph.

Figure 4.6. Analysis of pre-bleaching CFP- and YFP-fusion expression levels. CFP (A, B) and YFP (C, D) pre-bleaching expression levels relative to the indicated FRET pairs of samples such those in Figure 4.3A are shown.

Figure 4.7. Analysis of subcellular localization and molecular weight of expressed proteins. (A)HEK293 T cells were seeded in 24 well plate containing poly lysinated coverslip glasses and after 24h p.t. the cells were transfected with RLuc expressing plasmids and the subcellular localization of expressed proteins was investigated by inverted fluorescent microscope (Leica, DFC420 C), 48 h p.t.. (B) Western blotting analysis indicate that all fusion proteins could be readily detected at the expected molecular weight.

Figure 4.8. Analysis of protein expression levels mediated by BRET plasmids. Seeded $1x10^5$ HEK293 T cells per well of a 24 well plate, and 24h later, transfected cells using Lipofectamine 2000 with increasing amounts of plasmids (from 0 to 500ng) mediating the expression of either the YFP-UL44, the RLuc-UL44 or the RLuc-UL44(405-433) fusion proteins. 48h p.t. cells were processed for detection of fluorimetric (YFP-fusions) and luminescent (RLuc-fusion) expression by using a plate reader, 5' after addition of RLuc substrate CTZ (5µM).

Figure 4.9. Analysis of protein expression levels mediated by BRET plasmids. Seeded $1x10^5$ HEK293 T cells per well of a 24 well plate, and 24h later, transfected cells using Lipofectamine 2000 with increasing amounts of plasmids (from 0 to 500ng) mediating the expression of either the YFP-UL44, the RLuc-UL44 or the RLuc-UL44(405-433) fusion proteins. 48h p.t. cells were processed for detection of fluorimetric (YFP-fusions) and luminescent (RLuc-fusion) expression by using a plate reader, 5' after addition of RLuc substrate CTZ (5µM)

Figure 4.10. Detection of UL44 dimerization in living cells by BRET.

$1x10^5$ HEK293 T cells were seeded and transfected as above with either 25ng RLuc-UL44 or 12.5ng RLuc-UL44 (405-433) alone, or in combination with YFP-UL44 500ng. 48h p.t. later cells were processed for BRET analysis .

Figure 4.11.Saturations curve. HEK293 T cells were seeded $1x10^5$ in 24 well plates and transfected with either 25ng of RLuc-UL44 or 6.25ng of RLuc-UL44 (405-433), in the presence of increasing amounts of the YFP-UL44 (range: 0 to 900ng). 48h later cells were processed for BRET analysis. Data could be fitted to a one site-specific binding curve ($R^2 = 0.982$) to generate a logarithmic shaped curve, which reached a plateau,

indicative of a specific interaction. On the opposite, the BRET ratio relative to the RLuc-UL44 (405-433)/YFP-UL44 BRET pair slowly increased in a linear fashion, without reaching a plateau, indicative of random interaction due to protein overexpression.

Figure 4.12. Analysis of expression of UL44, UL54 and their mutants. We transfected $1x10^5$ HEK 293T cells, 24h later seeding in a 24 well plate, using different amount of plasmids mediating the expression of RLuc and YFP plasmids fused to the protein of interest. 48h p.t. cells were processed for detection of fluorimetric (YFP-fusions) and luminescent (RLuc-fusion) expression by using a plate reader, 5' after addition of RLuc substrate CTZ.

Figure 4.13. Saturation curves of UL44, UL54 and their mutants.

we transfected $1x10^5$ HEK 293T cells, 24h later seeding in a 24 well plate, using different amount of plasmids mediating the expression of RLuc and increasing amount of YFP fusions (0 to 900ng), processed samples for fluorimeteric/luminometric detection, and calculated saturation curves using data obtained 45 min after CTZ addition. We calculated similar Bmax and B50 values for BRET pair.

Figure 4.14. Study of UL44 dimerization by GST-pull down. We incubated the recombinant proteins 6His-UL44(1-290), 6His-UL44(1-290)-L86/L87A dimerization impaired point mutant, GST-UL44 (1-290) and GST [75, 77]. After incubation, the complexes were loaded on glutathione specific columns. After extensive washes with NETN buffer, complexes where eluted with NETN+GSH buffer. The Figure show Input, Wash and Eluted fractions loaded.

Figure 4.15 Determination of concentrations of selective agent to be used. (A), trend of all concentrations from 0 day to 10 days. (B) trend of work concentration.

Figure 4.16 Localizzation on Stable cell line by inverted microscopie.

Figure 4.17. Analysis of stable YFP-UL44 cell lines expression levels and BRET ratio in the presence of transiently expressed RLuc-UL44. $1x10^5$ HEK293 A-YFP-UL44 (68-1x, 68-2x, 68-3x) and HEK293 A-pWPI-puro (7-1x, 7-2x, 7-3x) in 24 well plates in duplicate, and after 24 hour we transfected them with either UL44 (25ng) or RLuc-UL44 (405-433) (12.5ng) as a control, or pCDNA3 empty vector to calculate background. 48h later cells were processed for BRET analysis.

Figure 4.18. Generation stable cell line YFP-UL44. Analysis of YFP expression (A), RLuc activity (B) and BRET ratio.

Figure 4.19. Analysis of the effect of DMSO on cell viability . (A) Curve of cell viability. (B) HEK293 A in 96 well at 24h $1x10^4$ cells/well and $0.5x10^4$ cells/well for 48h and we treaded the cells with DMSO a different concentrations (10%, 1%, 0.1%, 0.01% and 0%). After 24h or 48h depending on the plate, we add the WST-1 and analyzed the plate by ELISA plate reader

Figure 4.20. Analysis of the effect of SMs on cell BRET signal . $1x10^5$ of cells in 24 well plate and 24h later we transfected polyclonal, monoclonal and HEK293 A-pPWI-puro cells line with RLuc-UL44 (25ng) and HEK293 A with RLuc-UL44 (25ng) and YFP-UL44 (80ng) and we used mock-untransfected cells were processed in parallel. 6 h p.t. media was replaced with DMSO1% or with fresh DMEM. 48 h p.t. We evaluated the effect of DMSO 1% on YFP (A) expression levels and RLuc activity (B) and BRET ratio (C), Z' score (D).

Figure 4.21 . Evaluation of toxicity of SMs on HEK 293A cells by linear regression. $5x10^4$ HEK293 A were seeded into 96 well and 24h later were treated with increasing amounts of compounds, (3μM-200μM). 48h post treatment absorbance at 450 nm was measured . Data were analyzed and fitted with linear regression with the software Prism to calculate CC50.

Figure 4.22. Evaluation of toxicity of SMs on HEK 293A cells by 4 Parameter Logisitic Equation (Sigmoidal). $5x10^4$ HEK293 A were seeded into 96 well and 24h later were treated with increasing amounts of compounds, (3μM-200μM). 48h post treatment absorbance at 450 nm was measured. Data was analyzed and fitted to a 4 Parameter Logistic Equation (Sigmoidal), with the software Prism to calculate CC50.

Figure 4.23 . Evaluation of toxicity of SMs on HEK293 A cells by linear regression. $5x10^4$ HEK293 A were seeded into 96 well and 24h later were treated with increasing amounts of compounds, (3μM-200μM). 48h post treatment we evaluated the CC50 by visual inspections. Data was analyzed and fitted to a 4 Parameter Logistic Equation (Sigmoidal), with the software Prism to calculate CC50.

Figure 4.24. Evaluation of toxicity of SMs on HEK293 A cells by linear regression. $5x10^4$ HEK293 A were seeded into 96 well and 24h later were treated with increasing amounts of compounds, (3μM-200μM). 48h post treatment we evaluated the CC50 by visual inspections. Data were analyzed and fitted with linear regression with the software Prism to calculate CC50.

Figure 4.25 . Assessment of the effect of SMs on UL44 dimerization by means of BRET assays. Monoclonal cell line (1B2) cells were transfected with 25 ng of RLuc-UL44, either alone (*red rhombus)* or in the presence of 40ng of YFP-UL44 expressing plasmid (*other rhombuses*). 8h p.t. transfection media was changed with DMEM containing 1% DMSO (*empty rhombus*) or two different concentrations of the indicated SMs (*black rhombus*, see Table 4.1 for concentrations). 24h later, cells were processed for BRET measurements. The BRET ratio at 45' after n-CTZ substrate addition is reported for each condition.

Figure 4.26 . Generation double stable cell line RLuc-UL44/YFP-UL44. 1B2 cell lline was transfected with pre-linearized RLuc-UL44 in a 6 well plate, and cells expressing RLuc-UL44 were selected by treatment with neomycin (700µg/ml).

Figure 4.27. Dose dependent inhibition of BRET ratio by overexpression of BRET competitors using CTZ. Polyclonal , HEK 293 T and monoclonal and cells were transfected respectively with fixed amounts of RLuc-UL44/YFP-UL44, A-D; 0 ng for RLuc-UL44, 0 ng for YFP-UL44, E-H; 25ng for RLuc-UL44, 40 ng for YFP-UL44, and I-N; 25 ng for RLuc-UL44, 0 ng for YFP-UL44) expressing plasmids in the presence of increasing amounts of the indicated FLAG-tagged fusions expressing plasmids (FLAG-UL44, *empty circles*; FLAG-UL42, *filled squares*) and processed 48h pt before addition of CTZ and data acquisition and analysis to calculate BRET inhibition. BRET ratio (A, B, E, F, I L) and YFPnet (C, G, M), either as raw values (A, C, E, G, I,M) or as a percentage of values obtained for samples in the absence of competitor, are plotted against the amounts of competitor plasmids used to transfect cells.

Figure 4.28. Effect of substitution of CTZ with h-CTZ on RLuc activity.

293 T cells were transfected with 2.5 ng (h-CTZ) or 25 ng of RLuc-UL44 (CTZ) for 24h before being processed for RLuc measurement). Cells were further incubated with the indicated substrates (5 µM) before measuring RLuc activity at the indicated time points. Data shown are the mean ± standard deviation of the mean (S.D.) of three independent experiments.

293-T cells were transfected with the indicated amounts of RLuc-UL44 for 24h before being processed for RLuc measurement. Cells were incubated with the indicated concentrations of h-CTZ before measurement of RLuc activity, 15 min post substrate addition. Data show the RLuc activities (RLU) ± S.D. from three technical replicas relative to a single experiment.

293 T cells were transfected with increasing amounts of RLuc-UL44 and RLuc-UL54 as indicated, 24h and 48h before being processed for RLuc measurement. Cells were incubated with 5 µM h-CTZ before measurement of RLuc activity at 15 min post substrate addition. Data show the RLuc activities (RLU) ± S.D. at the different plasmid quantities.

Figure 4.29. Time dependent variations of RLuc activity and BRET ratio using CTZ or h-CTZ. Data from saturation experiments such those in Figure 4.5 were used to compare RLuc activity and BRET ratio values at the indicated time points after substrate addition (CTZ, *blue circles* or h-CTZ, *red circles*). RLuc activity and BRET ratio, relative to transfection with maximum amounts of acceptor plasmid (YFP-UL44) in the presence of fixed amounts of RLuc-UL44 (A-D; 2.5 ng for h-CTZ, 25 ng for CTZ) or RLuc-UL54 (E-H; 10 ng for h-CTZ, 100 ng for CTZ), are either shown as raw values (A, C, E, G) or normalized as a percentage of values obtained 5 min post substrate addition (B, D, F, H).

Figure 4.30. BRET saturation curves relative to the indicated BRET pairs obtained using CTZ or h-CTZ. HEK 293 T cells were transfected for BRET saturation experiments, and processed 48h later, before data acquisition and analysis to generate BRET saturation curves. Where indicated, data were normalized using the YFP/RLuc value relative to the RLuc-YFP control. For each condition, the BRET ratio is plotted against the relative YFP/RLuc signal. For CTZ based experiments, raw values are calculated 45 min post

substrate addition. In all other cases, values are derived from measurement performed 15 min post substrate addition. A representative curve for each condition is shown.

Figure 4.31 . Dose dependent inhibition of BRET ratio by overexpression of BRET competitors using CTZ. HEK 293 T cells were transfected with fixed amounts of RLuc-UL44/YFP-UL44 (A-D; 25 ng for RLuc-UL44, 40 ng for YFP-UL44) or RLuc-UL54/YFP-UL44 (E-H; 100 ng for RLuc-UL54, 40 ng for YFP-UL44) expressing plasmids in the presence of increasing amounts of the indicated FLAG-tagged fusions expressing plasmids (FLAG-UL44, *empty circles*; FLAG-UL42, *filled squares*) and processed 48h pt before addition of CTZ and data acquisition and analysis to calculate BRET inhibition. BRET ratio (A, B, E, F) and YFPnet (C, D, G, H), either as raw values (A, C, E, G) or as a percentage of values obtained for samples in the absence of competitor, are plotted against the amounts of competitor plasmids used to transfect cells.

Figure 4.32 . Dose dependent inhibition of BRET ratio by overexpression of BRET competitors using CTZ. HEK 293 T cells were transfected with fixed amounts of RLuc-UL44/YFP-UL44 (A-D; 25 ng for RLuc-UL44, 40 ng for YFP-UL44) or RLuc-UL54/YFP-UL44 (E-H; 100 ng for RLuc-UL54, 40 ng for YFP-UL44) expressing plasmids in the presence of increasing amounts of the indicated FLAG-tagged fusions expressing plasmids (FLAG-UL44, *empty circles*; FLAG-UL42, *filled squares*) and processed 48h pt before addition of CTZ and data acquisition and analysis to calculate BRET inhibition. BRET ratio (A, B, E, F) and YFPnet (C, D, G, H), either as raw values (A, C, E, G) or as a percentage of values obtained for samples in the absence of competitor, are plotted against the amounts of competitor plasmids used to transfect cells.

Figure 4.33 . Assessment of the effect of SMs on UL44 dimerization by means of BRET assays. HEK293 T cells were transfected with 2.5 ng of RLuc-UL44, either alone (*red rhombus)* or in the presence of 40 ng of YFP-UL44 expressing plasmid (*other rhombuses*). 8h p.t. transfection media was changed with DMEM containing 1% DMSO (*empty rhombus*) or two different concentrations of the indicated SMs (*black rhombus*, see Table 4.1 for concentrations). 24h later, cells were processed for BRET measurements. The BRET ratio at 15' after h-CTZ substrate addition is reported for each condition.

Figure 4.34. Effect of selected SMs, on BRET ratio relative to RLuc-UL44/YFP-UL44 and the control fusion protein RLuc-YFP. $2x10^5$ HEK 293-T cells were transfected with RLuc-UL44 (2.5ng) alone or in the presence of YFP-UL44 (40ng; black bars), or with a plasmid encoding the control fusion protein Rluc-YFP (22ng; white bars). 8h later cells media was replaced with DMEM containing either 1% DMSO or the indicated concentrations of SMs (Table 4.1). 24h pt cells were processed for measurement of BRET inhibition after 15' after addition of h-CTZ. For each BRET pair, BRET ratio (A, B), YFPnet (C, D), and Rluc activity (E, F) are shown, either as raw values (A, C, E) or as a percentage of values obtained for samples in the absence of compound (B, D, F).

Figure 4.35. Effect of AL18 treatment for 16h on UL54-UL44 interaction as detected by BRET. $2x10^5$ HEK293 T cells were transfected with plasmids expressing the indicated BRET expressing plasmids (2,5 ng of Rluc-UL44 + 40 ng of YFP-UL44; 10 ng of Rluc-UL54 + 40 ng of YFP-UL44; 22 ng of RLuc-YFP). 8h

p.i. media was substituted with DMEM containing either DMSO1% or AL18 at the indicated concentrations. 24h pt cells were processed for measurement of BRET inhibition after 15' after addition of h-CTZ. For each BRET pair are shown BRET ratio (A, B), YFPnet (C, D), and Rluc activity (E, F) either as raw values (A, C, E) or as a percentage of values obtained for samples in the absence of compound (B, D, F). Data are the mean ± S.D. of the mean relative to two independent experiments.

Figure 4.36. Effect of AL18 treatment for 40h on UL54-UL44 interaction as detected by BRET. $1x10^5$ HEK293 T cells were transfected with plasmids expressing the indicated BRET expressing plasmids (2,5 ng of Rluc-UL44 + 40 ng of YFP-UL44; 10 ng of Rluc-UL54 + 40 ng of YFP-UL44; 22 ng of RLuc-YFP). 8h p.i. media was substituted with DMEM containing either DMSO1% or AL18 at the indicated concentrations. 48h pt cells were processed for measurement of BRET inhibition after 15' after addition of h-CTZ. For each BRET pair are shown BRET ratio (A, B), YFPnet (C, D), and Rluc activity (E, F) either as raw values (A, C, E) or as a percentage of values obtained for samples in the absence of compound (B, D, F). Data are the mean ± S.D. of the mean relative to two independent experiments.

Figure 4.37. Effect of AL18 on subcellular localization relative to the indicated FRET fusion proteins. HEK283 T cells were seeded on glass coverslips and transfected with the indicated donor expression plasmids. 8h pt, media was replaced with DMEM containing either DMSO 1% or AL18 at the indicated concentration. 48h later cells were fixed and processed for IF, before being analyzed by CLSM to investigate the subcellular localization of the indicated fusion proteins. The subcellular localization of the indicated FRET pairs is shown for each condition (*left panels*) together with the correspondent RGB profiles (*right panels*).

Figure 4.38. Effect of AL18 on FRET efficiency relative to the indicated FRET pairs. Samples such as those shown in Figure 4.37 were subjected to FRET acceptor photobleaching analysis to calculate FRET efficiency. Data are shown as FRET efficiency relative to the indicated FRET pair (*panel A*) or the indicated donor fusions alone (*panel B*), upon treatment with the indicated concentration of DMSO or AL18.

Figure 4.39. Correlation between FRET efficiency % and fluorophore expression levels upon AL18 treatment. YFP and CFP pre-bleaching expression levels, relative to images, such those shown in Figure 4.18A, are plotted against FRET efficiency. Pearson r values relative correlations higher than 0.5 or lower than -0.5 are reported on the correspondent graph.

Figure 4.40. Correlation between FRET efficiency % and fluorophores expression levels upon AL18 treatment. YFP and CFP pre-bleaching expression levels, relative to images, such those shown in Figure 4.18B, are plotted against FRET efficiency. Pearson r values relative correlations higher than 0.5 or lower than -0.5 are reported on the correspondent graph.

Figure 4.41. Effect of AL18 treatment on CFP and YFP fusions expression levels. CFP and YFP pre-bleaching expression levels of samples such those in Figure 4.37, are shown.

Figure 4.42. Analysis of pre-bleaching CFP- and YFP-fusion expression levels. CFP (A, B) and YFP (C, D) pre-bleaching expression levels relative to the indicated FRET pairs of samples such those in Figure 4.3A are shown.

Figure 4.43. Test effect of DMSO by GST-pull down. tested the effect of DMSO on the ability of GST-UL44(1-290) to bind to 6His-UL44. To this end, recombinant proteins were incubated for 2h, either in binding buffer alone, or in binding buffer containing DMSO 1%, before being processed for GST-pull down analysis. We load Input, Wash 1 and the last (15°), Elution E1, E2, E3.

Figure 4.44. Identification of SMs inhibiting UL44 dimerization by GST-pull down. Test the effect of the 18 SMs identified as potentially important for UL44 dimerization by means of GST pull down assays. GST-UL44 (1-290) to bind to 6His-UL44 proteins were incubated for 2h, either in binding buffer alone, or in binding buffer containing DMSO 0.25%.

8. APPENDIX

8.1 Solutions

Elution buffer (Sigma)	Tris HCl, 10 mM
50x TAE buffer (1 litre)	242 g Tris base
	57.1 ml Glacial acetic acid
	100 ml 0.5 M EDTA pH 8.0
DNA loading buffer (6X)	30% (v/v) glycerol
	0.25% (w/v) bromophenol blue
	0.25% (w/v) xylene cyanol FF
Laemni loading buffer (5X)	0.25% Bromophenol blue
	0.5 M DTT (dithiothreitol)
	50% Glycerol
	10% SDS (sodium dodecyl sulfate)
	0.25 M Tris-Cl (pH 6.8)
Poly Lysine (100 mg/ml in H_2O)	5 mg poly-lysine (SIGMA 6282)
	50 ml sterile MQ H_2O
	The solution was stored at 4°C.
DNA loading dye 6X	0.25% (w/v) bromophenol blue
	0.25% (w/v) xylene cyanol FF
Running buffer gel (8.5%-15%)	H_2O
	30% acrylamide
	1.5M Tris pH 8.8

	10% SDS
	10% ammonium persulfate
	TEMED
Staking buffer gel (5%)	H_2O
	30% acrylamide
	1M Tris pH 6.8
	10% SDS
	10% ammonium persulfate
	TEMED
Running buffer pH 8.3	25mM Tris Base
	192mM glycine
	0.1% SDS
Transfer buffer pH 8.3	25mM Tris Base
	150mM glycine
	20% Methanol
Binding Buffer	25mM HEPES pH 7.5
	12.5 mM $MgCl_2$
	20% glycerol
	0.1% NP-40
	150mM KCL
	0.15 mg/ml Bovine Serum Albumin (BSA)
	1mM DTT
NETN Buffer	20mM Tris-HCL pH7.5
	100mM NaCl

0.1mM EDTA

0.5% NP-40

DMEM cpt (GIBCO, 500ml) FBS 1:10

Pen-strep 1:100

L-Glutammina 1:100

Non-Essential Amino Acids Solution (1:100)

Freezing media (50 ml) 45 ml DMEM

5 ml heath inactivated FBS (10 % v/v) Solution stored at -20°C.

0.5M PIPES (pH 6.7) 15.1 g of PIPES (pH 6.7)

pH of the solution was adjusted to 6.7 with5 M KOH. Sterilized solution stored frozen at -20°C.

PBS 10x (1 litre) 2.4 g KH2PO4

80 g NaCl

11.45 g Na2HPO4

2g KCL

LB (Luria Broth) media (1 liter) 10 g Bacto Tryptone

5 g Bacto Yeast Extract

10 g NaCl

H_2O up to 1 liter

The solution was autoclaved for sterilization and stored at room temperature (RT).

LB Agar for plates (1 liter) 10 g Bacto Tryptone

5 g Bacto Yeast Extract

10 g NaCl

15 g Agar

H_2O up to 1 liter

The solution was sterilized by autoclaving, cooled to 55/60°C prior to addition of the appropriate antibiotics (see table 8.1). Plates were stored at 4 °C for up to 3 weeks.

Antibiotic	Stock Solution	Working Solution	Dilution
Ampicillin	50mg/ml	50µg/ml	1:1000
Kanamkycin	50mg/ml	50µg/ml	1:1000
Gentamicin	10mg/ml	10µg/µl	1:500

Table 8.1. Antibiotics used in this study for bacterial selection

Inoue Transformation Buffer

The Inoue transformation buffer is composed by:

Reagent	Amount per Liter	Final Concentration
$MnCl_2$ x $4H_2O$	10.88 g	55mM
$CaCl_2$ x $2H_2O$	2.20 g	15mM
KCl	18.65 g	250mM
PIPES (0.5M, pH6.7)	20 ml	10mM
Water	to 1l	

Table 8.2.

Antibiotic for cells

We used for select cells different antibiotics: puromycin, (Clontech), blasticidin (Life Sciences) and neomycin (Life Sciences). Each antibiotic was resuspend in H_2O and filtrated. Store -20°C.

Antibiotic	Stock Solution	Working Solution	Dilution
Puromycin	10mg/ml	1µg/ml	1:10000
Blasticidin	5mg/ml	5µg/ml	1:1000
Neomycin	500mg/ml	700µg/µl	1:714

Table 8.3. Antibiotics used in this study for cells selection

DNA Markers

DirectLoad™ Wide Range DNA Marker

(SIGMA)

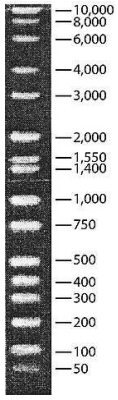

100 bp DNA Ladder

(Promega)

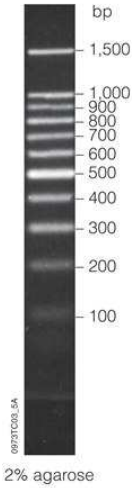

Protein marker

Prestained Protein SHARPMASS^{tm} VI

(Euroclone)

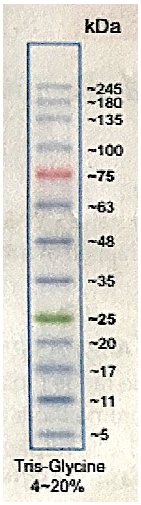

8.2 Cell used in this study

8.2.1 Bacterial cells

***E. Coli* DH5α,** Life Technologies F–Φ80*lac*ZΔM15Δ(*lac*ZYA-*arg*F)U169 *rec*A1 *end*A1 *hsd*R17 (rK–, mK+) *pho*A *sup*E44λ– *thi*-1 *gyr*A96 *rel*A1)**.** This *E. coli* strain is designed for general cloning and subcloning. It is, versatile strain that can be used in many everyday cloning applications. DH5α contains recA1 and endA1 mutations. The endA1 mutation greatly improves the quality of plasmid DNA, and the recA mutation helps ensure insert stability. Additionally, this strain lacks some endonucleases, which might digest the plasmids during the isolation procedure. DH5α is additionally competent for blue-white screening.

8.2.2 Mammalian cells

HEK293 T: HEK293 T is a cell line derived from Human Embryotic Kidney cells grown in tissue culture. This particular line was initiated by the transformation and culturing of normal HEK cells with sheared adenovirus 5 DNA (characteristics of a human cell line transformed by DNA from human adenovirus type 5).

The HEK293 T cell line (obtained from ATCC; ATCC CRL-11268) is an important variant of this cells line, because it stably expresses the SV40 large T- antigen, that allows episomal replications of transfected plasmids containing the SV40 origin of replication. This permits to increase protein production upon plasmid transfection (Vectors bicistronically linking a gene of interest to the SV40 large T antigen in combination with the SV40 origin of replication enhance transient protein expression and luciferase reporter activity).

HEK293 A: HEK293 A are a specific clone of HEK 293 cells, isolated because of its particular ability to adhere in cell culture. They display a typical flat phenotype. Cells were transformed by exposing them to sheared fragments of adenovirus type 5 DNA. The transformed cells exhibited many of the characteristics of transformed cells, including the expression of a virus-specific tumor antigen.

7.3 Plasmids

pDONOR207

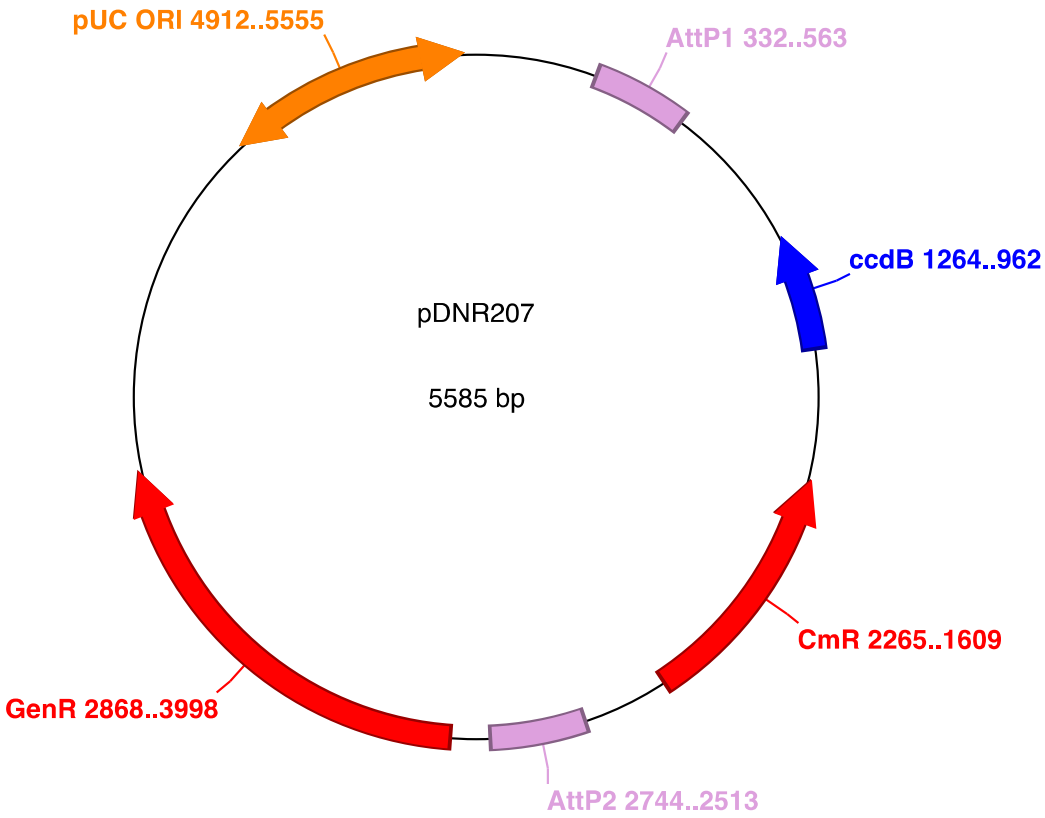

This vector contains a Gateway recombination cassette, containing the ccdB suicide gene and the chloramphenicol resistance (CmR) gene flanked by *att*P sites. The ccdB gene encodes a toxic product that interferes with E.coli gyrase, and propagation of such plasmid requires a ccdB resistant strain such a DB3.1 or 2T1R strains. This vector is designed to allow recombination between the Gateway recombination cassette flanked by attP sites, and a GOI flanked by attB sites (often represented by a *att*B-flanked PCR products), thus generating an *entry clone*. Such entry clone does not bear the ccdB gene and can grow in standard *E.coli* strains such as DH5α. The plasmid also contains the Gentamycin resistance gene (GenR), to allow a positive selection in E.coli.

pDEST-ntYFP

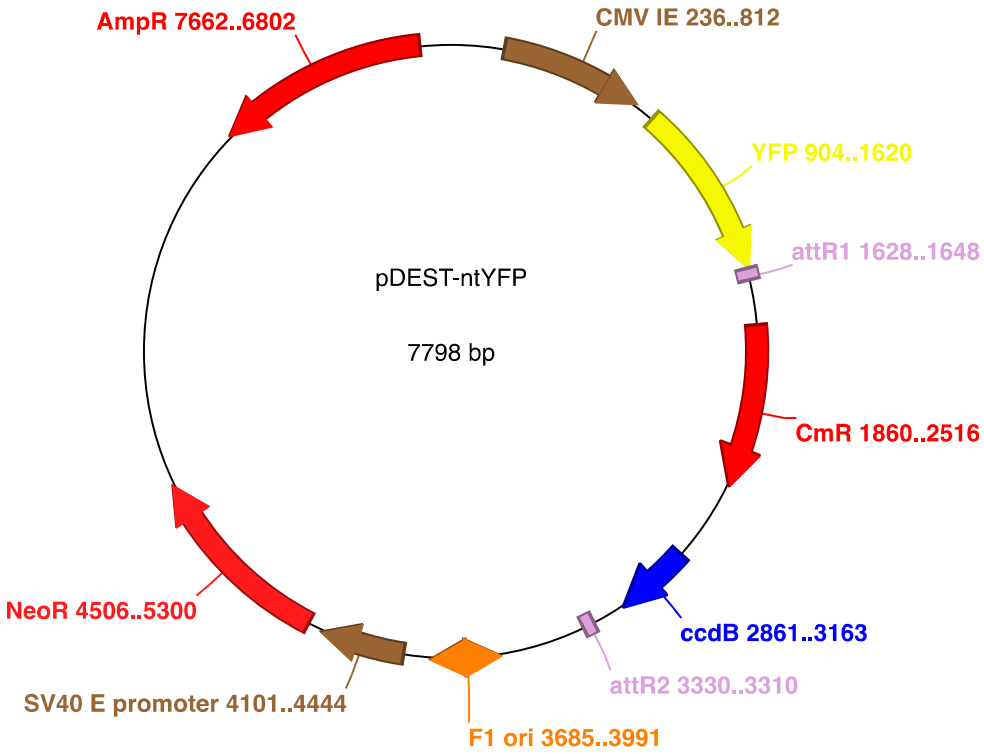

The pDEST-ntYFP vector [80] is a destination vector. It contains the YFP ORF under the control of the Human Cytomegalovirus (CMV) immediate early (IE) promoter, followed by the Gateway recombination cassette, whereby the *ccdB* suicide gene and the chloramphenicol resistance (CmR) gene are flanked by AttR sites. The *ccdB* gene encodes a toxic product, which interferes with *E.coli* gyrase, and propagation of such plasmid requires a ccdB resistant strain such a *E.coli* DB3.1 or 2T1R strains. It recombines with and *entry clone* via an LR reaction to generate an expression clone that contains elements necessary to express the GOI fused to the C-terminus of YFP in Mammalian cells under the control of the CMV IE promoter. It contains *Ampicillin* (AmpR) and *Neomycin* (NeoR) resistance genes to allow selection in bacterial and Mammalian cells, respectively. After a LR reaction with a suitable entry vector, the Gateway recombination cassette is replaced by the GOI enabling the expression of a YFP-GOI fusion, and allowing growth in standard E.coli strains such as DH5α.

pDEST-ntCFP

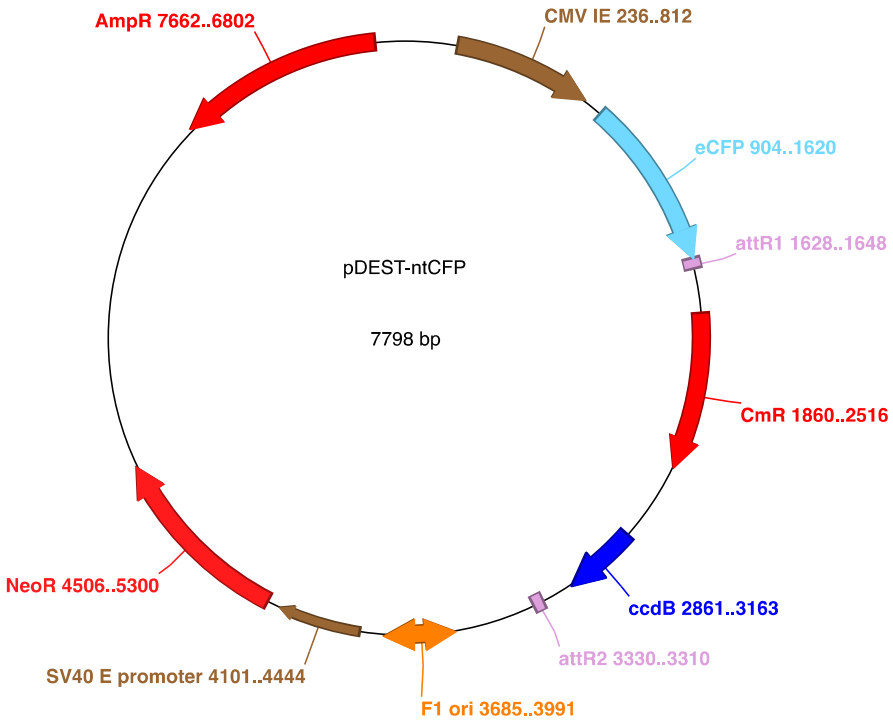

The pDEST-ntCFP vector [80] is a destination vector. It contains the CFP ORF under the control of the Human Cytomegalovirus (CMV) immediate early (IE) promoter, followed by the Gateway recombination cassette, whereby the *ccdB* suicide gene and the chloramphenicol resistance (CmR) gene are flanked by AttR sites. The *ccdB* gene encodes a toxic product, which interferes with *E.coli* gyrase, and propagation of such plasmid requires a ccdB resistant strain such a *E.coli* DB3.1 or 2T1R strains. It recombines with and *entry clone* via an LR reaction to generate an expression clone that contains elements necessary to express the GOI fused to the C-terminus of CFP in Mammalian cells under the control of the CMV IE promoter. It contains *Ampicillin* (AmpR) and *Neomycin* (NeoR) resistance genes to allow selection in bacterial and Mammalian cells, respectively. After a LR reaction with a suitable entry vector, the Gateway recombination cassette is replaced by the GOI enabling the expression of a CFP-GOI fusion, and allowing growth in standard E.coli strains such as DH5α.

pcDNA3RLuc-rfb

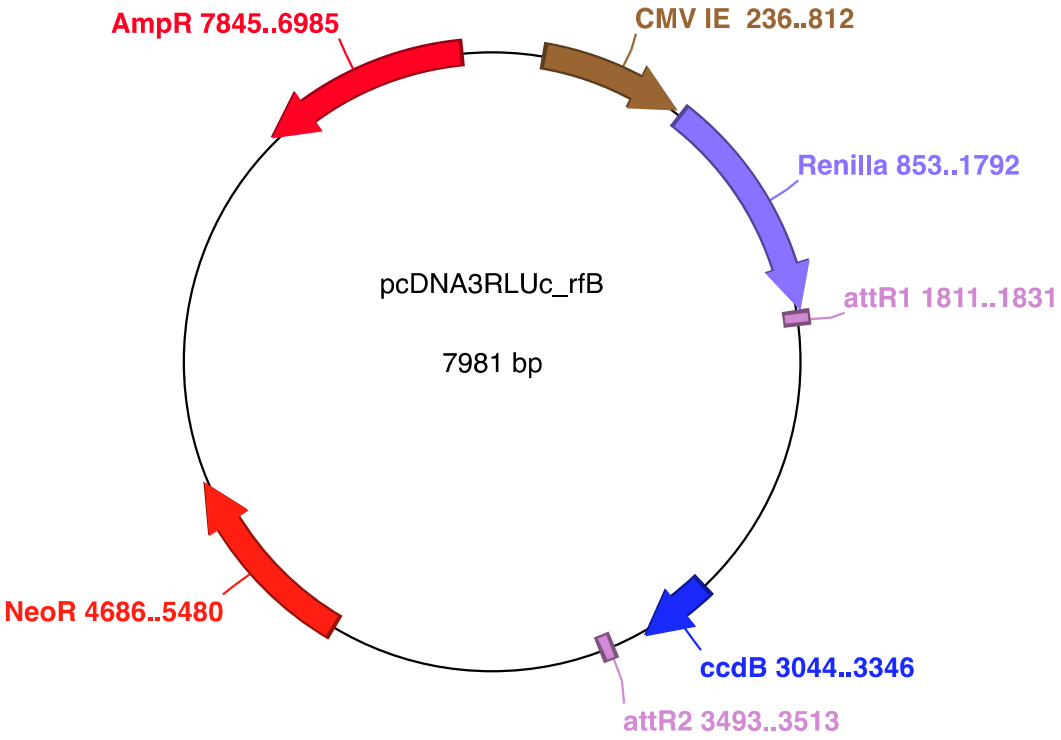

pWPI_BLR

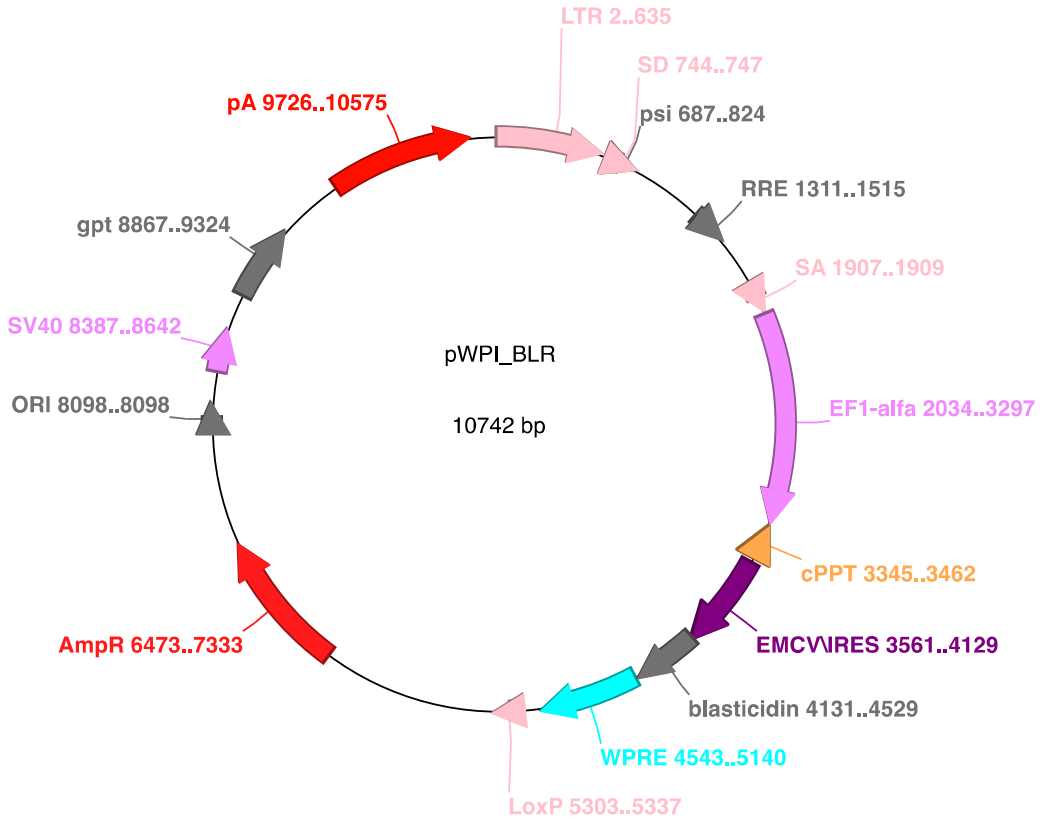
LTR 2..635
SD 744..747
psi 687..824
RRE 1311..1515
SA 1907..1909
EF1-alfa 2034..3297
cPPT 3345..3462
EMCV\IRES 3561..4129
blasticidin 4131..4529
WPRE 4543..5140
LoxP 5303..5337
AmpR 6473..7333
ORI 8098..8098
SV40 8387..8642
gpt 8867..9324
pA 9726..10575
pWPI_BLR
10742 bp

pMD2.G

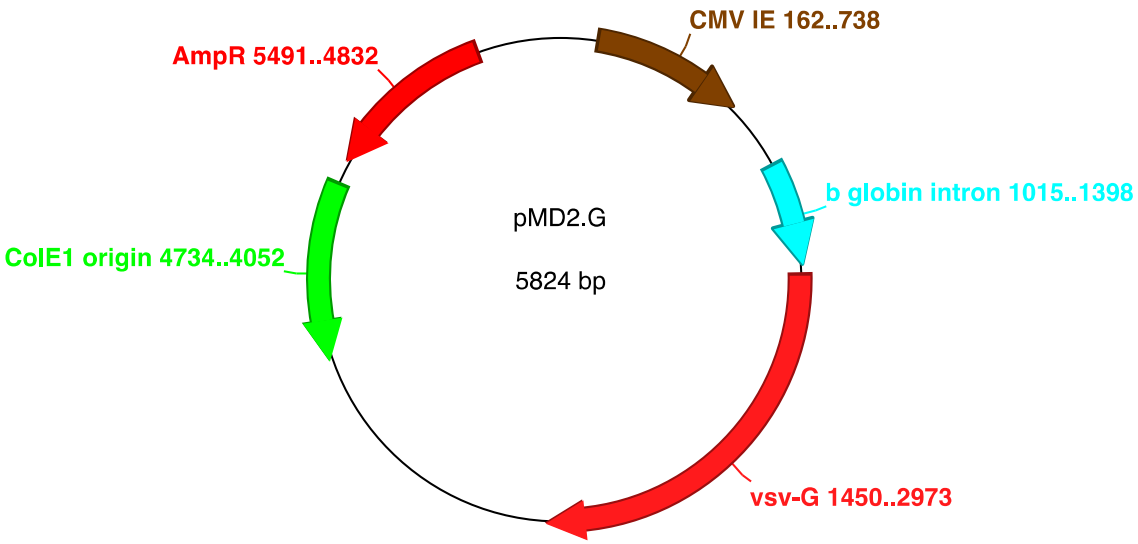
CMV IE 162..738
AmpR 5491..4832
b globin intron 1015..1398
pMD2.G
5824 bp
ColE1 origin 4734..4052
vsv-G 1450..2973

pCMVR8.74

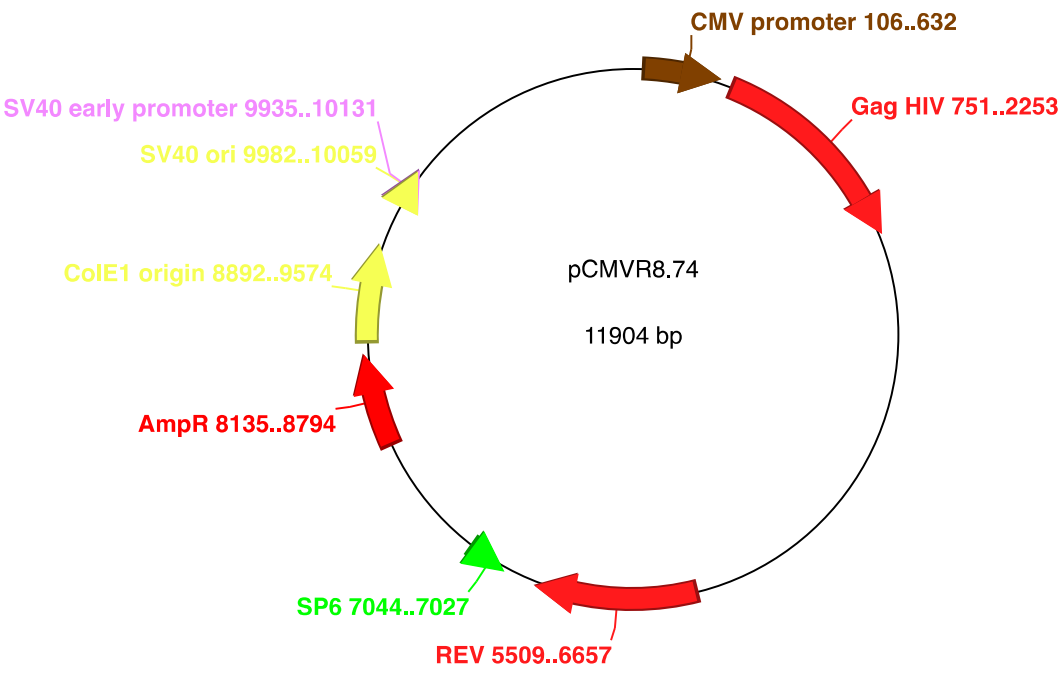
CMV promoter 106..632
Gag HIV 751..2253
SV40 early promoter 9935..10131
SV40 ori 9982..10059
ColE1 origin 8892..9574
pCMVR8.74
11904 bp
AmpR 8135..8794
SP6 7044..7027
REV 5509..6657

Entry clone pDONOR207-UL44 (2-433)

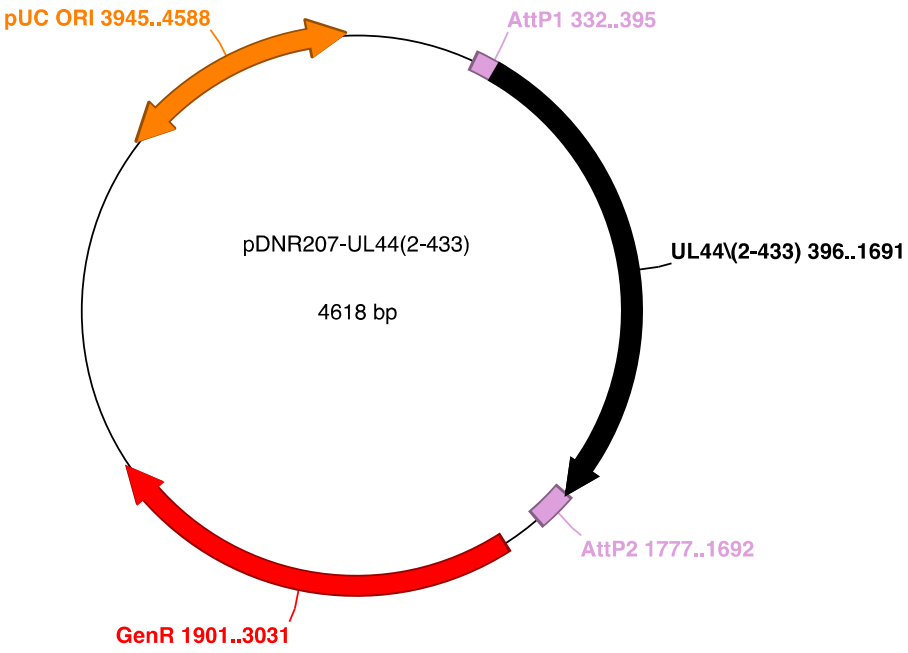

Unlike the parental pDONR207 plasmid from which it is derived, this vector does not contain the *ccdB* suicide gene and the CmR gene, and can be therefore grown in standard *E.coli* strains such as DH5α. It does not contain any promoter to drive the expression of UL44 (2-433) and only serves as a shuttle vector to generate *expression vectors* after recombination with destination vectors via LR reactions respect to the pDONOR207 plasmid, the Gateway recombination cassette is replaced with UL44 (2-433) coding sequence.

Entry clone pDONOR207-UL54 (1125-1242)

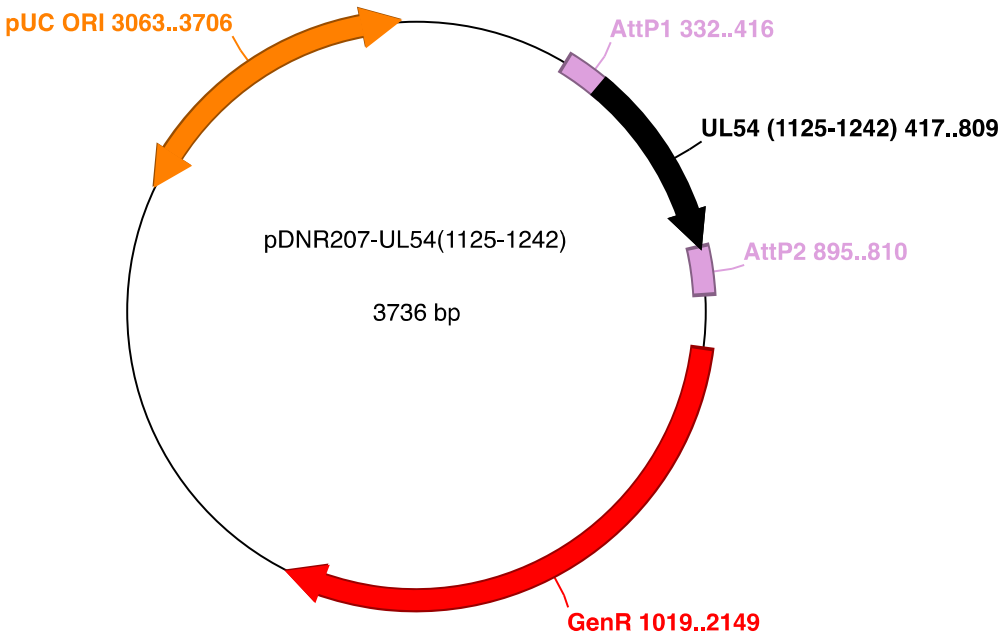

Unlike the parental pDONR207 plasmid from which it is derived, this vector does not contain the *ccdB* suicide gene and the CmR gene, and can be therefore grown in standard *E.coli* strains such as DH5α. It does not contain any promoter to drive the expression of UL54 (1125-1242) and only serves as a shuttle vector to generate *expression vectors* after recombination with destination vectors via LR reactions respect to the pDONOR207 plasmid, the Gateway recombination cassette is replaced with UL54 (1125-1242) coding sequence.

Entry clone pDONOR207-UL44 (405-433)

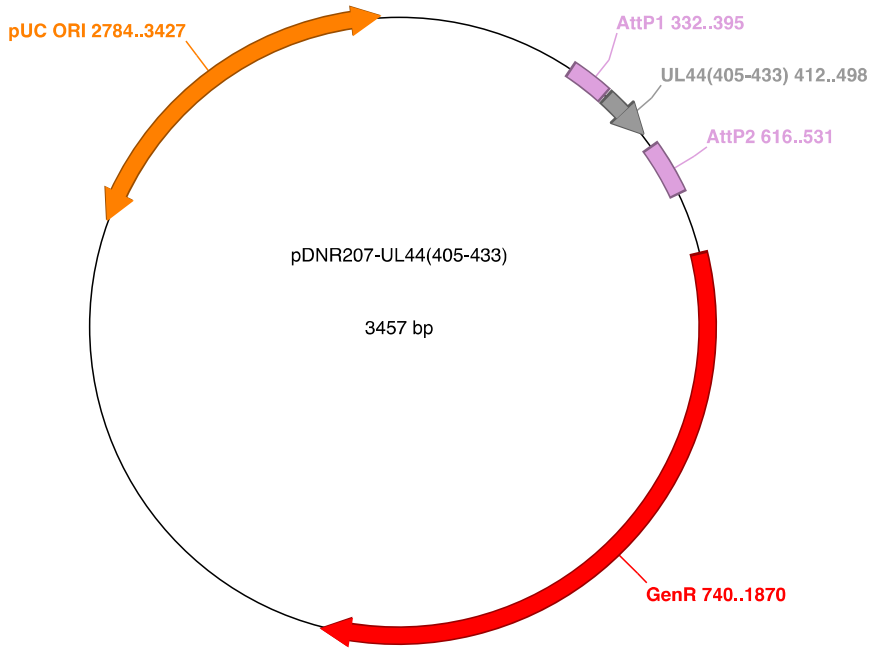

Unlike the parental pDONR207 plasmid from which it is derived, this vector does not contain the *ccdB* suicide gene and the CmR gene, and can be therefore grown in standard *E.coli* strains such as DH5α. It does not contain any promoter to drive the expression of UL44 (405-433) and only serves as a shuttle vector to generate *expression vectors* after recombination with destination vectors via LR reactions respect to the pDONOR207 plasmid, the Gateway recombination cassette is replaced with UL44 (405-433) coding sequence.

Entry clone pDONOR207-UL44 L86/L87A

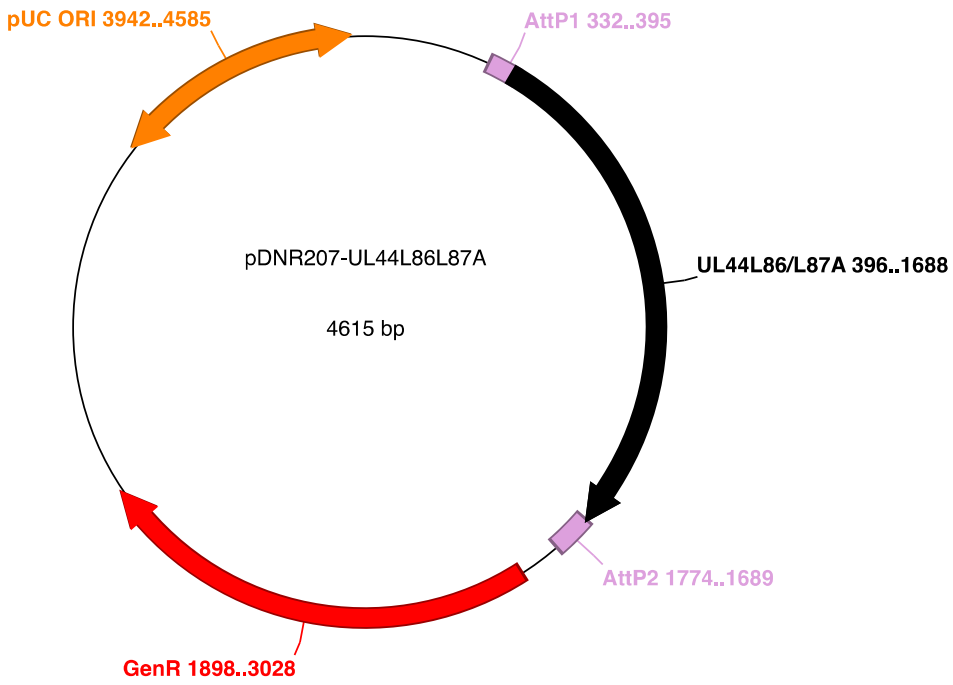

Unlike the parental pDONR207 plasmid from which it is derived, this vector does not contain the *ccdB* suicide gene and the CmR gene, and can be therefore grown in standard *E.coli* strains such as DH5α. It does not contain any promoter to drive the expression of UL44 L86/L87A and only serves as a shuttle vector to generate *expression vectors* after recombination with destination vectors via LR reactions respect to the pDONOR207 plasmid, the Gateway recombination cassette is replaced with UL44 L86/L87A coding sequence.

Entry clone pDONOR207-UL44 F121A

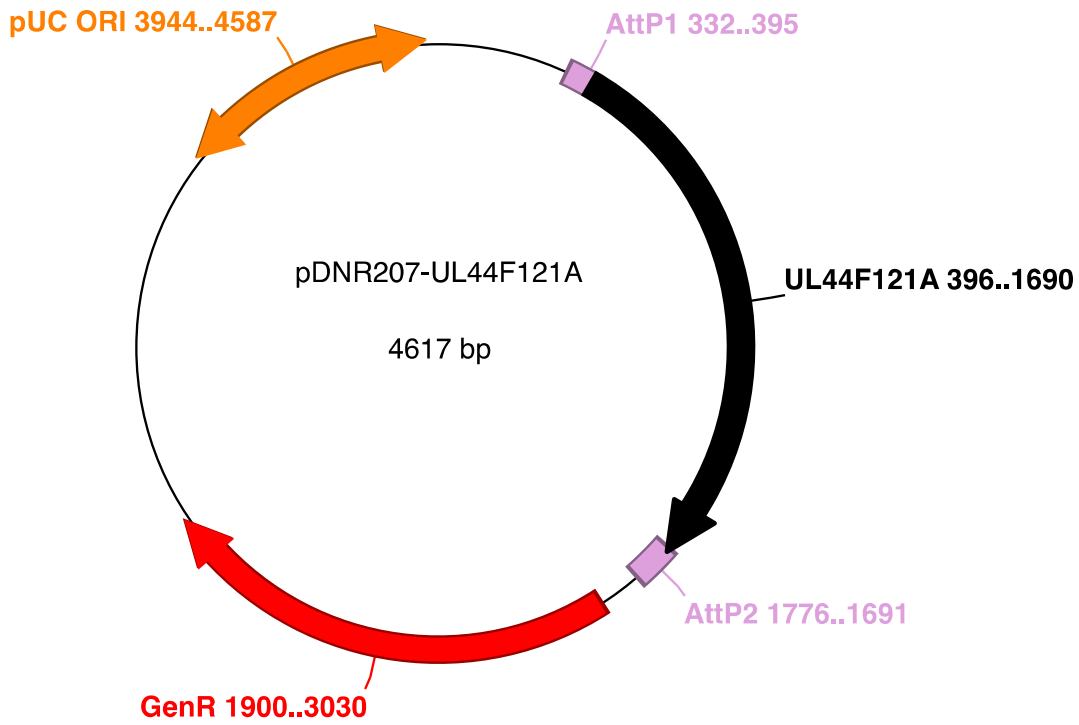

Unlike the parental pDONR207 plasmid from which it is derived, this vector does not contain the *ccdB* suicide gene and the CmR gene, and can be therefore grown in standard *E.coli* strains such as DH5α. It does not contain any promoter to drive the expression of UL44 F121A and only serves as a shuttle vector to generate *expression vectors* after recombination with destination vectors via LR reactions respect to the pDONOR207 plasmid, the Gateway recombination cassette is replaced with UL44 F121A coding sequence.

Entry clone pDONOR207-UL44 I135A

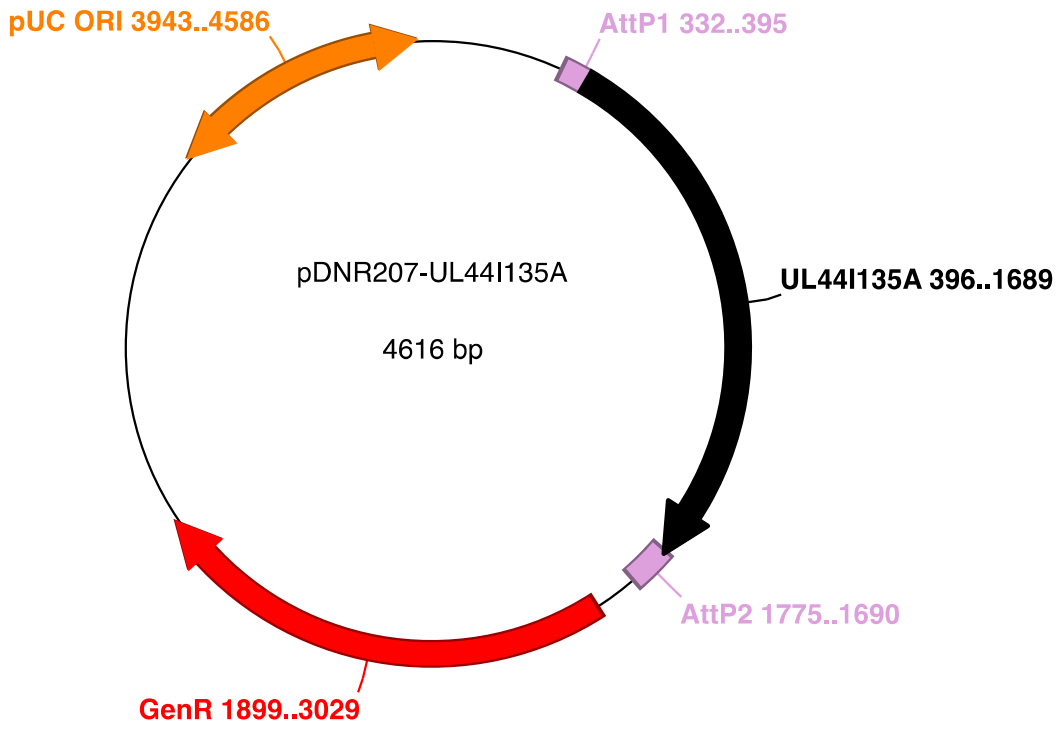

Unlike the parental pDONR207 plasmid from which it is derived, this vector does not contain the *ccdB* suicide gene and the CmR gene, and can be therefore grown in standard *E.coli* strains such as DH5α. It does not contain any promoter to drive the expression of UL44 I135A and only serves as a shuttle vector to generate *expression vectors* after recombination with destination vectors via LR reactions respect to the pDONOR207 plasmid, the Gateway recombination cassette is replaced with UL44 I135A coding sequence.

pWPI_puro-YFP-UL44

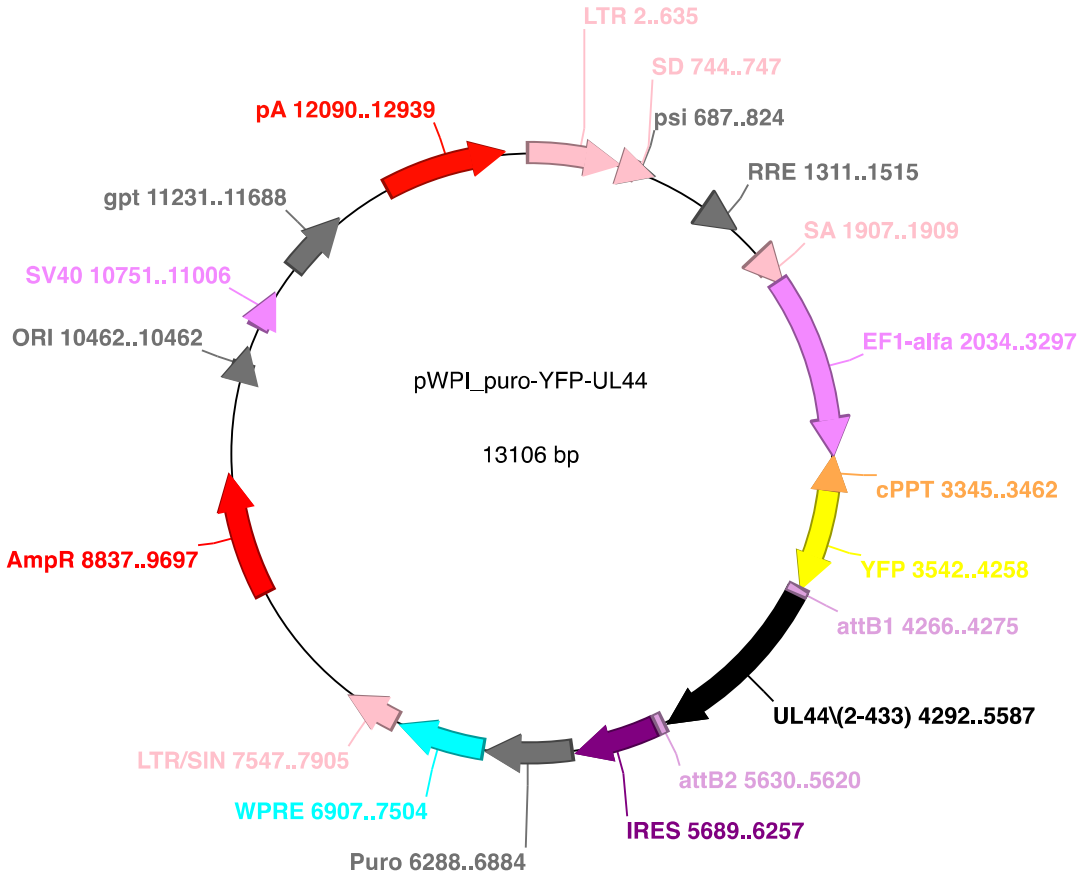

8.4 Primers used in this study

Primer Name	Primer Code	Sequence (5' - 3')
EGFP FW	A14	GATCACATGGTCCTGCTG
EGFP RW	A15	CCGTCCAGCTCGACCAG
pDNR RW	A16	GCAATGTAACATCAGAGAT
pDNR FW	A17	TAACGCTAGCATGGATCTC
T7 RW	A18	TAATACGACTCACTATAGGG
CMV FW	A19	CGCAAATGGGCGGTAGGCGTG
BGH RW	A28	TAGAAGGCACAGTCGAGG
AttB1-YFP-ATG	D21	GGGG**ACAAGTTTGTACAAAAAAGCAGGCT**GGATGGTGAGCAAGGGCGAGGAG
AttB1-YFP-noATG	D22	GGGG**ACAAGTTTGTACAAAAAAGCAGGCTT**GGTGAGCAAGGGCGAGGAG
AttB2-YFP-noSTOP	D23	GGGG**ACCACTTTGTACAAGAAAGCTGGGT**CCTTGTACAGCTCGTCCATGCC
AttB2-YFP-stop	D24	GGGG**ACCACTTTGTACAAGAAAGCTGGGT**TTACTTGTACAGCTCGTCCATGCC
AttB1-RLuc-ATG	D25	GGGG**ACAAGTTTGTACAAAAAAGCAGGCT**GGATGACCAGCAAGGTGTACGAC
AttB2-RLuc no STOP	D26	GGGG**ACCACTTTGTACAAGAAAGCTGGGT**CATCCCCCTGCTCGTTCTTCAGC
AttB2-RLuc-noATG	D27	GGGG**ACAAGTTTGTACAAAAAAGCAGGCT**TGACCAGCAAGGTGTACGAC
AttB2-RLuc-STOP	D28	GGGG**ACCACTTTGTACAAGAAAGCTGGGT**TTAGAGATCCCCCTGCTCGTTC

Table 8.4. List of primers used in this study. Where present, GatewayTM attB sites are in boldface

Table 8.5 Cloning vectors used in this study

Plasmid n.	Plasmid name	Description
GW5	pDONOR207	Gateway™ Destination vector containing the Gentamicin resistance gene and the ccdB suicide gene as well as the Cloranphenicol resistance gene (Invitrogen).
GW6	pDEST-EPI-GFP	Gateway™ Destination vector for mammalian episomal propagation and expression of N-terminal EGFP tagged fusion proteins [52].
GW14	pDEST-FLAG	Gateway™ Destination vector for Mammalian expression of N-terminal fusions with FLAG [81].
GW17	pDEST-ntCFP	Gateway™ Destination vector for Mammalian expression of CFP N-terminal tagged proteins. CMV promoter [82].
GW22	pDEST-ntYFP	Gateway™ Destination vector for Mammalian expression of tagRFP-T C-terminal tagged proteins. CMV promoter [82].
GW29	pCDNA3ntRLucGW	Gateway™ Destination vector for Mammalian expression of Renilla N-terminal tagged proteins [82].
6	pWPI-blr	Lentiviral vector for Mammalian expression. Blastadicin R. E2α promoter.

Table 8.6 Other plasmids used in this study

n.	Plasmid name	Description	Application
21	CFP-YFP	Mammalian Expression Vector encoding a fusion protein betrween CFP and YFP, connected fused through a 5-amino-acid (SGGGG) linker sequence under the control of the IE CMV promoter. REF	Positive control in FRET assays
24	pDESTntYFP-UL44	Mammalian Expression Vector encoding a N-terminal YFP-UL44(2-433) fusion protein, under the control of the IE CMV promoter. This study, see Table 6.6	FRET/BRET assays
30	pDESTntCFP-UL44	Mammalian Expression Vector encoding a N-terminal YFP-UL44(2-433) fusion protein, under the control of the IE CMV promoter. This study, see Table 6.6	FRET assays
57	pDESTntCFP-UL44-L86/L87A	Mammalian Expression Vector encoding a N-terminal CFP-UL44(2-433) fusion protein, bearing point mutations in the dimerization interface, under the control of the IE CMV promoter. This study, see Table 6.6	FRET assays
92	pDESTntYFP-UL44-F121A	Mammalian Expression Vector encoding a N-terminal YFP-UL44(2-433) fusion protein, bearing point mutations in the dimerization interface, under the control of the IE CMV promoter. This study, see Table 6.6	BRET assays
92	pDESTntRLuc-UL44-F121A	Mammalian Expression Vector encoding a N-terminal RLuc-UL44(2-433) fusion protein, bearing point mutations in the dimerization interface, under the control of the IE CMV promoter. This study, see Table 6.6	BRET assays
59	pDESTntRLuc UL44	Mammalian Expression clone encoding a N-terminal RLuc-UL44(2-433) fusion protein, under the control of the CMV promoter. This study, see Table 6.6	BRET assays
62	pcDNA.31	Empty vector. Invitrogen	BRET assays
82	pDESTntYFP-UL44-L86/L87A	Mammalian Expression Vector encoding a N-terminal YFP-UL44(2-433) fusion protein, bearing point mutations in the dimerization interface, under the control of the IE CMV promoter. This study, see Table 6.6	FRET/BRET assays

205	pDESTntRLuc-UL44-Δloop	Mammalian Expression Vector encoding a N-terminal RLuc-UL44(2-433) fusion protein, with point mutations within FL involved in DNA binding, under the control of the IE CMV promoter. This study, see Table 6.6	BRET assays
66	pDESTntYFP-UL44-Δloop	Mammalian Expression Vector encoding a N-terminal YFP-UL44(2-433) fusion protein, without flexible loop involved in DNA binding, under the control of the IE CMV promoter. This study, see Table 6.6	BRET assays
87	pCMVHA-X-CFP	Mammalian expression vector encoding HA-tagged Cyan Fluorescent Protein (CFP). [76]	FRET assays
88	pCMVFLAG-X-YFP	Mammalian expression vector encoding HA-tagged Yellow Fluorescent Protein (YFP). [76]	FRET assays
243	pDESTntYFP-UL44(I135A)	Mammalian Expression Vector encoding a N-terminal YFP-UL44(2-433) fusion protein, bearing point mutations in the connector loop preventing binding to UL54, under the control of the IE CMV promoter. This study, see Table 6.6.	BRET assays
249	pDESTntRLuc-UL54(1125-1242)	Mammalian Expression Vector encoding a N-terminalRLuc-UL54(1125-1242) fusion protein, containing UL54 binding site for UL44 as well as a classical NLS, under the control of the IE CMV promoter. This study, see Table 6.6	BRET assays
382	pDESTntCFP-UL54(1125-1242)	Mammalian Expression Vector encoding a N-terminal CFP-UL54(1125-1242) fusion protein, containing UL54 binding site for UL44 as well as a classical NLS, under the control of the IE CMV promoter. This study, see Table 6.6	FRET assays
242	pDESTntRLuc-UL54(1145-1213)	Mammalian Expression Vector encoding a N-terminalRLuc-UL54(1125-1242) fusion protein, containing point mutation for UL44, under the control of the IE CMV promoter. This study, see Table 6.6	FRET/BRET assays
241	pDESTntYFP-UL54(1145-1213)	Mammalian Expression Vector encoding a N-terminal YFP-UL54 UL54(1125-1242) fusion protein, containing point mutation for UL44, under the control of the IE CMV promoter. This study, see Table 6.6	BRET assays
341	pDEST-RLuc-YFP	Mammalian Expression Vector encoding a fusion protein betrween RLuc and YFP, under the control of the IE CMV promoter. This study, see Table 6.6	BRET assays

343	pDEST-FLAG-UL42	Mammalian Expression plasmid expressing full-lenght UL42 with a FLAG-terminal TAG, with point mutations within the bipartite NLS under the control of the CMV IE promoter. [48].	BRET assays
60	pcDNA.3 Rluc_rfB-UL44(405-433)	Mammalian Expression clone encoding a N-terminal RLuc-UL44(2-433) fusion protein impaired NLS, under the control of the CMV promoter. This study, see Table 6.6	BRET assays
247	pcDNA.3 Ubc9-FLAG	Mammalian Expression clone encoding a N-terminal FLAG-Ubc9 fusion protein, under the control of the CMV promoter. [54].	BRET assays
40	pDONOR-UL44(2-433)	Entry clone encoding a N-terminal UL44(2-433) fusion protein. [49].	Subcloning
39	pDONOR-UL54(1145-1213)	Entry clone encoding a N-terminal UL54(1145-1213) fusion protein, containing UL54 binding site for UL44 as well as a classical NLS. [49].	Subcloning
43	pDONOR-UL44(I135A)	Entry clone encoding full length UL44(2-433) fusion protein, bearing point mutations in the connector loop preventing binding to UL54. [83].	Subcloning
42	pDONOR-UL44-F121A	Entry clone encoding UL44 (2-433) fusion protein, bearing point mutations in the dimerization interface. [83].	Subcloning
41	pDONOR-UL44-L86/L87A	Entry clone encoding UL44 (2-433) fusion protein, bearing point mutations in the dimerization interface. [83].	Subcloning
54	pDONOR-UL44(405-433)	Entry clone encoding a N-terminal UL44 (2-433) fusion protein. [54].	Subcloning
126	pDONOR-UL44-Δloop	Entry clone encoding a N-terminal YFP-UL44(2-433) fusion protein, without flexible loop involved in DNA binding. [62].	Subcloning
237	pDONOR - UL54(1125-1242)	Entry clone encoding a UL54(1125-1242) fusion protein, containing UL54 binding site for UL44 as well as a classical NLS. [49].	Subcloning

333	pDONOR –RLuc noATG	Entry clone encoding a the Renilla luciferase gene. This study, see Table 6.7.	Subcloning

Table 8.7 LR reactions performed in this study

Description	Resulting Construct
LR reaction between GW17 pDEST-ntCFP and pDONOR-UL44(2-433)	30. pDEST-ntCFP-UL44
LR reaction between GW17 pDEST-ntCFP and 41 pDONOR-UL44-L86/L87A	57. pDEST-ntCFP-UL44-L86/L87A
LR reaction between GW22 pDEST-ntYFP and 126 pDONOR-UL44-Δloop	66. pDEST-ntYFP-UL44-Δloop
LR reaction between GW29 pcDNA3RLuc_rfb and 54 pDONOR-UL44(405-433)	60. pDEST-ntRLuc UL44(405-433)
LR reaction between GW29 pcDNA3RLuc_rfb and 60 pDONOR-UL44(2-433)	59. pDEST-ntRLuc-UL44(2-433)
LR reaction between GW22 pDEST-ntYFP and 42 pDONOR-UL44-F121A	92. pDEST-ntYFP-UL44-F121A
LR reaction between GW29 pcDNA3RLuc_rfb and 42 pDONOR-UL44-F121A	91. pDEST-ntRLuc-UL44-F121A
LR reaction between GW29 pcDNA3RLuc_rfb and 41 pDONOR-UL44-L86/L87A	90. pDEST-ntRLuc UL44-L86/L87A
LR reaction between GW29 pcDNA3RLuc_rfb and 126 pDONOR- UL44-Δloop	205. pDEST-ntRLuc UL44-Δloop
LR reaction between GW29 pcDNA3RLuc_rfb and 43 pDONOR- UL44(I135A)	244. pDEST-ntRLucUL44(I135A)
LR reaction between GW29 pcDNA3RLuc_rfb and 39 pDONOR-UL54(1145-1213)	243. pDEST-ntRLucUL54(1145-1213)
LR reaction between GW22 pDEST-ntYFP and 39 pDONOR-UL54(1145-1213)	241. pDEST-ntYFP-UL54(1145-1213)
LR reaction between GW29 pcDNA3RLuc_rfb	249. pDEST-ntRLuc-UL54(1125-1242)

and 237 pDONOR-UL54(1125-1242)	
LR reaction between GW22 pDEST-ntYFP and 237 pDONOR-UL54(1125-1242)	248. pDEST-ntYFP -UL54(1125-1242)
LR reaction between GW29 pcDNA3RLuc_rfb and 334 pDONOR-YFPnoATG	336.pDESTntYFP-RLuc
LR reaction between GW22 pDEST-ntYFP and 333 pDONOR-RLucnoATG	341.pDESTntRLuc-YFP
LR reaction between GW22 pDEST-ntYFP and pDESTntYFP-UL44	24.pDESTntYFP-UL44

Table 8.8 BP reactions performed in this study

Description	Resulting Construct
BP reaction between GW5 pDONOR207 and PCR_RLuc_noATG (primers D21,D22)	333. pDONOR- RLuc_noATG
BP reaction between GW5 pDONOR207 and 41 PCR_YFP_noATG (primers D22,D24)	334. pDONOR- YFP_noATG

Table 7.9 Ligations performed in this study

Description	Resulting Construct
Ligation reaction between 7 pWPI-Puro and 24 ntYFP-UL44wt	68. pWPI-Puro- ntYFP-UL44
Ligation reaction between 6 pWPI-Blr and 24 ntYFP-UL44wt	137. pWPI-Blr- ntYFP-UL44

Table 8.10 VIKTOR X2 acquisition settings for BRET experiments

Fluorometric detection of YFP signal (YFPNet)

Protocol name ..... yfp x BRET

Protocol number ..... N/A

Name of the plate type ..... Generic 8x12 size plate

Number of repeats 1

Delay between repeats ..... 0 s

Measurement height ..... Default

Protocol notes .....

Shaking duration ..... 1.0 s

Shaking speed ..... Normal

Shaking diameter ..... 0.10 mm

Shaking type ..... Double orbit

Repeated operation ..... Yes

Name of the label ..... Fluorescein (1.0s)

Label technology ..... Prompt fluorometry

CW-lamp filter name F485

CW-lamp filter slot A5

Emission filter name F535

Emission filter slot A5

Measurement time ..... 1.0 s

Emission aperture ..... Small

CW-lamp energy 8704

Second measurement CW-lamp energy. 0

Emission side ..... Above

CW-Lamp Control ..... Stabilized Energy

Excitation Aperture ..... N/A

Luminometric detection of YFP and RLuc signal

Protocol name ..... BRET 1 s filter Y/R

Protocol number ..... N/A

Name of the plate type ..... Generic 8x12 size plate

Number of repeats 1

Delay between repeats ..... 0 s

Measurement height ..... Default

Protocol notes .....

Shaking duration ..... 1.0 s

Shaking speed ..... Normal

Shaking diameter ..... 0.10 mm

Shaking type ..... Double orbit

Repeated operation ..... Yes

Name of the label ..... CPS 1 sec Normal YFP BRET

Label technology ..... Luminometry

Emission filter name F535

Emission filter slot A5

Measurement time ..... 1.0 s

Emission aperture ..... Normal

Name of the label ..... CPS 1 sec Normal Renilla BRET

Label technology ..... Luminometry

Emission filter name F460

Emission filter slot A6

Measurement time ..... 1.0 s

Emission aperture ..... Normal

9. References

1. Roizman, B., et al., *Herpesviridae. Definition, provisional nomenclature, and taxonomy. The Herpesvirus Study Group, the International Committee on Taxonomy of Viruses.* Intervirology, 1981. **16**(4): p. 201-17.
2. Kalejta, R.F., *Tegument proteins of human cytomegalovirus.* Microbiol Mol Biol Rev, 2008. **72**(2): p. 249-65, table of contents.
3. Pari, G.S., *Nuts and bolts of human cytomegalovirus lytic DNA replication.* Curr Top Microbiol Immunol, 2008. **325**: p. 153-66.
4. Gandhi, M.K. and R. Khanna, *Human cytomegalovirus: clinical aspects, immune regulation, and emerging treatments.* Lancet Infect Dis, 2004. **4**(12): p. 725-38.
5. Zaia, J.A., *Prevention and management of CMV-related problems after hematopoietic stem cell transplantation.* Bone Marrow Transplant, 2002. **29**(8): p. 633-8.
6. Mocarski, E.S., Jr., *Immune escape and exploitation strategies of cytomegaloviruses: impact on and imitation of the major histocompatibility system.* Cell Microbiol, 2004. **6**(8): p. 707-17.
7. Sissons, J.G., et al., *Human cytomegalovirus and immunopathology.* Springer Semin Immunopathol, 2002. **24**(2): p. 169-85.
8. Gandhi, M.K., et al., *Human cytomegalovirus-specific immunity following haemopoietic stem cell transplantation.* Blood Rev, 2003. **17**(4): p. 259-64.
9. Schottstedt, V., et al., *Human Cytomegalovirus (HCMV) - Revised.* Transfus Med Hemother, 2010. **37**(6): p. 365-375.
10. Kalejta, R.F., *Functions of human cytomegalovirus tegument proteins prior to immediate early gene expression.* Curr Top Microbiol Immunol, 2008. **325**: p. 101-15.
11. Fields, B.N., D.M. Knipe, and P.M. Howley, , *Fields virology. 4th ed.* ... [et al.] ed. 2001, ;: , ed. D.M.K. Fields virology. 4th ed. / editors-in-chief, Peter M. Howley, associate editors, Diane E. Griffin ... [et al.] ed. 2001, Philadelphia ; London: Lippincott Williams & Wilkins. 2001, London.
12. Kemble, G.W. and E.S. Mocarski, *A host cell protein binds to a highly conserved sequence element (pac-2) within the cytomegalovirus a sequence.* J Virol, 1989. **63**(11): p. 4715-28.
13. Van Damme, E. and M. Van Loock, *Functional annotation of human cytomegalovirus gene products: an update.* Front Microbiol, 2014. **5**: p. 218.
14. Karlin, S., E.S. Mocarski, and G.A. Schachtel, *Molecular evolution of herpesviruses: genomic and protein sequence comparisons.* J Virol, 1994. **68**(3): p. 1886-902.
15. Landolfo, S., et al., *The human cytomegalovirus.* Pharmacol Ther, 2003. **98**(3): p. 269-97.
16. Pari, G.S. and D.G. Anders, *Eleven loci encoding trans-acting factors are required for transient complementation of human cytomegalovirus oriLyt-dependent DNA replication.* J Virol, 1993. **67**(12): p. 6979-88.
17. Ertl, P.F. and K.L. Powell, *Physical and functional interaction of human cytomegalovirus DNA polymerase and its accessory protein (ICP36) expressed in insect cells*, in *J Virol*. 1992. p. 4126-33.
18. Tenney, D.J. and A.M. Colberg-Poley, *Human cytomegalovirus UL36-38 and US3 immediate-early genes: temporally regulated expression of nuclear, cytoplasmic, and polysome-associated transcripts during infection.* J Virol, 1991. **65**(12): p. 6724-34.
19. Skaletskaya, A., et al., *A cytomegalovirus-encoded inhibitor of apoptosis that suppresses caspase-8 activation.* Proc Natl Acad Sci U S A, 2001. **98**(14): p. 7829-34.
20. Goldmacher, V.S., et al., *A cytomegalovirus-encoded mitochondria-localized inhibitor of apoptosis structurally unrelated to Bcl-2.* Proc Natl Acad Sci U S A, 1999. **96**(22): p. 12536-41.
21. Terhune, S., et al., *Human cytomegalovirus UL38 protein blocks apoptosis.* J Virol, 2007. **81**(7): p. 3109-23.
22. Romanowski, M.J. and T. Shenk, *Characterization of the human cytomegalovirus irs1 and trs1 genes: a second immediate-early transcription unit within irs1 whose product antagonizes transcriptional activation.* J Virol, 1997. **71**(2): p. 1485-96.

23. Wright, D.A. and D.H. Spector, *Posttranscriptional regulation of a class of human cytomegalovirus phosphoproteins encoded by an early transcription unit.* J Virol, 1989. **63**(7): p. 3117-27.
24. Ahn, J.H., W.J. Jang, and G.S. Hayward, *The human cytomegalovirus IE2 and UL112-113 proteins accumulate in viral DNA replication compartments that initiate from the periphery of promyelocytic leukemia protein-associated nuclear bodies (PODs or ND10)*, in *J Virol*. 1999. p. 10458-71.
25. Park, M.Y., et al., *Interactions among four proteins encoded by the human cytomegalovirus UL112-113 region regulate their intranuclear targeting and the recruitment of UL44 to prereplication foci.* J Virol, 2006. **80**(6): p. 2718-27.
26. Tanner, N.K. and P. Linder, *DExD/H box RNA helicases: from generic motors to specific dissociation functions.* Mol Cell, 2001. **8**(2): p. 251-62.
27. Colletti, K.S., et al., *Human cytomegalovirus UL84 is a phosphoprotein that exhibits UTPase activity and is a putative member of the DExD/H box family of proteins.* J Biol Chem, 2005. **280**(12): p. 11955-60.
28. Gebert, S., et al., *The UL84 protein of human cytomegalovirus acts as a transdominant inhibitor of immediate-early-mediated transactivation that is able to prevent viral replication.* J Virol, 1997. **71**(9): p. 7048-60.
29. Lischka, P., et al., *Human cytomegalovirus UL84 protein contains two nuclear export signals and shuttles between the nucleus and the cytoplasm.* J Virol, 2006. **80**(20): p. 10274-80.
30. Xu, Y., et al., *Human cytomegalovirus UL84 insertion mutant defective for viral DNA synthesis and growth*, in *J Virol*. 2004. p. 10360-9.
31. Colletti, K.S., et al., *Human cytomegalovirus UL84 interacts with an RNA stem-loop sequence found within the RNA/DNA hybrid region of oriLyt.* J Virol, 2007. **81**(13): p. 7077-85.
32. Gao, Y., K. Colletti, and G.S. Pari, *Identification of human cytomegalovirus UL84 virus- and cell-encoded binding partners by using proteomics analysis.* J Virol, 2008. **82**(1): p. 96-104.
33. Digard, P., et al., *Functional analysis of the herpes simplex virus UL42 protein.* J Virol, 1993. **67**(3): p. 1159-68.
34. Gallo, M.L., et al., *The essential 65-kilodalton DNA-binding protein of herpes simplex virus stimulates the virus-encoded DNA polymerase.* J Virol, 1989. **63**(12): p. 5023-9.
35. Davison, A.J. and J.E. Scott, *The complete DNA sequence of varicella-zoster virus.* J Gen Virol, 1986. **67 (Pt 9)**: p. 1759-816.
36. Ertl, P.F. and K.L. Powell, *Physical and functional interaction of human cytomegalovirus DNA polymerase and its accessory protein (ICP36) expressed in insect cells.* J Virol, 1992. **66**(7): p. 4126-33.
37. Agulnick, A.D., et al., *Identification of a DNA-binding protein of human herpesvirus 6, a putative DNA polymerase stimulatory factor*, in *J Gen Virol*. 1993. p. 1003-9.
38. Nicholas, J., *Determination and analysis of the complete nucleotide sequence of human herpesvirus.* J Virol, 1996. **70**(9): p. 5975-89.
39. Lin, K., C.Y. Dai, and R.P. Ricciardi, *Cloning and functional analysis of Kaposi's sarcoma-associated herpesvirus DNA polymerase and its processivity factor.* J Virol, 1998. **72**(7): p. 6228-32.
40. Digard, P., et al., *The extreme C terminus of herpes simplex virus DNA polymerase is crucial for functional interaction with processivity factor UL42 and for viral replication.* J Virol, 1993. **67**(1): p. 398-406.
41. Tenney, D.J., et al., *Mutations in the C terminus of herpes simplex virus type 1 DNA polymerase can affect binding and stimulation by its accessory protein UL42 without affecting basal polymerase activity.* J Virol, 1993. **67**(1): p. 543-7.
42. Matthews, J.T., B.J. Terry, and A.K. Field, *The structure and function of the HSV DNA replication proteins: defining novel antiviral targets.* Antiviral Res, 1993. **20**(2): p. 89-114.
43. Larder, B.A., S.D. Kemp, and G. Darby, *Related functional domains in virus DNA polymerases.* EMBO J, 1987. **6**(1): p. 169-75.
44. Ye, L.B. and E.S. Huang, *In vitro expression of the human cytomegalovirus DNA polymerase gene: effects of sequence alterations on enzyme activity.* J Virol, 1993. **67**(11): p. 6339-47.

45. Nishiyama, Y., K. Maeno, and S. Yoshida, *Characterization of human cytomegalovirus-induced DNA polymerase and the associated 3'-to-5', exonuclease.* Virology, 1983. **124**(2): p. 221-31.
46. Alvisi, G., et al., *Human cytomegalovirus DNA polymerase catalytic subunit pUL54 possesses independently acting nuclear localization and ppUL44 binding motifs.* Traffic, 2006. **7**(10): p. 1322-32.
47. Loregian, A., et al., *The catalytic subunit of herpes simplex virus type 1 DNA polymerase contains a nuclear localization signal in the UL42-binding region.* Virology, 2000. **273**(1): p. 139-48.
48. Alvisi, G., et al., *Nuclear import of HSV-1 DNA polymerase processivity factor UL42 is mediated by a C-terminally located bipartite nuclear localization signal.* Biochemistry, 2008. **47**(52): p. 13764-77.
49. Alvisi, G., D.A. Jans, and A. Ripalti, *Human cytomegalovirus (HCMV) DNA polymerase processivity factor ppUL44 dimerizes in the cytosol before translocation to the nucleus.* Biochemistry, 2006. **45**(22): p. 6866-72.
50. Ripalti, A., et al., *Cytomegalovirus-mediated induction of antisense mRNA expression to UL44 inhibits virus replication in an astrocytoma cell line: identification of an essential gene.* J Virol, 1995. **69**(4): p. 2047-57.
51. Weiland, K.L., et al., *Functional analysis of human cytomegalovirus polymerase accessory protein*, in *Virus Res*. 1994. p. 191-206.
52. Alvisi, G., et al., *A protein kinase CK2 site flanking the nuclear targeting signal enhances nuclear transport of human cytomegalovirus ppUL44.* Traffic, 2005. **6**(11): p. 1002-13.
53. Alvisi, G., et al., *Multiple phosphorylation sites at the C-terminus regulate nuclear import of HCMV DNA polymerase processivity factor ppUL44.* Virology, 2011. **417**(2): p. 259-67.
54. Sinigalia, E., et al., *The human cytomegalovirus DNA polymerase processivity factor UL44 is modified by SUMO in a DNA-dependent manner.* PLoS One, 2012. **7**(11): p. e49630.
55. Mattoscio, D., C.V. Segre, and S. Chiocca, *Viral manipulation of cellular protein conjugation pathways: The SUMO lesson.* World J Virol, 2013. **2**(2): p. 79-90.
56. Appleton, B.A., et al., *The cytomegalovirus DNA polymerase subunit UL44 forms a C clamp-shaped dimer.* Mol Cell, 2004. **15**(2): p. 233-44.
57. Gulbis, J.M., et al., *Structure of the C-terminal region of p21(WAF1/CIP1) complexed with human PCNA.* Cell, 1996. **87**(2): p. 297-306.
58. Zuccola, H.J., et al., *The crystal structure of an unusual processivity factor, herpes simplex virus UL42, bound to the C terminus of its cognate polymerase.* Mol Cell, 2000. **5**(2): p. 267-78.
59. Appleton, B.A., et al., *Crystal structure of the cytomegalovirus DNA polymerase subunit UL44 in complex with the C terminus from the catalytic subunit. Differences in structure and function relative to unliganded UL44.* J Biol Chem, 2006. **281**(8): p. 5224-32.
60. Komazin-Meredith, G., et al., *The human cytomegalovirus UL44 C clamp wraps around DNA.* Structure, 2008. **16**(8): p. 1214-25.
61. Sinigalia, E., et al., *Role of homodimerization of human cytomegalovirus DNA polymerase accessory protein UL44 in origin-dependent DNA replication in cells.* J Virol, 2008. **82**(24): p. 12574-9.
62. Alvisi, G., et al., *The flexible loop of the human cytomegalovirus DNA polymerase processivity factor ppUL44 is required for efficient DNA binding and replication in cells.* J Virol, 2009. **83**(18): p. 9567-76.
63. Limaye, A.P., et al., *Late-onset cytomegalovirus disease in liver transplant recipients despite antiviral prophylaxis.* Transplantation, 2004. **78**(9): p. 1390-6.
64. Lurain, N.S. and S. Chou, *Antiviral drug resistance of human cytomegalovirus.* Clin Microbiol Rev, 2010. **23**(4): p. 689-712.
65. Razonable, R.R., V.C. Emery, and I. th Annual Meeting of the, *Management of CMV infection and disease in transplant patients. 27-29 February 2004.* Herpes, 2004. **11**(3): p. 77-86.
66. Loregian, A., H.S. Marsden, and G. Palu, *Protein-protein interactions as targets for antiviral chemotherapy.* Rev Med Virol, 2002. **12**(4): p. 239-62.
67. Loregian, A. and G. Palu, *Disruption of protein-protein interactions: towards new targets for chemotherapy.* J Cell Physiol, 2005. **204**(3): p. 750-62.
68. Scott, D.E., et al., *Small molecules, big targets: drug discovery faces the protein-protein interaction challenge.* Nat Rev Drug Discov, 2016. **15**(8): p. 533-50.

69. Cohen, E.A., et al., *Specific inhibition of herpesvirus ribonucleotide reductase by a nonapeptide derived from the carboxy terminus of subunit 2.* Nature, 1986. **321**(6068): p. 441-3.
70. Pilger, B.D., C. Cui, and D.M. Coen, *Identification of a small molecule that inhibits herpes simplex virus DNA Polymerase subunit interactions and viral replication.* Chem Biol, 2004. **11**(5): p. 647-54.
71. Loregian, A. and D.M. Coen, *Selective anti-cytomegalovirus compounds discovered by screening for inhibitors of subunit interactions of the viral polymerase*, in *Chem Biol*. 2006. p. 191-200.
72. Chautard, E., N. Thierry-Mieg, and S. Ricard-Blum, *Interaction networks: from protein functions to drug discovery. A review.* Pathol Biol (Paris), 2009. **57**(4): p. 324-33.
73. Cobret, L., et al., *Targeting the cis-dimerization of LINGO-1 with low MW compounds affects its downstream signalling.* Br J Pharmacol, 2015. **172**(3): p. 841-56.
74. Zhang, J.H., T.D. Chung, and K.R. Oldenburg, *A Simple Statistical Parameter for Use in Evaluation and Validation of High Throughput Screening Assays.* J Biomol Screen, 1999. **4**(2): p. 67-73.
75. Loregian, A., et al., *Residues of human cytomegalovirus DNA polymerase catalytic subunit UL54 that are necessary and sufficient for interaction with the accessory protein UL44.* J Virol, 2004. **78**(1): p. 158-67.
76. Paul, D., et al., *NS4B self-interaction through conserved C-terminal elements is required for the establishment of functional hepatitis C virus replication complexes.* J Virol, 2011. **85**(14): p. 6963-76.
77. Muratore, G., et al., *Small molecule inhibitors of influenza A and B viruses that act by disrupting subunit interactions of the viral polymerase.* Proc Natl Acad Sci U S A, 2012. **109**(16): p. 6247-52.
78. Loregian, A., et al., *Specific residues in the connector loop of the human cytomegalovirus DNA polymerase accessory protein UL44 are crucial for interaction with the UL54 catalytic subunit.* J Virol, 2004. **78**(17): p. 9084-92.
79. Corbel, C., et al., *First BRET-based screening assay performed in budding yeast leads to the discovery of CDK5/p25 interaction inhibitors.* Biotechnol J, 2011. **6**(7): p. 860-70.
80. Scaturro, P., et al., *Characterization of the mode of action of a potent dengue virus capsid inhibitor.* J Virol, 2014. **88**(19): p. 11540-55.
81. Panza, E., et al., *Transfection of the mutant MYH9 cDNA reproduces the most typical cellular phenotype of MYH9-related disease in different cell lines.* Pathogenetics, 2008. **1**(1): p. 5.
82. Scaturro, P., et al., *Characterization of the mode-of-action of a potent Dengue virus capsid inhibitor.* J Virol, 2014.
83. Mercorelli, B., et al., *A 6-aminoquinolone compound, WC5, with potent and selective anti-human cytomegalovirus activity.* Antimicrob Agents Chemother, 2009. **53**(1): p. 312-5.